Published in final edited form as:
Chem Rev. 2020 October 14; 120(19): 10695–10743. doi:10.1021/acs.chemrev.9b00810.

Photopolymerizable Biomaterials and Light-Based 3D Printing Strategies for Biomedical Applications

Claire Yu[#],
Department of NanoEngineering, University of California San Diego, La Jolla, California 92093, United States

Jacob Schimelman[#],
Department of NanoEngineering, University of California San Diego, La Jolla, California 92093, United States

Pengrui Wang,
Materials Science and Engineering Program, University of California San Diego, La Jolla, California 92093, United States

Kathleen L. Miller,
Department of NanoEngineering, University of California San Diego, La Jolla, California 92093, United States

Xuanyi Ma,
Department of Bioengineering, University of California San Diego, La Jolla, California 92093, United States

Shangting You,
Department of NanoEngineering, University of California San Diego, La Jolla, California 92093, United States

Jiaao Guan,
Department of Electrical and Computer Engineering, University of California San Diego, La Jolla, California 92093, United States

Bingjie Sun,
Department of NanoEngineering, University of California San Diego, La Jolla, California 92093, United States

Wei Zhu,
Department of NanoEngineering, University of California San Diego, La Jolla, California 92093, United States

Shaochen Chen

Corresponding Author: Shaochen Chen - Phone: 858-822-7856; chen168@eng.ucsd.edu; Fax: 858-534-9553.

[#] C.Y. and J.S. contributed equally to this publication.

The authors declare no competing financial interest.

Complete contact information is available at: https://pubs.acs.org/10.1021/acs.chemrev.9b00810

Department of NanoEngineering, Materials Science and Engineering Program, Department of Bioengineering, and Chemical Engineering Program, University of California San Diego, La Jolla, California 92093, United States;

Abstract

Since the advent of additive manufacturing, known commonly as 3D printing, this technology has revolutionized the biofabrication landscape and driven numerous pivotal advancements in tissue engineering and regenerative medicine. Many 3D printing methods were developed in short course after Charles Hull first introduced the power of stereolithography to the world. However, materials development was not met with the same enthusiasm and remained the bottleneck in the field for some time. Only in the past decade has there been deliberate development to expand the materials toolbox for 3D printing applications to meet the true potential of 3D printing technologies. Herein, we review the development of biomaterials suited for light-based 3D printing modalities with an emphasis on bioprinting applications. We discuss the chemical mechanisms that govern photopolymerization and highlight the application of natural, synthetic, and composite biomaterials as 3D printed hydrogels. Because the quality of a 3D printed construct is highly dependent on both the material properties and processing technique, we included a final section on the theoretical and practical aspects behind light-based 3D printing as well as ways to employ that knowledge to troubleshoot and standardize the optimization of printing parameters.

Graphical Abstract

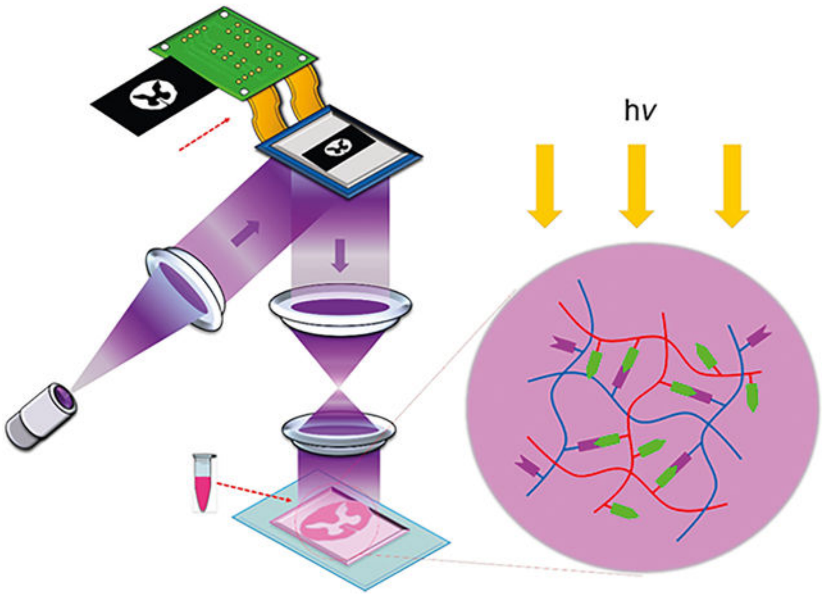

1. INTRODUCTION

The emergence of 3D printing technologies in tissue engineering has caused a paradigm shift in traditional biofabrication strategies by enabling precise spatiotemporal control over the placement of cells and biomaterials to form complex constructs. These advanced 3D printing platforms have become increasingly important as we move toward the adoption of

3D cell culture systems due to the inadequacies of conventional 2D cell culture. Specifically, it has been well documented now that rigid monolayer culture systems do not appropriately recapitulate the inherent complexities within the native tissue microenvironment. Thus, cells grown under these 2D conditions poorly reflect the in vivo functionality, phenotype, morphology, and differentiation potential.[1–3] The reason for this disparity is because cells residing in their natural milieu are highly influenced by their surroundings known as the extracellular matrix (ECM) and maintaining this dynamic reciprocity within a 3D microenvironment is crucial to restoring appropriate biological behaviors in vitro.[4] As such, 3D cell culture systems have gained wide attraction in the fields of tissue engineering and regenerative medicine. To properly mimic the 3D ECM environment, a fabrication method is needed that can precisely control the mechanical, physical, and viscoelastic properties of a material in a 3D space. Recent advances in 3D printing techniques have shown their promise at addressing these requirements. The level of control offered by 3D printers has led to many noteworthy advancements in the production of physiologically relevant biomimetic tissue and organ substitutes for drug testing, elucidation of biological mechanisms, disease models, translational medicine, and surgical implants.[5–8]

Over the years, the evolution of 3D printing technologies has seen significant advancements since the early stereolithography (SLA) fabrication systems first introduced in the 1980s by Charles Hull.[9] Today, a wide range of 3D printing modalities have been developed, with the most common being traditional nozzle-based printers in the form of inkjet and extrusion platforms. These printing platforms operate in a rasterized direct-write format by building a structure layer-by-layer and have been used extensively in bioprinting applications to fabricate various tissue models including perfusable kidneys, vascularized cardiac tissues, and cellularized neural grafts for repair of the damaged central nervous system.[10–12] Complementing these traditional platforms, light-based 3D printing technologies have recently gained popularity by offering improved spatial resolution, pattern fidelity, and fabrication speeds. Most current light-based 3D printers operate using digital light processing (DLP) technology controlled by a digital micromirror device (DMD) invented by Larry J. Hornbeck at Texas Instruments in 1987.[13] Notably, the introduction of the DMD chip has revolutionized projection display by offering excellent image stability, fidelity, and reliability while serving as a crucial element in DLP-based 3D printers. The device is comprised of an array of millions of micromirrors that each correspond to a pixel in the image being displayed, which can be individually rotated to create an “on” or “off” state to control the reflection of the projected light. By modulating these “on” or “off” states digitally, different light patterns can be rapidly projected onto a photocurable reservoir to enable selective solidification. Moreover, the contactless nature of these printers permits the fabrication of complex structures with micrometer-level resolution and overhanging or hollow geometries that can be completed rapidly on the order of seconds via plane-by-plane or volumetric projection rather than dot-by-dot or line-by-line as in SLA, inkjet, and extrusion printing formats.[14] Because of these features, the application of light-based 3D printers in tissue fabrication has led to the creation of highly elaborate cellularized constructs possessing tissue-scale features that can be produced in a continuous fashion with smooth topographies not attainable in layer-by-layer processes.[14] Several prominent examples showcasing the development of elaborate physiologically relevant tissues using

DLP-based 3D printing technology include a multicomponent human liver triculture model for drug testing, biomimetic implant containing multiple microchannels to guide nerve regeneration for spinal cord repair, and anatomically correct trabecular bone models embedded with angiogenic sprouts and meniscal grafts.[15–17]

Given the promising use of light-based 3D printing in tissue engineering, the success of these platforms is also dependent on the development of compatible biomaterials available for these systems to suit various biomedical applications. Owing to the light-based nature of these printing platforms, a key factor in bioink development is to incorporate photoreactive moieties (e.g., methacrylate, acrylate, or thiol–ene groups) to enable fast and selective solidification of the prepolymer. Photopolymerization occurs when UV or visible light interacts with light-sensitive compounds known as photoinitiators to produce free radicals that initiate the polymerization process to form a covalently cross-linked hydrogel.[18] Compared to conventional polymerization methods, photopolymerization reactions present several advantages, including rapid curing rates under low light intensity, short exposure times with minimal heat production, and potential for spatiotemporal control.[19] Furthermore, these reactions can be performed under physiological conditions in aqueous solutions without harsh cytotoxic reagents that make it favorable for cell-based bioprinting applications.[19] To date, a number of synthetic and naturally derived photopolymerizable biomaterials for biocompatible and biodegradable hydrogels have been investigated that were addressed in several excellent reviews.[19–21] Among the many types of photoreactive biomaterials, there are several criteria that must be considered upon selection for compatibility with light-based 3D printing setups and their utility in tissue engineering applications as summarized in Figure 1. In general, the key evaluation criteria include: (1) biodegradative properties to ensure appropriate tissue remodeling without deleterious byproducts, (2) biocompatibility in the presence of cells with minimal immunogenicity, (3) mechanical properties attainable with the selected biomaterial formulation, (4) structural stability of the final printed construct, (5) appropriate polymerization mechanism to achieve the desired hydrogel properties for the intended biological application, and (6) optical properties of the biomaterial composition and 3D printer settings to ensure optimal printing conditions can be reached.

The scope of this paper is to provide a comprehensive review on photopolymerizable biomaterials and current state-of-the-art on 3D light-based printing technologies, with a focus on biomedical applications. While there are several exceptional reviews on 3D printing, including works by Murphy et al.[6] and Mandrycky et al.,[22] they primarily cover methods and applications of traditional nozzle-based 3D printers. Our aim is to present a detailed overview that spans the development of photoreactive bioinks to light-based 3D printing strategies as a guide to address the growing adoption and development of light-based additive manufacturing. We begin by introducing fundamental principles and mechanisms of photopolymerization reactions employed in photocurable biomaterials followed by a summary of commonly used photoinhibiting and photolabile chemistries to control polymerization kinetics. Next, we provide a discussion on the current literature for photo-cross-linkable natural, synthetic, and composite biomaterials used in light-based printing as well as their application in tissue engineering and regenerative medicine. Finally, we review the progress and evolution of recent light-based 3D printing modalities ranging from serial to planar to volumetric build platforms and discuss strategies to improve control over print resolution and quality to serve as a framework to standardize future printing optimization methodologies. Overall, we envision that the expansion and development of novel photocurable biomaterial libraries will help facilitate and broaden the utility of light-based 3D printing systems such that we can further exploit their fabrication potential for the advancement of next-generation scaffolds and biomimetic tissues.

2. PHOTOPOLYMERIZATION MECHANISMS

2.1. Free-Radical Chain Growth Polymerization

The majority of photoreactive biomaterial systems primarily undergo free-radical chain-growth polymerization upon light irradiation to form a cross-linked hydrogel. Specifically, photoinitiators decompose upon light exposure at 263 a specific wavelength (i.e., commonly 365 nm) into radicals, which serve as kinetic-chain carriers by attacking free monomers to initiate a chain reaction of attacking nearby monomers and adding them to the growing polymer chain.

2.1.1. Mechanism.—Chain-growth polymerization is defined by three distinct stages: (1) initiation, (2) propagation, and (3) termination. In initiation, monomers typically have the structure $CH_2{=}CR_1R_2$, where the carbon–carbon double bond (“active center”) is rearranged by free radical initiators. R_2 is commonly either a hydrogen or methyl group, and for simplicity we will write it as an H group in the following schemes.[23,24] Upon light exposure, the photoinitiator molecule decomposes homolytically into two free radicals (Scheme 1A) via bond cleavage at sites such as C–C, C–Cl, C–O, or C–S bonds.[23,24] The free radicals are then able to initiate polymer chain growth by reacting with a monomer as depicted in Scheme 1B. The newly radicalized monomer is able to react with another monomer and this continues to propagate in a chain-like fashion (Scheme 1C,D).[23]

The propagation of the polymer chain continues until a termination reaction occurs. There are four different ways a reaction can be terminated: (1) combination of two propagating chains (Scheme 1E), (2) a propagating chain reacts with an initiator radical, (3) chain transfer occurs (i.e., the free radical is transferred to another molecule), or (4) an interaction with impurities or inhibitors. However, chain ends can also react with each other via hydrogen abstraction, also known as disproportionation, which results in two separate terminated polymer chains. Whether the two chains react via combination or disproportionation depends on the monomer type as well as the reaction temperature.[23,24]

Impurities and inhibitors are also a major consideration during photopolymerization in DLP-based 3D printing. In particular, oxygen impurities can react with free radicals, thus impeding their propagation within the prepolymer system. As oxygen can diffuse into a material overtime, this means that a material may exhibit different printing properties (i.e., lower resolution and requiring higher exposure times) as the material is used over a period of time. Sometimes free radical inhibitors are used in a controlled manner to improve printing resolution. Since free radicals are very active and can diffuse quickly from an activated area, inhibitors can capture the free radicals to mitigate propagation.[23,24]

2.1.2. Kinetics.

The rate of photopolymerization can be described by the following equation:

$$\upsilon_{\mathrm{pp}} = k_{\mathrm{pp}}(\phi \varepsilon I_0 / k_{\mathrm{t}})^{1/2}[M]^{3/2} \qquad (1)$$

where v_{pp} is the rate of photopolymerization, k_{pp} is the photopropagation rate constant, ϕ is quantum yield, ε is extinction coefficient, I_0 is the incident light intensity, k_{t} is the termination rate constant, and M is the monomer concentration. From eq 1, a few observations can be noted. First, the rate of polymerization is dependent on the initial monomer concentration by a power of 1.5, indicating that an increase in monomer concentration will lead to a nonlinear increase in polymerization rate. Moreover, the efficiency of the photoinitiator is related to the polymerization rate by its square root, which is discussed further in section 2.1.5.[23]

2.1.3. RAFT and ATRP.

Because of the multiple termination reactions in free-radical polymerization, the polymer chain lengths are highly dispersed within a solution. To reduce the polydispersion, “living” radical polymerizations that moderate the termination reactions were developed. Generally, the free radical is reversibly “trapped” in a secondary chain transfer agent, rendering it dormant and reducing the overall concentration of free radicals in the prepolymer solution. This results in a controlled linear growth in polymer length. Two of the “living” or controlled radical polymerizations are reversible addition/fragmentation chain transfer (RAFT) and atom transfer radical polymerization (ATRP).

In ATRP, an alkyl halide (R–X) and a transition metal halide catalyst (Mt^{z}Y/ligand) are used to reversibly trap the free radical (Scheme 2, top). The kinetics for the deactivation rate (k_{d}) compared to activation rate (k_{a}) are much higher, meaning that the radical is mostly kept dormant. This in turn means that the termination reaction will have less probability to occur and will therefore be suppressed. ATRP methods are used with styrenes, (meth)acrylates, (meth)acrylamides, and acrylonitrile. Moreover, ATRP can be used with free radical initiation in a method termed reverse ATRP. Free radicals are rendered dormant by an alkyl halide complex in a higher oxidation state, where one alkyl molecule can reversibly react with the radicalized polymer chain (Scheme 2, bottom).[23]

RAFT is another common living polymerization technique, where a molecule can reversibly cap one or two growing polymer chains at once. This molecule contains dithiol compounds which will be bonded to the central carbon atom by single or double bonds. The Z compound is typically an aryl, alkyl, SR, OR, or NR_2 group. Lastly, a good leaving group with respect to the polymer chain, P_{m} or P_{n}, is initially bonded to one of the sulfur atoms and supplanted by a free radical upon initiation. Scheme 3 describes the equilibrium reaction and showcases how the growing polymer chains spend most of their time dormant and thereby suppressing termination reactions and allowing for a controlled growth of the polymer chains.[23]

Capping agents such as 2,2,6,6-tetramethyl-1-piperidinyloxy (TEMPO) have also been used to help prevent free radical diffusion within a solution and can be added to a prepolymer solution before printing.[25] Although less widely applicable, TEMPO is used in nitroxide-mediated polymerization and can reversibly cap the growing polymer chain, suppressing termination reactions.[23]

2.1.4. Functional Groups.—

Because not all monomers contain the desired reactive alkene for free-radical polymerization, functional groups can be modified onto a synthetic monomer or onto the backbone of a natural polymer. In the case of free radical polymerization, acrylates and methacryloyls have been commonly used with prepolymer materials. For example, poly(ethylene glycol) diacrylate (PEGDA) is a popular synthetic polymer for biomedical applications containing two acrylate groups. Moreover, natural polymers such as gelatin and hyaluronic acid have been functionalized with methacryloyl groups, sometimes commonly referred to as methacrylate groups.[26]

2.1.5. Photoinitiators.—

In DLP printing, photoinitiator choice is very important as it can determine the efficiency of polymerization, which in turn will impact the printing time, power, and resolution as covered in greater detail in section 9. Type I photoinitiators, commonly used in light-based 3D printing, generate two free radicals upon exposure to light of a specific wavelength.[19,27,28] The kinetics of a photoinitiator can be described by the following equation, where R_i is the initiation rate:

$$R_i = \frac{2\phi\varepsilon I f C_i}{N_A h \upsilon} \tag{2}$$

Here, I is the incident light intensity (units of power/area), C_i is the photoinitiator concentration, ε is the extinction coefficient, ϕ is the quantum yield, and f is the photoinitiator efficiency. In the denominator are Avogadro's number (N_A), Planck's constant (h), and the frequency of initiating light (v). By examining the equation, one can see that increasing incident light intensity (I) will increase the rate of initiation, as more energy will be transferred to breaking bonds in the photoinitiator. As well, initiator concentration (C_i) has a direct impact on the initiation rate.[23]

The initiation rate in turn has an indirect relationship with polymerization rate (eq 3), which can be derived using the steady-state approximation. The polymerization rate (R_p) is directly related to the square root of the initiation rate (R_i). In eq 3, k_p is the rate constant for chain propagation, M is the monomer concentration, and k_t is the rate constant for termination.

$$R_p = k_p[M]\left(\frac{R_i}{2k_t}\right)^{1/2} \tag{3}$$

More specifically, the polymerization rate will have a square root dependence on the photoinitiator concentration and light intensity. However, these equations describe local relationships, and depending on the spatial position, the rates will change due to local incident light variation that is caused by light-path distance and diffraction as well as by monomer concentration. As such, more complex equations can be used to describe these circumstances.[24]

To determine the appropriate photoinitiator choice, one must first consider the wavelength of the light source used. Three of the most common photoinitiators used in bioprinting are Irgacure-2959, lithium phenyl-2,4,6-trimethylbenzoylphosphi-nate (LAP), and eosin Y.[26] Both Igracure-2959 and LAP are commonly used with a near-UV (i.e., 365 nm) light source. Consequently, there is some concern about using near-UV light on prepolymer solutions containing cells due to the known cell damage caused by prolonged UV irradiation. To address this concern, Ruskowitz et al. recently tested the impact of low-dose near-UV exposure on the apoptosis and proliferation of mouse fibroblasts (i.e., NIH/3T3) as well as human mesenchymal stem cells (hMSCs) and found no significant effects.[29] However, further experiments on more cell types are needed to fully conclude the impact of near-UV wavelengths on cells, although their findings point to the concentration of free radicals present as what may directly impact cell viability.[29] Irgacure-2959 has low cytotoxicity, minimal immunogenicity, and is often used with solely synthetic polymer systems due to its low water solubility (<0.5 wt %). Moreover, due to its low molar absorptivity at 365 nm ($\varepsilon < 10\ \mathrm{m}^{-1}\ \mathrm{cm}^{-1}$), high concentrations must be added to the prepolymer solution. On the other hand, LAP is a highly water-soluble photoinitiator and is a good choice for prepolymer systems incorporating natural polymers. LAP also has a very high molar absorptivity ($\varepsilon \approx 200\ \mathrm{M}^{-1}\ \mathrm{cm}^{-1}$), which makes it much more efficient than Irgacure-2959 and can be used at much lower concentrations. To illustrate, Fairbanks et al. compared the time to gelation with equal concentrations of LAP and Irgacure-2959 in a PEGDA solution and demonstrated that the samples containing LAP gelled almost a magnitude faster than those containing Irgacure-2959.[26,28,30] Although less common, visible light photoinitiators have also been reported as an alternative to circumvent potential cytotoxic effects with near-UV light photoinitiators. For example, LAP can also be used with a 405 nm light source, although its molar absorptivity is lower at this wavelength. In the same experiment as discussed earlier, Fairbanks et al. found that the time to gelation was five times longer with LAP when a 405 nm light source was used compared to a 365 nm light source.[26,28] Another common and cytocompatible visible light photoinitiator is the xanthene dye, eosin Y, commonly used in histological staining. Unlike the other photoinitiators discussed, eosin Y is a type II photoinitiator that generates a secondary free radical from a co-initiator via hydrogen abstraction. When excited by light at wavelengths between 490 and 650 nm, it requires both a co-initiator (i.e., triethanolamine (TEOA)) as well as a comonomer (i.e., 1-vinyl-2 pyrrolidinone (NVP)) to generate free radicals.[30,31]

2.2. Orthogonal Step Growth Polymerization

2.2.1. Click Chemistry for Hydrogel Formation.—One undesired aspect of free-radical chain-growth polymerization is that it produces inhomogeneous networks which correspond to inconsistent mechanical and physical properties within a polymerized matrix.[32] An inhomogeneous network structure will lead to a mismatch between bulk and local (microscale) properties, which is not ideal for controlled 3D cell culture. For example, the bulk properties could be consistent from sample to sample, however, the directionality of the local properties could vary and may lead to observed differences in cell responses due to cells' natural sensitivity toward mechanical cues or physical gradients.[33] Many click chemistry reactions have been developed and exploited for tuned facile hydrogel formation.[34–38]

2.2.2. Photoinduced Thiol–Ene Click Chemistry.—

Most click reactions occur either spontaneously or via catalysis, although few can be controlled with light.[34,39–42] One that has been exploited recently, although its mechanism has been known for some time,[43] is the photoinduced thiol–ene reaction.[34,36,44–50] For context, the thiol–ene reaction is historically differentiated from the Michael addition reaction based upon the reaction condition. Specifically, the thiol–ene reaction requires a free-radical initiator, whereas the thiol-Michael addition requires a chemical catalyst, although some consider the photoinduced mechanism to be a type of thiol-Michael addition pathway.[34,37] The orthogonal nature of the thiol–ene mechanism allows for the formation of homogeneous hydrogel networks of consistent properties. Free-radical chain growth primarily produces spatially inhomogeneous networks, especially in acrylate-based photopolymerization common to 3D printing and bioprinting.[32,45]

2.2.3. Mechanism.—

Alhough the thiol–ene reaction is similar to the photoinduced chain-growth mechanism in that both are initiated via free radicals, it follows a free radical-mediated step-growth mechanism which achieves a higher rate of conversion in a shorter period of time, especially as compared to the textbook step-growth polymerization kinetics.[51] Due to the photoclickable nature of thiol–ene reactions, it is orthogonal, such that each available thiol group only reacts once with each available double bond. There have been multiple publications taking advantage of this selective behavior by using off-stoichiometric ratios of thiol to alkene in the fabrication of cross-linked networks that have available functional groups for post functionalization.[39,52–58] The nature of interaction between thiol groups and oxygen also renders thiol–ene reactions less susceptible to oxygen inhibition compared to traditional free radical chain growth mechanisms. In this case, oxygen tends to abstract the hydrogen from a thiol group to regenerate the thiyl radical and thus permits continued polymerization.[59] The step-growth thiol–ene polymerization mechanism is detailed in Figure 2.[60]

A dosage of light is used to generate a free radical either by cleaving an initiator which abstracts the thiol hydrogen or by cleaving the hydrogen directly from the thiol. The resultant thiyl radical reacts with the alkene double bond. This reaction proceeds in a step-growth manner due to a chain transfer reaction predominantly occurring (Figure 2, mechanism II), where the free radical on the propagating chain is transferred to an available thiol group, thus regenerating the thiyl radical. As such, these reactions theoretically require a lower initiator concentration to proceed.

2.2.4. Reaction Kinetics.—

Bowman and his coauthors have extensively studied the thiol–ene reaction and its kinetics.[37,61–66] They have found that the rate order is determined by k_p/k_{CT}, where k_p is the rate of propagation and k_{CT} is the rate of chain transfer.[62,67,68] When k_p dominates, the rate is first-order with respect to the thiol concentration, when k_{CT} dominates, the rate is first-order with respect to the alkene concentration, and when $k_p \approx k_{CT}$, the rate is half-order with respect to both the thiol and alkene concentrations.[67] The specific values of k_p and k_{CT} depend on the reaction conditions such as the alkene group used.[67] Thus, the kinetics of the thiol–ene reaction is dependent on the chosen alkene reactivity. The reactivity of the alkene group decreases as the electron density of the double bond decreases.[69] Northrop and Coffey have modeled the kinetics of the radical-initiated thiol–ene reaction between a methyl mercaptan ($H_3C–SH$) and a series of different alkenes.[67] As can be seen in Figure 3, the kinetics of the thiol–ene reaction is highly dependent on the reactivity of the chosen alkene, with norbornene proving to have the highest reactivity. The inherent ring strain of norbornene causes its double bond to be highly reactive for a thiyl radical attack as well as a radical intermediate for abstracting the thiol hydrogen to generate the thiyl radical.[45,69] As such, thiol–norbornene chemistry has been a popular choice in the literature for light-based 3D printing.[52,70–77]

2.2.5. Orthogonal Cross-linking and Off-Stoichiometry Thiol–Ene.

—One of the benefits of implementing photoinduced thiol–ene chemistry is its orthogonal behavior, such that one thiol group will react only once with one alkene double bond (i.e., no intrinsic reaction propagation). Additionally, if the appropriate alkene is chosen, an alkene will specifically only react with a thiol and vice versa. This specificity allows for greater control of the network formation as shown in Figure 4C, where an end-functional multiarm PEG is used to produce a regular and homogeneous network.[78]

When one reacts a 1:1 stoichiometric ratio of thiol to alkene groups, theoretically each group should be fully consumed under the assumption that a sufficient concentration of free radicals is present to take the reaction to full conversion. However, if an excess of either thiol or alkene groups is present, the excess components will remain after complete photo-cross-linking due to the orthogonal nature of the thiol–ene reaction. The remaining free thiol or alkene groups can then be readily used for postfunctionalization of the thiol–ene hydrogel, as has been reported in several works under the term off-stoichiometry thiol–ene (OSTE).[39,55,79–82] Typically, the thiol is preferred as the excess reagent as it is widely used in click chemistry, especially for bioconjugation,[48,83] and the free thiol groups can undergo reversible disulfide bond formation to drive dynamic hydrogel behavior.[84]

3. PHOTOINHIBITING CHEMISTRY AND MECHANISMS

Controlling polymerization of various biomaterials is necessary to ensure high resolution and appropriate shape fidelity in light-based 3D printing. This is particularly important in DLP-based printing systems, where the $x-y$ resolution of the construct is determined by the projected light path, meanwhile the resolution in the z direction is dependent on additives to provide photoinhibiting or light attenuating properties to eliminate out-of-focus light to achieve the desired layered thickness. This section provides a review of general strategies to control free-radical chain growth polymerization in (meth)-acrylate-based biomaterial systems for improving photopatterning conformity and feature resolution. Furthermore, a summary of commonly used photoinhibitors and photoabsorbers is provided in Table 1.

3.1. Photoinhibitor Additives

Photoinhibition strategies involve the addition of light-activated molecules to mediate free-radical polymerization by producing radicals that function to terminate chain growth. As such, these molecules can offer improved photocontrolled reactions by employing dual wavelengths of activation that are sufficiently far apart to give independent control over photoinitiation and photoinhibition in a localized manner. This was first demonstrated by

Scott et al. by using two-color irradiation single-photon absorption of the camphorquinone (CQ)/ethyl 4-(dimethylamino)benzoate (EDAB) visible-light (i.e., 469 nm) photoinitiator in combination with the near UV-active (i.e., 365 nm) tetraethylthiuram disulfide (TETD) photoinhibitor to permit controlled direct-write photolithography of triethylene glycol dimethacrylate (TEGDMA).[85] In this system, UV irradiation leads to cleavage of TETD to form a sulfur-centered dithiocarbamyl radical that terminates polymerization by end-capping the growing polymer chain to slow the rapid polymerization rates upon visible light irradiation.[85] This photoinitiation and photoinhibition system allows for submicrometer resolutions as small as 65 nm that are comparable to length scales in two-photon photopolymerization systems.[85] Moreover, by using a single-photon approach to nanolithography, they were able to achieve higher fabrication velocities with the use of less expensive continuous wave diode lasers relative to conventional two-photon polymerization techniques.[85] Similarly, Lovell et al. evaluated the effects of controlled polymerization kinetics of TEGDMA as a function of wavelength by incorporating varying ratios of 2,2-dimethoxy-2-phenylacetophenone (DMPA) as the photoinitiator and TED as the photoinhibitor.[86] In this case, both photoinitiator and photoinhibitor species were activated at wavelengths ranging between 290 and 365 nm to control the degree of iniferter or “living” radical polymerization.[86] It was found that the influence of wavelength was greater on polymerization rate compared to the ratio of DMPA to TED because the rates of sulfur–carbon chain breaking was directly correlated as a function of wavelength, which could then be used as another factor to control resolution and thus pattern fidelity.[86] In another study, van der Laan et al. explored the use of butyl nitrite as an UV activated photoinhibitor of blue light induced photopolymerization reactions coupled with CQ/EDAB as the visible light photoinitiator.[87] Butyl nitrite functions as a photoinhibitor via the formation of nitric oxide upon photolysis which then efficiently terminates free-radical polymerization as well as generates alkoxide radicals to yield a net of two termination events.[87,88] Here, two perpendicular irradiation light paths, one at near-UV wavelengths and the other at blue visible wavelength, were utilized to achieve independent control over initiation and inhibition for volumetric 3D printing.[87] It was found that polymerization inhibition with butyl nitrite terminates immediately upon cessation of near-UV irradiation such that photopolymerization can continue without delay.[87] This is contrary to other near-UV photoinhibitors, such as bis[2-(*o*-chlorophenyl)-4,5-diphenyl imidazole] (*o*-Cl-HABI), where inhibition persists for several seconds after irradiation.[89] As a result, highly selective polymerization of methacrylate resins can be achieved to form complex 3D geometries in a single exposure. For instance, concurrent perpendicular photoinhibition and photopolymerization enabled confinement of depth during fabrication by illuminating both near-UV and visible light through a circular and triangular photomask, respectively. The resulting structure produced a triangular prism with hollow circular regions throughout the depth of the construct, which cannot be fabricated using a single exposure with traditional photolithography techniques.[87]

Photoinhibitor species can also be used in light-based 3D printing to achieve rapid and continuous stereolithographic additive manufacturing. Using two-color irradiation, de Beer et al. demonstrated that the incorporation of *o*-Cl-HABI near-UV photoinhibitor in combination with CQ/EDAB blue visible light photoinitiator into trimethylolpropane triacrylate could be used to provide controlled photopolymerization confinement at the polymerization window.[89] In the absence of co-initiators, photolysis of *o*-Cl-HABI produces lophyl radicals that rapidly combine with propagating carbon-centered radicals to terminate polymerization.[89] As such, upon concurrent irradiation of near-UV and blue visible light, a layer of no polymerization occurs at the fabrication window, meanwhile above this region polymerization occurs such that continuous 3D printing can be achieved without adhesion of the object.[89] The thickness of the inhibited layer is dependent on the incident radiation and concentration of the UV absorber.[89] Typical inhibition methods require oxygen inhibition at the window that is tens of micrometers in thickness,[90] whereas this technique allows for variable control to achieve thickness in the hundreds of micrometers to accommodate for viscous biomaterials or geometries with large surface areas.[89]

Stable radicals such as TEMPO and its derivatives are also ideal candidates as photoinhibiting species to mediate well-controlled free-radical polymerization. The stable free-radical property of TEMPO is attributed to steric bulk of the substituent groups that function to impede the reaction of other free radicals to continue polymerization. Specifically, in free-radical polymerization, TEMPO acts as a free radical quencher by adding to the end of a growing polymer chain to terminate polymerization and thus provide control over the polymerization kinetics.[91] For instance, the addition of TEMPO at low concentrations into methacrylate prepolymers (e.g., GelMA) have been reported to improve printing resolution in dynamic optical projection stereolithography (DOPsL) for the fabrication of micrometer scale topographies with overhanging structures as 3D extracellular microenvironments.[92]

3.2. Photoabsorber Additives

An alternate strategy to control for polymerization is the addition of photoabsorbing species, which function as light-attenuating additives to absorb excess light and therefore improve pattern fidelity by prompting a dose-dependent delay in the initiation of photopolymerization. Commonly used photoabsorbers include natural or synthetic food dyes that absorb in the visible light range and are compatible with aqueous prepolymer formulations. A yellow food dye, tartrazine (absorbance peak at ~405 nm), is a candidate photoabsorber for 3D bioprinting due to its biocompatibility, low toxicity, wide use in the food industry, and hydrophilic nature that allows for sufficient elution to yield transparent hydrogels post fabrication.[93] Grigoryan et al. demonstrated the addition of tartrazine in PEGDA hydrogels to enable visible light 3D printing via continuous liquid interface production (CLIP) of complex multivascular networks.[94] In particular, this group was able to fabricate an alveolar model topology with voxel resolutions of 5 pl with perfusable open channels measuring as small as 300 μm in diameter.[94] Other food additives that can function as photoabsorbers include curcumin (absorbance peak at ~425 nm) derived from turmeric that is lipophilic in nature which can cause staining of the hydrogel, while anthocyanin (absorbance peak ~510 nm) derived from blueberries will require high concentrations to provide suitable light attenuation under visible light due to the offset in peak absorbance.[94–97] Reactive orange 16 is another water-soluble anionic azo dye that can be used to achieve DLP-based 3D printed features as small as 200 μm with PEGDA with a peak absorbance of 493 nm.[98,99] The addition of nanoparticles is also a viable strategy to attenuate light with the use of inorganic gold nanoparticles that are biocompatible for tissue engineering applications.[100] Depending on the diameter of the gold nanoparticles, peak absorbance can be achieved in the range of ~520–530 nm.[100] Lastly, 2-hydroxy-4-methoxybenzophenone-5-sulfonic acid (HMBS) has been used as an additive that is biocompatible at low concentrations and is a commonly used FDA approved chemical used in sunscreen and cosmetic products.[92]

4. PHOTOLABILE CHEMISTRY AND MECHANISMS

Photolabile molecules refer to chemical compounds that react under the presence of light to cleave a specific covalent bond, effectively separating the compound into two moieties. They have been widely used both in organic synthesis as removable protection groups as well as in biochemistry as caged compounds.[104] In biology, caged compounds are biomolecules temporarily deactivated by photosensitive functional groups. Upon photoirradiation, the photosensitive groups (i.e., photolabile groups) are separated from the molecular structure, thus reactivating the biomolecule. This section illustrates the structural basis of photolabile molecules and strategies for incorporating these molecules into biological systems. Biological applications of representative cases are also discussed to demonstrate their important roles in dynamic biological studies.

4.1. o-Nitrobenzyl and Related Groups

Light-induced and electronically excited 2-nitrobenzol compounds have demonstrated fast reaction rates (<1 ns) as well as high reversibility in aqueous solutions.[105] In particular, tautomerization of 2-nitrotoluene into quinonoid aci-nitro tautomer aci-1 has served as a benchmark for widely used nitrobenzyl flash photolysis as shown in Figure 5.[106] The primary photochemical process involved is intramolecular H-abstraction by the excited nitro group, which is followed by the formation of the aci-nitro form and the rearrangement to the nitroso derivatives. The quantum yield for this simple hydrogen shift varied from less than 1% for 2-nitrotoluene, 0.6% for 1-(2-nitrophenyl)ethyl derivatives, and 0.3% for α,α,α-trideuterated 2-nitrotoluene. The benzylic position in 2-nitrotulene could be triggered by laser with $\lambda_{\max} \approx 400$ nm after functionalization with a leaving group. In particular, *o*-nitrobenzyloxycarbonyl caged compounds undergo photolysis and release −COOH, which will further decarboxylate to give −H as the final uncaged product. The reaction rates are dependent on the functional group, pH of aqueous solution, and the type of solvent used.

To expand the application to biological systems, structural modifications have been applied on the leaving groups of *o*-nitrobenzyl molecules such as adding substitution groups on the phenyl ring. For example, the two substitutions on the phenyl ring in 3,5-dimethoxy-*o*-nitrobenzyl reduced the triggering wavelength to 365 nm.[107] Substitution on the benzylic carbon of *o*-nitrobenzyl molecules is also common. For example, monosubstitution at the α-position increases the photorelease rates. Furthermore, the addition of a carboxylic group on the benzylic carbon has demonstrated even higher release rate for the glutamate-caged system.[108] Replacing the phenyl group with other aromatic groups, such as naphthalene or dibenzofuran, has also demonstrated a shift in triggering the wavelength to 350–400 nm. In particular, a nitrodibenzofuran caged calcium chelator demonstrated a large two-photon excitation and fast photorelease with high efficiency of photolysis.[109] More research efforts should be applied to develop nitrodibenzofuran-based photorelease systems for both one- and two-photon triggered release in situ.

4.2. Coumarin-4-yl Esters and Related Groups

Coumarin-4-yl methylate photolabile caging groups can typically cage carboxylic acids and phosphate groups by 7-methyoxycoumarin-4-ylmethyl (MCM) groups through an ester bond. The photolysis process of coumarin-4-ylmethyl groups is initiated by heterolysis of the C–O ester bond from photo-excitation to form coumarinylmethyl carbocation and anions.[110] The ion pair is then separated and isolated by a polar solvent to give 4-hydroxylmethyl coumarin and released payloads. The addition of a carbonyl group on MCM could expand the caging units to amino and hydroxyl groups by decarboxylation after the aforementioned photolysis step. One of the notable applications of MCM is the study of cyclic nucleotide-dependent cellular activity by caging secondary messengers adenosine 3′,5′-cyclic monophosphate (cAMP).[111]

4.3. p-Hydroxyphenacyl Groups

The *p*-hydroxyphenacyl (pHP) photolysis is a promising alternative to nitrobenzyl-based photolysis for biomedical applications. It is typically used in caging carboxylates and phosphate groups with remarkably fast release rates.[112] The mechanism often results in high quantum yields, fast reaction rates, good solubility, stability, and biocompatibility under physiological conditions although some of the detailed kinetics have yet to be elucidated. In aqueous solutions, the photorelease of pHP yields *p*-hydroxy-phenylacetic acid and then an uncaged molecule.

4.4. Other Photolabile Groups

There are some photoliable reactions that have just been recently discovered and yet to have been fully elucidated. Notably, 4-methoxyl-nitroindolinyl caged glutamate has been synthesized and demonstrated as an excellent potential neurotransmitter. The byproduct of photolysis was found to be 7-nitroxoindole instead of nitroindoline, thus the mechanism is different from common deprotonation processes and has yet to be determined.[113]

5. NATURAL BIOMATERIALS

5.1. Gelatin Methacrylate (GelMA)

Gelatin is a biodegradable polypeptide derived from the partial hydrolysis of collagen and has been widely investigated for cell-based studies in tissue engineering due to its excellent biocompatibility, tunability, as well as bioactive and cell adhesive properties (e.g., arginine–glycine–aspartic acid (RGD) motifs).[114] Moreover, the thermogelling properties of gelatin through its conversion from a liquid to gel state in response to a change in temperature permits its use for various applications such as a 2D coating or 3D hydrogel matrix.[114] In the case of nozzle-based 3D printing processes, little chemical modification of gelatin is needed as most strategies rely on thermogelation to increase viscosity to stabilize 3D patterns of gelatin-based matrices (Table 2).[114] However, for light-based 3D printing systems, gelatin must be made photo-cross-linkable to enable rapid and selective solidification to form a covalently cross-linked hydrogel. The most commonly used method of functionalizing gelatin with a photo-cross-linkable moiety is the synthesis of gelatin methacrylate (GelMA), which Van de Bulcke et al. first reported in 2000.[115] The general process involves reacting gelatin with methacrylic anhydride via one-pot synthesis to conjugate methacryloyl groups, commonly referred to as methacrylate groups in literature, to predominantly amine groups and less so to the hydroxyl groups present along the gelatin backbone.[116,117] Recently, a group of researchers have systematically optimized the reaction conditions of GelMA to achieve: (a) consistent batch-to-batch degree of substitution (DS), (b) a linear relationship of methacrylic anhydride concentration to DS to controllably tune the DS, and (c) an increased reaction efficiency of near-complete amine substitution.[118–120] Upon light exposure from the relevant wavelength in the presence of a photoinitiator, the GelMA prepolymer is permanently cross-linked into a hydrogel through free radical chain growth photopolymerization.

By employing a light-based approach to GelMA hydrogel fabrication, this enables high tunability of mechanical properties by varying factors such as light exposure time, irradiation, intensity, and concentration. This is critically important in the fabrication of biomimetic tissues because cell fate is influenced by biomechanical cues from the surrounding extracellular matrix, thus recapitulating the modulus of native tissues is necessary to ensure desired behavioral outcomes in vitro. GelMA hydrogel stiffness can be tuned by varying the DS, the GelMA concentration, and the exposure time and intensity to cover a wide-range of biomimetic stiffnesses ranging from brain tissue to cardiac tissue to cartilage.[121,122] For instance, Ma et al. demonstrated that DLP-based 3D printing can be used to modulate the stiffness of GelMA-based bioinks to mimic moduli corresponding to different stages of liver cirrhosis by simply changing the exposure time regionally.[123] Upon fabricating a tissue model to monitor the progression of hepatocellular carcinoma progression, it was found that embedded HepG2 matrices of liver cancer cells favored cirrhotic stiffness by exhibiting more migratory and invasive phenotype.[123] The main disadvantage of GelMA is its mechanical robustness; as a protein biopolymer, it is susceptible to hydrolytic and enzymatic degradation and it has a relatively narrow stiffness range. To overcome this, GelMA is commonly implemented in composite biomaterials (see section 7). Overall, since the introduction of GelMA, it has been demonstrated extensively to support a range of engineered 3D tissue constructs including liver, cardiac, and nerve tissues.[15,117,123–125]

5.2. Thiol–Ene Gelatin

Currently, the functionalization of gelatin with methacrylate groups remains the most widely adopted approach with reactions proceeding via free-radical chain growth photopolymerization. However, there are several critical drawbacks regarding classical free-radical photopolymerization mechanisms including the formation of heterogeneous polymer networks, oxygen inhibition, and complex polymerization kinetics.[64] An alternate strategy to overcome many of these challenges is by employing light-mediated radical thiol–ene click chemistry as the photopolymerization mechanism. Thiol–ene radical reactions combine the advantages of photoinitiated processes and the orthogonality of click-based reactions. Such reactions proceed under mild conditions via a highly efficient step-growth manner to form homogeneous polymer networks, produce high yields, rapid reaction rate, possess inherent regiospecificity and stereospecificity, and is insensitive to oxygen inhibition.[64] Together, these characteristics make thiol–ene radical photopolymerization ideal for the formation of hydrogels in tissue engineering applications and is suitable for some cell types that are sensitive to radical-mediated damage.[74]

While using thiol–ene photoclick chemistry has been investigated in functionalized synthetic biomaterials such as PEG-norbornene,[63,126] there are current efforts to translate these methods toward the functionalization of natural biomaterials. The general thiol–ene photopolymerization mechanism involves the reaction between thiols with an inactivated alkene group in the presence of a radical photoinitiator. Among the possible alkene groups available for thiol–ene click reactions, norbornene is a favored alkene moiety due to its exceptionally rapid reaction with thiols via free-radical addition compared to electron deficient alkenes due to a combination of significant ring strain relief and low homopolymerization.[64] As such, synthesis methods have been developed by Munoz et al. for the functionalization of gelatin with norbornene groups to form GelNB that can be stably cross-linked in the presence of thiol-containing linkers for 3D cell encapsulation.[74] Preparation of GelNB involves reacting gelatin with carbic anhydride at 50 °C in aqueous buffer solutions under basic conditions (pH 8) to yield moderate degrees of substitution (i.e., ~44%).[74] Munoz et al. demonstrated the formation of hydrogels by cross-linking GelNB with the bifunctional cross-linker dithiothreitol (DTT) at varied concentrations upon UV irradiation and demonstrated that higher cytocompatibility of encapsulated hMSCs than GelMA hydrogels.[74] In the same study, GelNB was cross-linked with the tetra-functional thiol cross-linker PEG4SH compared to DTT and determined that changes in cross-linker functionality directly affected the step-growth efficiency and thus the resulting physical properties of the hydrogel. For instance, by keeping the concentration of the GelNB component constant as well as stoichiometric ratio between the alkene and thiol groups, it was found that reacting with PEGSH yielded an increase in equilibrium shear modulus to 5 kPa compared to 0.4 kPa when reacted with DTT while inversely affecting swelling equilibrium.[74] Unlike conventional chain growth polymerization such as with GelMA where increasing stiffness is directly associated with increased bioink concentrations, thiol–ene step-growth systems enable changes in mechanical properties independently of the concentration by employing cross-linkers of different functionality and modulating the ratio between thiol and alkene groups.[127] Recently, thiol–ene photoclickable gelatin bioinks have been developed for both DLP-based and extrusion-based 3D printing modalities. Here, Bertlein et al. synthesized allylated gelatin (GelAGE) that was cross-linked with DTT in the presence of either Irgacure 2959 as the UV-photoinitiator or tris(2,2′-bipyridyl)dichloro-ruthenium(II) hexahydrate with sodium persulfate (Ru/SPS) as the visible light photoinitiator.[128] Similar to other work, mechanical properties of the printed hydrogels were tunable by varying the ratio of GelAGE to DTT composition. GelAGE as a bioink for DLP-based 3D printing was advantageous in that it lacked physical gelation and remained at low viscosities at high concentration solutions (i.e., 10–20% w/v) at room temperature, which enabled fabrication of porous lattice structures with 250 μm struts with high shape fidelity.[128] For extrusion-based printing applications, a less degraded GelAGE bioink formulation at high concentration (i.e., 30% w/v) retained its thermal gelation properties necessary for shear thinning behavior at low temperatures (i.e., 4–7 °C). Extrusion printing of GelAGE produced constructs with resolutions of 500 μm and supported high cytocompatibility of encapsulated porcine chondrocytes.[128]

5.3. Collagen

Collagen is the most abundant extracellular matrix protein found in tissues within the body and has been extensively studied as a bioscaffold material due to its innate biocompatibility, biodegradability, bioactive adhesion sites, and supportive properties for regulating various cellular behaviors such as proliferation and differentiation as well as its critical role in wound healing processes.[129] Altogether, a total of 29 distinct collagen types have been identified, and among them, collagen type I, classified as fibrillar collagen, is the most utilized for scaffold development in tissue engineering applications.[130,131] At the molecular level, collagen is arranged in a triple-helical structure consisting of the repeating amino acids glycine−X−Y, where X and Y are typically proline or hydroxyproline.[132] These helical strands join via lateral interactions to form fibrils with diameters ranging between 50 to 200 nm and are arranged in a periodic array to produce the characteristic straited morphology of collagen fibrils.[132] This arrangement of collagen fibrils thus provides the high tensile strength, and when packed in parallel bundles they form the collagen fibers present in dense connective tissues including tendons, bone, and muscle.[132] Furthermore, the inherent ability of collagen type I to self-assemble via fibrillogenesis at physiological pH and temperature has been exploited for the production of soft hydrogels. However, these hydrogels are mechanically weak, therefore various cross-linking methods have been developed to improve control over material properties, physical stability, and resistance to enzymatic degradation.

Common techniques to cross-link collagen involve chemical and enzymatic methods such as using glutaraldehyde, genipin, and transglutaminase, but these approaches come with several drawbacks concerning long cross-linking times, lack of localized control over mechanical properties, and cytotoxicity of the cross-linking agents.[133–135] In the context of 3D printing, pure collagen bioinks have been mostly used in nozzle-based systems by relying on fibrillogenesis to complete in a timely manner such that the structure will not collapse. For instance, using a method called free-form reversible embedding of suspended hydrogels (FRESH), Hinton et al. demonstrated the deposition of collagen type I into a HEPES and gelatin slurry bath to maintain structural suspension during the print and ensure proper pH and temperature control for collagen self-assembly to occur.[136] Moreover, Lee et al. further demonstrated the potential of the FRESH method to build porous collagen scaffolds resembling patient-specific anatomical structures of the human heart.[137] While this technique is capable of achieving 200 μm spatial resolution, inherent issues such as clogging in nozzle-based printing systems are especially challenging for higher concentration bioinks needed to match tissue-specific properties. As a result, several groups have developed strategies to modify collagen type I for light-based 3D printing modalities to take advantage of the rapid printing speeds, ability to produce complex geometrical designs, and improve control over material properties. In one example, Drzewiecki et al. produced collagen methacrylamide (CMA) bioinks by first reacting 1-ethyl-3-[3-(dimethylamino)propyl] carbodiimide (EDC) and *N*-hydroxysuccinimide (NHS) in MES buffer with methacrylic acid for 10 min, followed by the addition of collagen in 0.02 M acetic acid to react for total of 24 h.[138] This synthesis method preserves the spontaneous fibrillar self-assembly and thermoreversible properties of native collagen while also enabling photo-cross-linking capability upon UV irradiation at 365 nm.[139] Using a free-form fabrication approach, the CMA material is first self-assembled at 37 °C to create a hydrogel, followed by UV light exposure with a photomask to solidify the desired geometry. Next, the entire construct was cooled to 4 °C to cold-melt the nonphotopolymerized regions to yield a stable construct with a 5-fold increase in storage modulus compared to thermally gelled CMA controls with fabrication resolutions around 350 μm.[138,139] To achieve greater printing resolution, multiphoton 3D printing techniques were applied by Bell et al. on collagen bioinks to attain micrometer-scale resolutions with greater precision over producing complex microarchitectures.[140] The bioink consisted of unmodified collagen type I that has been acid solubilized and mixed with 5′-phosphorylated flavin mononucleotide (FMN), which is a biocompatible photosensitizer compatible in low pH solutions.[140] Using a titanium–sapphire femtosecond laser, complex geometric shapes were produced, including multilayered woodpile structures with struts measuring ~12.5 μm and pore sizes as small as 12 μm.[140] This work demonstrates the capability of printing unmodified collagen type I with micrometer scale resolution and extends the utility of collagen biomaterials for 3D free-form fabrication techniques.

5.4. Hyaluronic Acid (HA) and Derivatives

Hyaluronic acid (HA) is a nonsulfated glycosaminoglycan present in the extracellular matrix and can be found in many tissues within the body including epithelial, connective, and neural tissues.[141] In vivo, HA has several important functions such as tissue hydrodynamics, joint lubrication, providing a network onto which cells are able to migrate, involvement in regulating wound healing, and promoting endothelial cell growth and angiogenesis.[142,143] Like gelatin and collagen, HA can be cross-linked into a hydrogel without chemical modifications. For example, previous studies have shown that HA can been cross-linked under alkaline conditions such as using bisepoxide and under acidic conditions by chemicals like glutaraldehyde and multifunctional hydrazides.[144] Compared to the native HA, the cross-linked hydrogels demonstrated more robust mechanical properties and stability and can be utilized in various 3D printing processes like in extrusion-based 3D printing modalities.[144]

When applied to light-based 3D printing systems, HA can be chemically modified by the addition of (meth)acrylate groups to impart photo-cross-linkable properties. This can be achieved by reacting HA with chemicals such as glycidyl methacrylate to form glycidyl methacrylate-HA (GM-HA).[15,144] The resultant HA derivatives can be covalently cross-linked into permanent hydrogels via free radical polymerization using light in the presence of a photoinitiator. The cross-linking density and thus mechanical property of GM-HA hydrogel can then be further controlled using various factors like light exposure time and photoinitiator concentration.[144]

5.5. Decellularized Extracellular Matrix (dECM)

The extracellular matrix (ECM) present in tissues within the body serves as structural support containing fibrous proteins as well as glycosaminoglycans (GAGs) that help modulate various cellular behaviors including proliferation, differentiation, and migration.[145,146] More specifically, the constituents of the ECM are unique to each individual tissue or organ system to form "tissue-specific" microenvironments tailored to support distinct cell populations in vivo. Tissue specificity in the context of biomaterials development is critically important as well-designed biomaterials aimed to recapitulate the complex biochemical makeup specific to the native ECM microenvironment of the tissue of interest to improve cell functionality, phenotype, and maturation.[145] One top-down approach to biomaterials development is the production of naturally derived decellularized extracellular matrices (dECM), which involves processing native tissues to yield an ECM scaffold material. This can be accomplished by treating the native tissue using a combination of mechanical disruption, enzymatic digestion, and chemical washes to produce an ECM material void of cells while retaining the ECM constituents unique to the original tissue. For instance, physical methods include snap freezing to form ice crystals for cell disruption, washes in hypertonic and/or hypotonic solutions, and agitation can be employed to improve diffusion and wash efficiency in facilitating the removal of cell debris. Furthermore, chemical and enzymatic approaches include washing in acidic and/or alkaline solutions, ionic and/or nonionic detergent solutions, and treatment with trypsin or nucleases to remove residual DNA and RNA within the tissues. It is important that the protocols employed ensure that the ECM is completely free of cellular remnants to prevent immunogenicity. To date, many protocols have been established in literature for the processing of various dECM including heart, lung, liver, adipose, brain, muscle, and intestine.[145,147] These dECM scaffolding materials can be processed into a variety of forms including whole intact decellularized organs, porous dECM foam scaffolds, thermally gelled dECM hydrogels, or powdered dECM to meet the requirements of different tissue engineering applications.

A common approach to process dECM into suitable bioinks for 3D printing is by pepsin digesting the dECM to yield a solubilized form of the product. Because of the thermal gelling properties of dECM, it can be readily deposited using conventional extrusion-based 3D printers and solidified at 37 °C post printing.[148] However, dECM hydrogels are inherently weak and lack structural integrity with little control over modulation of the physical properties, which impedes its utility as a scaffolding material. As such, additional stiffer biomaterials such as polycaprolactone (PCL) supports are typically required during extrusion 3D printing of dECM bioinks to prevent collapse and maintain structural fidelity of the entire construct.[148] In a different approach, the viscosity of the dECM bioink can also be increased to improve extrudability and avoid the need for nondegradable support structures. For instance, Skardel et al. developed a multicomponent liver dECM bioink capable of two-stage polymerization that facilitates proper extrusion and enables control over the final mechanical properties of the printed construct.[149] Here, solubilized liver dECM was mixed with a combination of thiolated gelatin and hyaluronic acid as well as PEG acrylate and PEG alkyl components.[149] Primary spontaneous cross-linking between the thiol and PEG acrylate groups enabled the formation of an extrudable hydrogel, meanwhile secondary cross-linking between the remaining thiol and PEG alkyl groups via UV irradiation post printing stabilized the construct well as increase its stiffness.[149] In another example, Jang et al. incorporated vitamin B2 (i.e., riboflavin), which is a biocompatible photo-cross-linking agent, into heart dECM bioinks to improve extrusion and attain mechanical stiffnesses close to that of native cardiac tissue.[150] Heart dECM of appropriate viscosities for extrusion-based printing were first deposited, followed by photo-cross-linking via UVA irradiation after every successive printed layer and thermal gelation at 37 °C of the completed construct to ensure physical stability. As highlighted, the majority of dECM bioinks developed have been limited to extrusion-based 3D printing modalities with moderate feature resolutions of no less than 100 μm, simple lattice-like geometrical designs, and slow fabrication speeds which hinders their scalability.[151] To overcome these challenges, processing of dECM bioinks suitable for DLP-based 3D printing systems have recently been developed to enable rapid fabrication and the production of complex structures at high resolutions. Yu et al. established a multistep process to make dECM biomaterials readily miscible with GelMA to form a photo-cross-linkable bioink by using a combination of mild pepsin solubilization, lyophilization, and cryomilling.[152] By using this technique, the dECM materials are physically processed into powdered form as an off-the-shelf dry product that can be readily reconstituted into a homogeneous dECM-GelMA solution that remains liquid at room temperature ideal for DLP-based 3D printing setups. Here, tissue-scale biomimetic microgeometries of the heart and liver unit structures (i.e., striated and hexagonal lobular patterns, respectively) were printed with up to 30 μm resolution.[152] The mechanical properties could also be easily modulated to match that of the desired native tissue by simply varying exposure time during printing.[152] To illustrate, this approach was used to create a biomimetic model composed of liver dECM-GelMA to monitor hepatocellular carcinoma progression of HepG2 cells by locally tuning the modulus of the printed scaffold to recapitulate regions of healthy and cirrhotic liver tissue stiffnesses.[123]

5.6. Alginate

Alginate is derived from alginic acid and has been broadly used as a biomaterial in extrusion-based and inkjet-based bioprinting applications.[153] Alginate can be obtained from calcium, magnesium, and sodium alginate salts isolated from the cell walls and intracellular spaces of brown algae.[153] Little chemical modification is needed when used in most 3D bioprinting applications due to its ability to ionically cross-link. Specifically, multivalent cations such as calcium ions can induce fast gelation of alginate through ionic interchain bridge formation.[153] By modulating the alginate solution concentration, molecular weight, and cross-linker ratio, alginate hydrogel stiffness can be controlled through changes in cross-linking density.[154] In the context of light-based 3D printing, alginate macromers have also been methacrylated by reacting sodium alginate and 2-aminoethyl methacrylate via EDC/NHS chemistry.[155] Upon photopolymerization of the methacrylated alginate hydrogels, greater stability and mechanical strength can be achieved when compared to ionically cross-linked alginate hydrogels that lose structural integrity over time.[156] To date, several studies have demonstrated the cytocompatibility of photo-cross-linked alginate hydrogels to serve as biodegradable scaffolds to support encapsulated chondrocytes for cartilage repair as well as maintaining viability of nucleus pulposus cells to treat intervertebral disc degeneration.[155–157]

5.7. Physical Characterization

5.7.1. Mechanical Properties.—Mechanical properties play a critical role in affecting cellular behavior. Characterization of mechanical properties largely focuses on stiffness which is quantified by elastic modulus, in the form of tensile and compressive moduli depending on the application of the material. The bulk elastic modulus is prevalently used, while point stiffness is typically measured in cases where the local mechanical properties is of interest or the bulk modulus is too difficult to effectively measure, such as with some hydrogels or thin films. The measurement tools used in the field vary from commercially available instruments to custom designed setups. Naturally derived materials with or without chemical modification are generally softer than synthetic materials. The typical stiffness of collagen and gelatin-based hydrogel materials that have been applied in biological applications is in the range of 0.01 kPa for thermally gelled collagen hydrogels to 10 kPa for covalently cross-linked GelMA hydrogels.[15,117,123,137,158] The mechanical properties of collagen and gelatin-based hydrogel highly depends on material concentration as well as cross-linking mechanism and conditions.[15,117,123,137,158] Similarly, HA-based hydrogels demonstrate a stiffness value ranging from 0.01 kPa to a few kPa,[159] depending on the HA concentration and cross-linking conditions. Alginate-based hydrogels have a stiffness range of 0.5–30 kPa and their mechanical properties can be effectively tuned with multivalent cross-linker concentration in addition to alginate concentration and percent modification with methacrylate groups.[154,156,160,161] In addition to factors like material concentration and cross-linking condition, combining multiple types of natural materials to form a composite can be used to further enhance mechanical properties. For example, 3D printed dECM/GelMA hydrogels demonstrated a stiffness range of 1–15 kPa.[123] Similarly, composite materials formed by combining natural and synthetic biomaterials, such as PEGDA, have also been used to enhance the mechanical properties to make suitable for surgical handling and implantation.[16,162]

5.7.2. Ultrastructure and Porosity.—The ultrastructure of hydrogels is another important factor affecting cell behavior by mediating physical interactions between cells and materials as well as the transport of signaling molecules. Studies have demonstrated that the ultrastructure of the material has been demonstrated to affect cellular migration,[163,164] thus mimicking native ultrastructure during fabrication can be used to improve recapitulating in vivo behavior in vitro. For instance, light-based 3D printing was employed to create tissue-scale striated patterns that promoted the alignment of encapsulated human cardiac cells and resulted in more uniform beating as well as maturation.[152] Material porosity is also important in affecting cell function and can be measured using several techniques including scanning electron microscopy (SEM) imaging, quantifying the efficiency of molecular transport, and monitoring cellular movement within the bulk hydrogel. In general, lower material concentrations and cross-linking density results in decreased material stiffness and larger pore size.[123]

5.7.3. Swelling Properties.—The evaluation of swelling properties is often conducted to determine the structural stability as well as maintenance of shape and pattern fidelity of hydrogels over time at physiological conditions.[152] In general, natural materials exhibit increased swelling at lower concentrations and cross-linking densities.[165] Swelling properties are also dependent on the nature of the material itself. For example, HA is a polysaccharide with a high density of negative charges which have an affinity to trap water molecules and thus swell to a greater extent.[166] Taking into account the swelling property of the hydrogel provides better prediction of the structural integrity and performance of biomaterials within in vitro or in vivo microenvironments.

5.8. Soft Tissue Applications

Natural materials have been extensively applied to the 3D printing of soft tissues. In particular, collagen and gelatin-based materials have been used for the production of cardiac, liver, and various cancer models due to their abundance within these tissues (Figure 6).[15,117,124,152] For instance, Liu et al. demonstrated the use of GelMA in the 3D printing of cantilever cardiac tissue models comprised of human embryonic stem cell derived cardiomyocytes to measure force generation.[117] Ma et al. also showed the successful application of GelMA and GM-HA in a 3D printed biomimetic multicellular liver tissue model possessing endothelial networks applicable for drug testing applications.[15] 3D printed GelMA hydrogels have also been used to build various cancer models include hepatocellular carcinoma progression and HeLa cell migration behavior.[123,124] Furthermore, dECM materials have also been widely adopted for 3D printed tissues in vitro to provide a more physiologically relevant and complex microenvironment. Recently, Yu et al. demonstrated that 3D-printed dECM bioinks derived from heart and liver tissues were able to promote the phenotype and maturation of induced pluripotent stem cell (iPSC)-derived cardiomyocytes and hepatocytes, respectively, in a tissue-specific manner.[152] Similarly, Ma et al. utilized liver dECM bioinks to 3D print a hepatic cancer model with tissue-matched pattern and mechanical properties to recapitulate various stages of fibrotic liver disease.[123] In other examples, HA-based materials have also been employed to fabricate highly vascularized organs and brain tissue due to its important role in promoting endothelial cell growth and rich presence in the ECM of the central nervous system.[15,167]

6. SYNTHETIC BIOMATERIALS

6.1. Polyethylene Glycol

Compared to naturally derived biomaterials, synthetic polymers allow for more precise and consistent control over their physical and chemical properties (e.g., molecular weight, functional groups) at both the monomer and polymer level. One class of the most commonly used synthetic polymers for biomedical applications are polyethylene glycol (PEG) and its derivatives such as PEG diacrylate (PEGDA), PEG dimethacrylate (PEGDMA), and multiarmed PEGs.[19] PEG-based hydrogels are versatile in tissue engineering and bioprinting applications. PEG-based hydrogels exhibit high biocompatibility with minimal to no immunogenicity and have been approved by the Food and Drug Administration (FDA) for use within various biomedical applications.[168,169] In addition, the chain length and concentration of the PEG monomer can be readily modified to tune the material and physical properties of the corresponding hydrogels such as stiffness and porosity.[170] Furthermore, PEG-based hydrogels are inherently nonadhesive to cells or proteins, providing a blank building block for adding desired biologically or chemically functional moieties.[171] For instance, cell adhesive peptides (e.g., Arg-Gly-Asp-Ser (RGDS)) can be patterned to specific areas of a PEG hydrogel for studying localized cell–material interactions with defined cellular distributions.[172] Additionally, PEG modified with acrylate groups can be readily photopolymerized into hydrogels under mild conditions (i.e., room temperature and low near UV exposure), which makes it a popular bioink choice for light-based bioprinting of scaffolds or tissues with high fidelity and cell viability.[173] Lastly, PEG can also be mixed or conjugated with other types of monomers to form copolymers with unique material properties that cannot be achieved by the individual components.[174,175] With these advantageous material properties, PEG-based hydrogels have found numerous applications in the research of basic cell biology, biomedical devices, tissue engineering, and regenerative medicine. This section will cover these applications while highlighting the various 3D printed PEG hydrogel constructs fabricated by light-based bioprinting platforms.

6.1.1. PEG-Based Hydrogels for Cell Biology.—In the field of stem cell biology, there has been increasing interest in studying the impacts of geometric cues on the cell behaviors including proliferation and differentiation. The underlying hypothesis of such studies is that physical cues from the surrounding matrix can guide cellular alignment and thus introduce patterned stresses to the cells which in turn modulates the cell fate.[172] Because of its nonadhesive blank slate property, PEG-based hydrogels serve as an ideal candidate for providing such geometric cues without introducing other chemical or physical influences. Qu et al. designed a facile approach to incorporate geometric guidance via digital light processing (DLP) based bioprinting of PEGDA.[172] Briefly, three PEGDA patterns (i.e., stripes, symmetric forks, and asymmetric forks) were 3D printed on a glass substrate for the seeding of adipose derived stem cells (ADSCs) (Figure 7A,B). The nonadhesive PEGDA walls confined the cells into different multicellular forms, resulting in different levels of cellular alignment and stress which directed the ADSCs into different lineages without the need for differentiation media or growth factors.[172] Other examples of PEG-based 3D structures being used to guide cell growth also include 3D printed microwell arrays for multicellular spheroid and embryoid body culture (Figure 7C),[14,176] as well as nature-inspired fractal patterns for investigating cell organization behaviors (Figure 7D).[177] In addition to these static 3D geometrical designs, the versatility of PEG also enables the 3D printing of flexible structures with high resolution and fidelity for dynamic cell studies at the micrometer scale. For instance, Zhang et al. utilized PEGDA and a two-photon laser direct writing system to fabricate suspended web structures with microscale units featuring positive and negative Poisson’s ratios to study the dynamic cell response to Poisson’s ratio (Figure 7E).[178] Unusual cell division on the negative Poisson’s ratio structures were observed, which could potentially indicate Poisson’s ratio as another material parameter with direct influence on cell fate in addition to elastic modulus.[179]

6.1.2. PEG-Based Hydrogels for Tissue Engineering and Regenerative Medicine.—Because PEG-based hydrogels are highly biocompatible and elicit minimal to no immunogenicity in vivo, they have been used in numerous tissue engineering and regenerative medicine applications including injury repair, wound healing, and tissue modeling. For instance, biomimetic spinal cord scaffolds have been recently 3D printed with a mixture of PEGDA and GelMA to treat severe spinal cord injuries (Figure 8A,B).[16] Here, linear microchannel arrays with high fidelity were fabricated to guide the regeneration and directional growth of the axons in the lesion site. PEGDA imparted the tunable mechanical properties of the 3D printed scaffolds to match the elastic modulus of the native spinal cord, while GelMA faciliated the attachment of cells. This material combination was proven to significantly reduce foreign body reactions as compared to other scaffolding materials (e.g., agarose), which contributed to the significantly improved functional recovery of the injured animals.[16] Similarly, PEG-based hydrogels were also used to 3D print nerve guidance conduits for peripheral nerve regeneration (Figure 8C,D).[162] The excellent 3D printability of PEG-based hydrogels enabled the scalable fabrication of patient specific scaffolds based on magnetic resonance imaging (MRI), computed tomography (CT) scan, or computer-aided design (CAD).

6.2. Poly(glycerol-*co*-sebacate)

Poly(glycerol-*co*-sebacate) (PGS) was first developed by Robert Langer's group in 2002 to address the need for a strong, biodegradable, and biocompatible elastomer that can withstand dynamic tissue environments.[180] PGS is the copolymer of glycerol and sebacic acid, which are both naturally occurring substances and commonly in used in FDA-approved medical devices.[181,182] Upon the introduction of PGS, many studies have demonstrated its broad versatility in biomedical engineering.[183,184] To illustrate, PGS has been utilized in cardiac tissue engineering,[185–195] vascular conduits,[196,197] retinal transplantation,[198] skin regeneration,[199] neural repair,[200–203] vocal fold repair,[204] cartilage applications,[205–207] as well as bone and dental engineering.[208–213]

PGS is synthesized through a polycondensation reaction followed by thermal cross-linking. However, the reaction and curing conditions of PGS are difficult to repeat with consistency and often require long reaction times under harsh conditions (e.g., 8–48 h reaction durations under vacuum and high temperatures to enable the secondary thermal curing process).[180,214,215] As such, this can severely limit the production and processability of PGS and hinder its applications. To simplify the synthesis of the PGS, photocurable PGS was later successfully synthesized by Langer's group in 2007 through the functionalization of PGS with acrylate groups to produce poly(glycerol-*co*-sebacate) acrylate (PGSA).[181] Photo-cross-linking of PGSA is much more convenient than the thermal curing of PGS. Under UV or visible light, PGSA can be easily cross-linked within 10 min at room temperature in the presence of a photoinitiator.[181,216] Because of its intrinsic biomimetic properties and ease of processing, PGSA has been widely employed in biomedical applications such as cell encapsulation,[217] surgical adhesives,[218,219] and 3D printing.[216,220] Additionally, PGS has been also modified with other functional groups, such as methacrylate,[221,222] norbornene,[223] 2-isocyanatoethy methacrylate,[224] cinnamates,[225] and fumarate[226] by different chemical reactions to explore wider manufacturing methods and further their applicability.

The mechanical properties of cross-linked PGS polymers can be tuned by changing the molecular weight of the polymer or cross-linking density by varying the conditions of the polycondensation reaction or curing process.[193,205,227,228] For example, Chen et al. synthesized PGS prepolymers at 110, 120, and 130 °C to obtain Young's moduli of 0.056, 0.22, and 1.2 MPa, respectively.[193] Besides varying the curing time of the PGS, Hollister et al. were also able to adjust the elastic modulus of PGS by varying the molar ratios between glycerol and sebacic acid (3:4, 1:1, and 4:3) when synthesizing the PGS prepolymers.[205] Meanwhile, the mechanical properties of PGSA can be tailored by changing the molecular weight of its precursor, degree of acrylation, and photocuring conditions such as light exposure time and intensity.[181] Typically, the ultimate tensile strength and Young's modulus of the photo-cross-linked PGSA increases with higher degree of acrylation at the same molecular weight. Langer's group tested PGSA polymers with 17–54% degree of acrylation and found that ultimate tensile strength ranged from 0.05 to 0.50 MPa, Young's modulus ranged from 0.05 to 1.38 MPa, and elongation at break ranged from 170% to 47.4%, respectively.[181] Because of the tunable mechanical properties of PGS and PGSA, these biomaterials have become prime candidates in tissue engineering to accommodate various cases including the fabrication of hard tissues by using stiff and less elastic PGS/PGSA, while soft and stretchable properties would be ideal for soft tissue applications.

The biodegradability of PGS and PGSA has been studied through both in vitro and in vivo experiments.[180,194,214,219,229–231] On the basis of these studies, PGS is known to degrade primarily by surface erosion via the cleavage of ester bonds.[232,233] Surface erosion is more favorable than bulk erosion in tissue engineering and drug delivery applications because it does not change the mechanical strength of the polymer during degradation and allows for controlled, tuned degradation.[180] However, PGS typically had slower degradation rates under in vitro conditions than in vivo environments.[180] For example, Wang et al. found that PGS only degraded about 17% of its dry weight under in vitro incubation in PBS at 37 °C for 60 days, while PGS implants in seven-week-old female Sprague–Dawley rats completely degraded after the same time frame.[180] It was proposed that the enzymes and macrophages present within the implant site might have contributed to accelerated degradation in vivo. This was confirmed by in vitro enzymatic and hydrolytic degradation studies wherein mass lost in PGS was reported to be 60% degraded in 48 h and 100% degraded in 6 h after incubation in enzymatic and hydrolytic conditions, respectively.[180] In other works, Chen et al. also reported that the degradation behavior of PGS was tunable by changing the synthesis conditions.[193] For instance, under in vitro conditions in PBS or cell culture media, PGS synthesized at 130 °C barely degraded while PGS synthesized at 120 °C showed a much slower degradation rate than PGS synthesized at 110 °C.[193] With regards to PGSA, it also exhibits similar degradation behavior to PGS. The degradation rate of PGSA can also be easily tuned by varying the degree of acrylation such that a high degree of acrylation resulted in slower degradation rates.[181]

The biocompatibility of PGS and PGSA have been well studied both in vitro and in vivo due to the wide biomedical applications of these materials.[184,220] Wang et al. cultured NIH/3T3 fibroblast cells onto PGS coated Petri dishes with a PLGA-coated Petri dish as the control due to the popularity of PLGA in biomedical applications.[180] It was found that PGS supported more adherent cells possessing better morphology than the PLGA after 6 days in culture. Furthermore, in vivo studies comparing PGS with PLGA scaffolds through subcutaneous implantations in Sprague–Dawley rats concluded that PGS introduced similar levels of inflammatory response as PLGA but caused much less formation of fibrous capsules over a 35 day period.[180] In similar work, Yeh et al. assessed the cytocompatibility of PGSA by culturing NIH/3T3 fibroblast cells onto 3D printed PGSA scaffolds for up to 4 days and found that these scaffolds were able to support the cell growth and proliferation comparable to that of bulk PGSA.[220]

6.2.1. PGS and PGSA for Tissue Engineering Applications.

—3D printing is an effective fabrication technique to form complex geometries that would expand the biomedical applications of PGS and PGSA. For extrusion-based 3D printing, the viscosity of the bioink plays a key role in determining the stability of the printed structure and whether it can be extruded continuously. As such, Yeh et al. developed printable PGSA bioinks with viscosities ranging from 3.18 to 8.78 Pa·s by altering the molecular weights of PGSA through changing the polycondensation time of the PGS prepolymer prior to acrylation.[220] In particular, optimal viscosity was achieved by mixing 10% of low molecular weight (M_n = 5.78 kDa) PGSA with 90% of high molecular weight (M_n = 6.32 kDa) PGSA along with the addition of 0.5 wt % 2,2-dimethoxy-2-phenylacetophenone (DMPA) as the photoinitiator. This mixture can be rapidly photopolymerized within 1 min upon UV light exposure after being extruded from the 3D printer. Examples of 3D printed structures include the lateral meniscus of a knee and the cartilaginous structure of an ear.[220] Considering the excellent printability of PGSA, including high resolution, ability to form macroscale complexity within printed structures, and superior mechanical performance, this material shows great potential in tissue regeneration and in vivo applications. In similar studies, Yeh et al. also developed another type of photocurable PGS derivative known as norbornene-functionalized PGS (Nor-PGS).[223] In this case, Nor-PGS macromers can be cross-linked by four-arm thiolated cross-linker based on thiol–ene click chemistry in the presence of a photoinitiator and UV light. Herein, an extrusion-based 3D printer was used to fabricate Nor-PGS scaffolds, including porous open-lattice cube, nose, and ear shaped structures (Figure 9). The mechanical properties and degradation rates of the photocured Nor-PGS can be adjusted by varying concentrations of the cross-linker. Similar to PGSA, Nor-PGS had higher modulus and ultimate strength along with less stretchability and slower degradation rates at higher cross-linking densities. Subsequent cell studies confirmed that 3D printed Nor-PGS scaffolds supported the viability and proliferation of NIH/3T3 fibroblasts cells, which demonstrate Nor-PGS as a biocompatible material for tissue engineering applications.

6.2.2. Poly(glycerol-*co*-sebacate methacrylate) as Nerve Guidance Conduits.

—Toward the development of implantable nerve guidance conduits, Singh et al. developed a novel type of PGS derivative known as poly(glycerol-*co*-sebacate methacrylate) (PGSM), which can also be rapidly photo-cross-linked by light in the presence of photoinitiator.[221] Here, they 3D printed the PGSM into hollow cylindrical conduits by using a DLP-based 3D printer integrated with a 405 nm wavelength light source. It was found that the modulus of the photo-cross-linked PGSM conduits measured an average of 3.2 MPa,[221] which is close to the upper stiffness range of native nerve tissue (i.e., 0.45–3.0 MPa).[234] In comparison, the modulus of the commonly reported materials for peripheral nerve repair, including polycaprolactone, poly(3-hydroxybutyrate), and poly-L-lactide, are normally over 100 times stiffer.[235–237] In vivo studies demonstrated that the PGSM nerve guidance conduits informed the regeneration of axons grown throughout the scaffold and into the distal stump after 21 days.[221]

6.3. Polyurethanes

Polyurethanes (PUs) are a diverse family of polymers that all have a urethane (−NHCOO−) group in the polymer backbone. They are commonly derived from condensation reactions between nucleophilic diisocyanate and electrophilic agents such as alcohols and amines in the presence of a chain extender, catalyst, and/or other additives.[238] The reaction mechanisms vary and could be classified by one-stage polymerization, where diisocyanates, oligodiols, and chain extenders are reacted simultaneously, or via two-stage reactions, where the remaining two components are reacted and chain extenders are added in a separate reaction as shown in Figure 10.[239]

Both aromatic and aliphatic isocyanates can be used in PU synthesis. Compared to aliphatic isocyanates, aromatic isocyanates, such as diphenylmethane diisocyanates (MDI) or toluene diisocyanates (TDI), shown in Figure 11, are more widely used in industry owing to their high reactivity and better mechanical properties of the PUs produced. The oligodiols can be categorized as polyether, polyester, and other special polyols such as polycarbonate, polycaprolactone, and polybutadienes, as shown in Figure 12. Polyether-based PUs are linear polymers commonly made from polyether such as polyethylene glycol (PEG) and poly(tetramethylene-ether) glycol. They have demonstrated high flexibility and hydrolytic resistance. However, researchers have found that they were susceptible to oxidative and thermal stress, excluding them from standard decontamination process such as autoclave. To improve PUs performance at elevated temperatures, polyester-based PUs were developed.[240]

In particular, polyester-based PUs were commonly synthesized from diols such as poly(ethylene adipate)diol and poly(butylene adipate)diol. The ester bonds are more stable than ethers at elevated temperatures, thus resulting in higher heat resistance. However, these ester bonds are more prone to hydrolytic degradation, which limit their applications in aqueous environments as biomaterials. To improve PU stability in heat and aqueous conditions, specially derived polycarbonate-based PUs were developed.[240] They have demonstrated superior mechanical properties and thermal stabilities in addition to improved biodurability and hydrolytic resistance.[241] The chain extenders and cross-linkers used in synthesizing PUs are generally diols and diamines of lower molecular weight such as ethylene glycol, 1,4-butanediol, and cyclohexane dimethanol. These are incorporated into the polymer chains to introduce more cross-links and hydrogen bonding to enhance the mechanical properties of PUs.

On the basis of the reaction mechanism and polymer backbone structures, PUs can be categorized as thermoplastic or thermosetting, as shown in Figure 13.[242] The main difference is the presence of covalent cross-linking sites on the polymer backbones. Thermoplastic PUs (TpPUs) are linear block polymers synthesized from reagents with difunctional groups such as diols and diamines without cross-linkers. They typically have a low melting point and exhibit poor mechanical performance at elevated temperatures. Furthermore, they can be readily dissolved into polar solvent, which makes them easily adapted by traditional processing techniques such as solvent casting and fiber spinning. Owing to their mechanical properties, lower glass transition temperature, and solubility in polar solvents, TpPUs have also been widely investigated in additive manufacturing such as 3D printing. Thermoset PUs (TsPUs) are synthesized from reagents with multiple functional groups such as trimethylolpropane and glycerol and/or in the presence of cross-linkers such as excess isocyanates. Because of the covalent network structures of TsPUs, they do not have a melting point and do not experience strength reduction at elevated temperatures. PUs can also form interpenetrating polymer networks (IPN) with other polymers such as epoxy and acrylates without bulk phase separation. These IPNs have enhanced mechanical performance by combining the advantageous properties of the components. For example, PU/epoxy IPNs have both the flexibility of PU and toughness of epoxy.[243] One of the most important contributors to PUs mechanical properties is microphase separation within the chemical structures as shown in Figure 14.[245] This is due to the complex backbone structures of PUs with hard segments such as benzenes and soft segments such as esters. The hard segments can act as physical cross-linking points, whereas the soft segments can rotate freely. In the presence of external forces, the hard segments can retain the integrity of the overall structure and the soft segments can absorb the energy and dissipate it as heat. Current developments have been focusing on improving their biostability and flexibility such as enhancing the hydrogen bonding of hard segments and adjusting microphase separation. Recent discoveries in PUs have also demonstrated their tunable physical, chemical, and biological properties. Coupled with the advancements in 3D printing technologies, it is both possible and desirable to expand the utilization of PU. In this section, we report some recent examples illustrating the usage of PUs in 3D printing for various biomedical applications.

6.3.1. Soft Robotics Applications.—Soft robotics are automated machines made using intrinsically soft materials such as fluids, gels, and elastomers.[246] Conventionally, they are fabricated by casting soft materials, such as PUs, followed by the assembly of different parts. Direct fabrication of soft robotics by 3D printing could reduce the overall processing time and hence reduce cost of fabrication. In one example, Patel et al. developed a family of highly stretchable with aliphatic urethane diacrylate as cross-linkers to print robotic hands.[247] In this work, some of the printed structures have achieved failure strain as high as 1100%.[247] With these PUs, they have demonstrated direct 3D printing of a set of pneumatically actuated grippers that could pick up an object. In other works, Gul et al. utilized a multiheaded extrusion 3D printer with light-assisted curing to build a three-legged soft robot from epoxy and polyurethane as structural components. Furthermore, they embedded shape memory alloy wires as actuators and demonstrated locomotion similar to a spider’s gait.[248] Similarly, Yang et al. used a fused deposition modeling (FDM) 3D printer to fabricate a polyurethane-based shape memory polymer (SMP) and conductive thermoplastic polyurethane (TPU) to make a pneumatically driven gripper with variable stiffness and active position feedback.[249] When current is applied to the TPU component, the resultant heating will soften the SMP, which induces shape change to work as a gripper. By controlling the piezo-resistance behavior of the TPU parts, they could monitor and control the grippers to grasp objects. Components like these could be readily transferred to biomedical applications such as surgical catheters.

6.3.2. Tissue Engineering Applications.—The excellent biocompatibility, adjustable biodegradation, and versatile mechanical properties of PUs have made them good candidates for tissue engineering and regenerative medicine applications.[250] For example, Whatley et al. utilized biodegradable and elastic PU to fabricate intervertebral disk scaffolds via FDM

3D printing. The printed structures demonstrated high fidelity and accuracy in replicating the lamellae structures of injury sites at both micro- and macroscales.[251] Neural cells seeded on the scaffolds aligned along the concentric lamellae following the topographical cues provided by the printed structures indicating potential neural repair. Xu et al. used biodegradable PUs to make vascular stents via liquid-frozen deposition manufacturing (LFDM) 3D printing.[252] Their results from in vivo studies showed early vascularization along the stent. In follow-up work, they also added heparin into the resin to enhance angiogenesis. This work has demonstrated the suitable elasticity, anticoagulation, and biodegradation of PUs for vascularization work. Furthermore, the inclusion of proteins also shows the potential of PUs in applications such as drug delivery and functional scaffolds for tissue repair.

Water-based PUs have also been used in various cell encapsulation works. Hung et al. developed water-based composites with PU nanoparticles and printed them by LFDM to make scaffolds for cartilage repair.[253] Compared to the PLGA scaffold which was fabricated in the same fashion, the PU nanoparticles improved the elasticity and proliferation of chondrocytes. Another water-based PU material for 3D printing developed by Hsieh et al. was printed into conduits by LFDM while encapsulating neural stems cells (NSCs). These conduits were implanted into adult zebra fish with traumatic brain injury. After 4 weeks of observation, these conduits showed significant improvements in recovery of locomotion and survival rates compared to the untreated group.[254] Following this study, Lin et al. incorporated soy protein isolate into the polymer matrix to further improve the survival and proliferation of NSCs.[255] Similarly, Huang et al. introduced water-dispersible graphene and graphene oxides into the polymer matrix to enhance the conductivity of the scaffolds.[255] The printed scaffolds demonstrated significant improvement in oxygen metabolism as well as differentiation of the encapsulated NSCs. In a recent work by Sanlin et al. using a DLP-based 3D printer, they printed a patient-specific left atrial appendage occluder implant based on a CT scan image using a PU-acrylate resin.[256] The structures were printed with microscale resolutions and smooth surfaces to meet the requirements of a functional occluder. Moreover, the mechanical properties of the scaffold successfully maintained the stress response of the actual part and showed promise as a strategy to functionally repair damaged tissues.[256]

6.3.3. Surgical Guides and Dental Applications.—The rapid prototyping of structures based on 3D designs also enabled construction of customized surgical guides for medical operations. Current surgical guides were manufactured in a mass-production fashion, which follows the same design with marginal fitting to the patients. This process becomes challenging if it cannot perfectly fit into the patient’s body during surgery, especially in operations on internal organs such as coronary heart diseases. The surgical guide also needs to possess adequate mechanical properties to be able to withstand damages incurred during surgery while also not eliciting adverse short-term immune response. The excellent precision and strength offered by 3D printing PUs have been employed for constructing customized surgical guides with high precision and durability. For example, Holzapfel et al. printed a pelvis based on a reconstructed model from CT scans of a patient with periacetabular tumor.[257] The printed structure closely imitated the modified scanning model. During the operation, the guides were capable of withstanding the operation with no adverse effects on the patient.[257] Apart from surgical guides, 3D printing of PUs has also been used in dental applications such as aligners to correct malocclusion. One of the commercially available products, Invisalign, consist of a series of computer-generated custom aligner molds to mobilize teeth into proper alignment. It has generated commercial success since its introduction in 1999 and further demonstrates the potential of PUs and 3D printing to bring similar products in other biomedical fields in the future.

6.4. Physical Characterization

6.4.1. Mechanical Properties.—An advantage of synthetic biomaterials is the ability to tailor properties for specialized applications by changing the molecular weight, functional groups, or polymerization chemistry to tune the final mechanical properties. This flexibility allows for a much greater range of material properties in synthetic biomaterials compared to naturally derived biomaterials that are often mechanically weak coupled with fast degradation which limits their usage. A key property is stiffness or elastic modulus, which can be readily controlled by the molecular weight of the polymer and degree of polymerization.[258] Like natural biomaterials discussed earlier, tuning the modulus to match that of the native tissue is critical to create an optimal environment to support cells and/or host tissues. In the context of implantable synthetic biomaterials, a combination of sufficient compressive, tensile, and shear strength is also important in order to be able to withstand forces exerted and prevent fractures while improving functional stability.[259] Appropriate yield and fatigue strength are also vital factors to consider to ensure the materials can tolerate cyclic loading and minimize internal stresses within the implant.[259]

6.4.2. Biodegradation Properties.—With the growing application of synthetic polymers in biomedical science, it is critical to evaluate the biodegradative properties in aqueous environments to determine their suitability in various tissue engineering related applications. For many years, synthetic polymers have been widely used as scaffolding materials, drug release systems, and implantable medical devices, thus a thorough understanding of their degradation rate and mechanism in vivo is important in the design of novel therapeutic approaches. Degradable polymer matrices can undergo two types of erosion via hydrolysis: surface erosion or bulk erosion. For surface erosion, degradation proceeds at a constant velocity throughout the erosion period and typically occurs in materials possessing functional groups that have short hydrolysis half-lives.[260] Meanwhile, bulk erosion does not progress under constant erosion velocity and the erosion mechanisms are often more complex in nature such that erosion occurs suddenly after a long period of no mass loss.[261] Another important mechanism to consider is oxidative degradation that occurs in vivo when peroxides produced by the body in response to an inflammatory reaction can create oxidative agents that cause polymers to degrade. Specifically, the main players being foreign body giant cells as well as macrophages produce peroxides produced near the polymer to initiate degradation. Synthetic polymers more susceptible to oxidative degradation include polyether polyurethanes and polyethylene, which have chemical groups that more readily form free radicals to facilitate the conversion of long polymer chains into shorter ones in the presence of oxidative products.[262] Other degradative mechanisms that occur also include enzymatic degradation due to biological enzymes present in vivo and physical degradation as a result of mechanical loading, swelling of the polymers, and friction forces.[262] The highly dynamic expression of enzymes is currently too complex to adequately model in vitro, making an in vivo assessment of the biodegradation rate of a biomaterial still necessary.

6.4.3. Biocompatibility.—Given the versatility of synthetic polymers in health care, it is critical to evaluate the biocompatibility of these materials both in vitro and in vivo to provide an overview of host interactions. Namely, biocompatibility is defined as a biomaterial that is able to perform its intended function without eliciting undesirable effects.[263] Several factors taken into consideration include a combination of chemical, physical, and mechanical properties. Furthermore, unlike naturally derived polymers that more closely mimic the native ECM both in terms of physical and chemical composition, it is important to also consider the cytotoxicity of degradation products from synthetic materials. Methods of biocompatibility testing involve several levels in which cytotoxicity as well as systemic toxicity in animal studies are evaluated. For instance, preliminary tests can be performed in vitro by testing the viability, growth, and metabolism of cultured cells (e.g., macrophages, fibroblasts, lymphocytes) on the selected synthetic biomaterial.[264] This can be coupled with in vivo tests where the material is often implanted into the subcutaneous or intramuscular regions of rodent animal models and observed for a period of time to assess the extent of any potential foreign body response, mutagenicity, toxicity, and carcinogenic effects.[264]

7. COMPOSITE BIOMATERIALS

7.1. Nanoparticle-Enabled Hydrogels

To improve the functionality of hydrogels, researchers have begun to explore the application of nanocomposite hydrogels to provide additional properties (Figure 15). For instance, common nanomaterials can be classified as organic, inorganic, metallic, or polymeric.[265,266] Thus, the incorporation of different nanomaterials into a 3D printed hydrogel can be used to improve the mechanical properties of the hydrogel (organic and inorganic materials), electrical properties (metallic nanomaterials), and drug delivery capabilities (polymeric nanomaterials). Given the wide applicability of nanocomposite materials, there are currently few studies examining the direct incorporation of nanoparticles into hydrogels or their interaction with cells. To translate the usage of nanocomposites in the field of tissue engineering to serve as feasible biomaterials, further research on the how nanomaterials impact cell growth, proliferation, and functionality are necessary. In this section, we will highlight commonly used nanocomposite biomaterials used in 3D printing to achieve different physical properties and functionalities within the printed hydrogel constructs.

7.1.1. Organic Nanomaterials.—Organic nanomaterials have been shown to increase both the electrical and mechanical properties of hydrogels.[266–268] Common examples of nanomaterials include carbon nanotubes (CNTs) and graphene oxide (GO). CNTs in particular are attractive due to their high mechanical strength and conductivity.[269] In one example, Shin et al. successfully incorporated CNTs into GelMA hydrogels to produce a conductive cellularized scaffold (Figure 16). Here, CNTs were coated with a thin layer of GelMA, allowing them to homogeneously disperse throughout the hydrogel. Following this, NIH/3T3 fibroblasts were encapsulated within the CNT-GelMA prepolymer solution and patterned into microdiscs. The fibroblasts retained high viability even at the highest concentration of CNTs incorporated, with no statistical difference relative to the control. More importantly, the mechanical properties of the hydrogels increased from 15 kPa (5% GelMA) to ~60 kPa with the addition of 0.5 mg/mL CNTs. This was attributed by the observed increase in nanofiber web-like structures formed by the CNTs as seen in the SEM images. As hydrogels are notoriously soft, especially GelMA, enhancing the mechanical properties while retaining the porosity and bioactivity of scaffold is highly advantageous.[268] In a follow up study by the same group, CNTs were incorporated at a higher concentration to form cardiac patches. This resulted in increased mechanical properties and electrical properties of the hydrogels, which ultimately led to improved beating uniformity of neonatal rat cardiomyocytes within the scaffold. After measuring a much lower excitation threshold in scaffolds with CNTs, they hypothesized that the lower potential reduced local pH gradients and gas generation, reducing possible damage to the tissue and thus producing a more stable tissue.[269] It has also been noted that because more electrical pathways are formed with the incorporations on CNTs, a higher concentration leads to lower resistivity, which is important in cardiac, muscle, and nerve tissues.[266,270]

GO is another popular form of carbon used in nanocomposites and the oxygen-containing hydrophilic groups on GO prevent sheet agglomeration, which make it advantageous for homogeneous dispersion in prepolymer solutions. By incorporating GO into GelMA, the compressive modulus of the gel increased from 4 to 24 kPa. Interestingly, it was found that the failure strain of the gels decreased from ~90% to ~55% after GO addition, indicating that the hydrogels were much more rigid. Furthermore, the porosity of the hydrogels was unaffected and supported the encapsulation of NIH/3T3 cells by maintaining high viability.[267] Chiaponne et al. also explored DLP-based 3D printing with GO by incorporating into a PEGDA hydrogel. Here, an increase in mechanical properties and slight improvement on electrical conductance was also observed.[271]

A challenge of using organic nanomaterials is that incorporating higher concentrations typically increases the opacity of the prepolymer solution. This is the case for many of the nanocomposite materials, such as with CNTs incorporated into GelMA as shown in Figure 16A. The darker solution absorbs more UV light and subsequently decreases photoinitiator conversion and can impede light-based 3D printing processes (Figure 16C), although it is worth noting that CNTs appear to be evenly distributed in the prepolymer solution (Figure 16B) and do not phase separate upon hydrogel formation (Figure 16D), thus indicating good miscibility between GelMA and CNTs. As the nanofiller concentration increases, longer exposure times and/or higher power light sources are required to compensate for the absorbed light. At a certain point, the solution will become too opaque to print with good resolution. Moreover, in the case of 3D bioprinting, longer and higher power exposure times can also have a negative impact on cell viability which would also have to be taken into consideration when optimizing the nanocomposite material composition and exposure parameters.

7.1.2. Metallic Nanomaterials.—

Metallic nanoparticles are incorporated into hydrogels to improve the conductivity of the hydrogel (e.g., gold and silver nanoparticles) or for their magnetic properties (e.g., iron-based nanoparticles).[265,266] In literature, gold and silver nanoparticles are most frequently incorporated into “smart” hydrogels that are responsive to external factors such as solution composition, pH, and temperature. In response to environmental changes, these hydrogels will either swell or shrink depending on the ionization of their side chains that function to move the encapsulated nanoparticles farther apart or closer together. This in turn directly impacts the electrical conductivity of the hydrogel, meaning that the conductivity can be a “switch” to control for external factors.[272] Moreover, these “smart” polymers have demonstrated to be compatible for 3D printing. For example, poly(*N*-isopropylacrylamide) [PNIPAm] has been printed through a DLP-based setup and was able to retain its reversible swelling/shrinking properties after printing.[273]

Hydrogels such as polycarboxyls or polyamines are also cell compatible due to the adsorption of extracellular matrix proteins which act to facilitate cell adhesion. For instance, PNIPAm is a common material that been used to effectively create cell sheets. Above the lower critical solution temperature (LCST), the hydrogel is hydrophobic and intramolecular hydrogen bonding in the polymer chains dominate which assists protein adsorption. Below the LCST, the surface becomes hydrophilic and the adhered cells detach thus forming a cell sheet.[274] Good cell adhesion has also been noted on poly(acrylic acid)/polyacrylamide gels and poly(acrylic acid)/poly(allylamine hydrochloride) gels.[275,276] Though it has not yet been demonstrated, it is expected that many of the smart hydrogels may have temperature-controlled adhesion similar to PNIPAm.

Janovák et al. explored the properties of two different hydrogels, poly(acrylamide) [PAAm] and PNIPAm with encapsulated nanoparticles. Here, gold nanoparticles (AuNPs) were added into each hydrogel and UV cured followed by an investigation on the effect of AuNP concentration on the overall hydrogel conductivity. Unsurprisingly, the conductivity increased with higher concentrations due to a rise in possible electrical flow pathways and decrease in the average nanoparticle separation distance. However, the impact of temperature on the gel conductivity was only seen at higher AuNP concentration. In particular, the group observed two different phenomena in the hydrogels where in the case of PAAm the conductivity of the sample decreased with increasing temperatures due to continuous swelling, compared to PNIPAAm where conductivity increased up to the point of its collapse at around 32 °C.[272] Zhao et al. also incorporated AuNPs into a PNIPAAm hydrogel by conjugating a vinyl group to the AuNPs and covalently linking the nanoparticles into the hydrogel as opposed to physical confinement, which can lead to leaking of AuNPs out of the hydrogel over time. After conducting multiple heating and cooling cycles, they discovered that the hydrogels were robust and had reversible electrical properties.[277] Similar findings were also discovered when incorporating silver nanoparticles (AgNPs) in poly(acrylic acid), showing that swelling can be a useful strategy for both AuNPs and AgNPs.[278]

Iron-based metallic nanomaterials are of considerable interest due to their magnetic properties. Magnetic nanoparticles (MNPs) are usually composed of Fe_3O_4, a compound called magnetite. Magnetite consists of Fe^{2+} and Fe^{3+} ions ordered unequally, resulting in a net magnetization ability and superparametric capability that has been used as a hypothermic agent in drug delivery as well as for MRI imaging. Another MNP is hematite, Fe_2O_3, which can be functionalized with fullerenes for use in drug delivery, MRI contrast agents, and nonviral gene delivery.[279]

When MNPs are incorporated into hydrogels they can also be used to impart mobility within hydrogels. For example, Zhu et al. 3D printed a PEGDA "microfish" by incorporating iron oxide nanoparticles into the head for directionality, platinum nanoparticles in the tail for propulsion, and polydiacetylene in the body for melittin toxin sensing (Figure 17).[280] Here, the MNPs were physically bound within the PEGDA hydrogel, which enabled the whole "microfish" to move in a controlled fashion with the use of a magnetic guide.[280] MNP incorporation has also been used in tissue culture applications. For instance, Xu et al. developed a GelMA-based hydrogel incorporating MNPs termed "M-gels".[281] By creating multiple small M-gels, a low intensity magnetic field was used to create multiple layers of spheroids. Following this, NIH/3T3 cells were encapsulated within these M-gels and were demonstrated to support high viability after 5 days in culture.[282] However, the MNPs presence did lower cell proliferation, which suggests that their long-term effects on cell behavior warrants further investigated. The MNPs also had an impact on the degradation of the hydrogel such that high concentrations of MNPs led to a faster degradation rate. The porosity was also significantly lower when 5% MNP was added to GelMA. Moreover, the ultimate stress and failure strain was increased after the addition of MNPs (1% and 5%) to the GelMA, however, the compressive modulus was unaffected. With regards to mechanical properties, MNPs are not as effective as the organic nanomaterials in increasing the material strength of the hydrogels.[281]

7.1.3. Inorganic Nanomaterials.—Hydrogels incorporating inorganic materials are primarily used for improving mechanical properties. For instance, common materials include hydroxyapatite, silicate nanoparticles, glass, and silica.[265,266] In one study, Gaharwar et al. incorporated silica nanospheres into PEGDA to increase the strength and the toughness of the hydrogel networks.[283] By increasing the concentration of the nanospheres up to 10%, this increased the opacity of the prepolymer solution in addition to the formation of silica aggregates due to higher silica content.[283] The same group also explored the covalent cross-linking of silicate nanoparticles to PEGDA. They found that the addition of silicate significantly increased fracture strength, ultimate strain, and toughness, yet it did not impact the compressive modulus. Moreover, although up to 5% silicate was incorporated, the transparency of the hydrogels was maintained which indicates that DLP-based 3D printing would be more feasible with silicate nanoparticles compared to silica nanospheres. Lastly, the adhesion properties of PEGDA after silicate incorporation was also improved upon by adding 5% silicate nanoparticles for the culture of MC3T3-E1 preosteoblast cells.[284]

Hydroxyapatite has also been incorporated into hydrogels, which has been shown to promote bone formation. For example, Zuo et al. mixed hydroxyapatite precursors into GelMA by physically constraining the particles within the hydrogel upon UV exposure.[285] It was demonstrated that an increase in the compressive modulus of the hydrogel from ~13 to ~23 kPa for pure GelMA to GelMA with 2% (w/v) hydroxyapatite was observed. Moreover, a modular scaffold of a cortical bone was fabricated by encapsulating both human umbilical cord vein endothelial cells (HUVECs) and MG63 cells that have high potential to be differentiated into bone as representative cell types (Figure 18). Gene expression analysis after 7 days of culture revealed an increase in collagen I expression and osteogenic genes, with the exception of osteocalcin and alkaline phosphatase in the scaffold containing hydroxyapatite.[285] Gaharwar et al. also mixed hydroxyapatite into PEGDA hydrogels in the form of preformed nanoparticles instead of precursors.[286] Doing so enabled a much higher concentration of nanoparticles being incorporated into the hydrogel, although aggregates began forming at 15% hydroxyapatite content. Regardless, the addition of the nanoparticles did not significantly change the pore size or shape of the hydrogel. The hydroxyapatite nanoparticles were also able to improve the mechanical properties of PEGDA, resulting in a 10-fold increase in toughness, an 8-fold increase in fracture strength, and a 3-fold increase in tensile modulus after the addition of 15% hydroxyapatite. Despite the constant pore size, the swelling degree was also decreased with increasing nanoparticle concentration. Moreover, cell adhesion of MC3T3-E1 preosteoblasts cells was improved due to the increased adsorption of proteins to the PEGDA hydrogel.[286]

7.1.4. Polymeric Nanomaterials.—Polymeric nanomaterials, such as dendrimers, hyperbranched polymers, liposomes, polymeric micelles, nanogels, and core–shell polymeric particles, have been incorporated into hydrogels.[265,266] These nanocomposite hydrogels are most often used for one of the four following areas: passively controlled drug release, stimuli responsive drug delivery, site-specific drug delivery, and detoxification. To form these nanocomposites, there are a few different methods. Common to the previous nanocomposites, the nanoparticles can be directly incorporated into the prepolymer solution prior to UV-cross-linking. The nanoparticles can also be synthesized within the prepolymer solution by adding the precursors into the solution. Lastly, the nanoparticles can also be "breathed in" by the hydrogel after its formation.[287]

In passively controlled drug release, liposomes are often physically trapped within the hydrogel and released by diffusion overtime. Because they are not covalently bonded to the hydrogel, their release can be modulated by the hydrogel porosity. The liposomes containing a drug either inside their structure, within their walls, or attached to the outside will then be able to dispense their effect.[287] Alternatively, dendrimers and hyperbranched polymers can help with the release directly from the hydrogel as opposed to release from liposomes or micelles from the hydrogel. Desai et al. integrated a polyamidoamine (PAMAM) dendrimer by covalently linking it to a PEG-acrylate molecule. The resulting hydrogel could contain either a hydrophilic or hydrophobic drug based on the surface charges of the dendrimer.[288] Zhang et al. also made a hydrogel entirely from hyperbranched polymers functionalized with acrylate groups. The authors successfully UV patterned the hyperbranched polymers, as well as encapsulated a hydrophobic drug that was passively released overtime.[289]

Drug delivery can also be done using "smart" hydrogels for stimuli responsive or site-specific drug delivery. In our previous discussion of "smart" hydrogels, we covered how in response to solution composition, pH, and temperature the hydrogels will shrink or swell.[272] When a drug is encapsulated within the hydrogel, it will diffuse faster when the pore size is larger (i.e., a swollen hydrogel) compared to a smaller pore size (i.e., a shrunken hydrogel). Thus, by changing external factors, the drug release profile can be controlled. Moreover, considerations about the environment where the drug should be released can be used. For example, an anti-inflammatory tripeptide was loaded into a hydrogel to alleviate inflammatory bowel disease. At the site the drug needs to be released, the pH of the environment was different and thus this external factor would trigger drug release at the correct site.[289]

Hydrogels can also be used as toxin absorbers as demonstrated by Gou et al., where the 3D printing of a liver-inspired detoxification device was made by mixing functional polydiacetylene nanoparticles in PEGDA for light-projection printing of a multilayered structure mimicking the liver microarchitecture (Figure 19).[290] In this detoxification device, the polydiacetylene nanoparticles served as the functional elements to sense, attract, and capture the toxins, while PEGDA served as the matrix to hold the functional nanoparticles in place inside the 3D liver-inspired microstructures to facilitate the diffusion and neutralization of toxins.[290]

7.2. Hybrid Polymeric Hydrogels

The extracellular matrix (ECM) provides the necessary mechanical and chemical signaling cues for cells to interact with and respond accordingly. The ECM is a composite material, composed of a myriad of biopolymers made up of various proteins (e.g., collagen, fibronectin, fibrinogen) and polysaccharides (e.g., hyaluronic acid and other GAGs).[291,292] Depending on the tissue system, the ECM composition will vary depending on the need for certain integrin-binding domains,[293] mechanical and viscoelastic properties,[294] and physical properties (e.g., swelling, pore size, porosity).[295,296] This complexity in material composition allows for a wide range of desirable mechanical, chemical, and spatiotemporal properties based on the same base biopolymers. In designing ECM-mimic materials for tissue engineering and regenerative medicine, it is useful to determine the minimum complexity necessary to successfully recapitulate a desired microenvironment.

7.2.1. Composite Natural Hydrogels.—There have been many investigations into combining ECM-derived natural biopolymers to better mimic the respective ECM environment. Using prepolymers modified for photo-cross-linking, light-based 3D printing can readily incorporate multiple materials into a single cross-linked hydrogel. For light-based bioprinting, GelMA is typically a main candidate for one of the materials as it has the common cell-attachment site RGD, which allows it to bind with many cell types. The disadvantage of using GelMA is that its mechanical properties have limited tunability.[297] Thus, secondary biomaterials are usually chosen to improve the structural and mechanical properties of the hydrogel. Garcia-Lizarribar et al. explored using two different nonmammalian polysaccharides, carboxymethyl cellulose (CMC) and alginate, to tune the degradation rate, swelling, and stiffness.[297] As with GelMA, they modified the alginate and CMC with a methacrylate group to create AlgMA and CMCMA to impart photo-cross-linkability. The benefit of using nonmammalian biopolymers is that cells cannot enzymatically degrade them. They demonstrated this in a degradation study by incubating the GelMA, GelMA–CMCMA, and GelMA–AlgMA in a collagenase type II solution. The GelMA-only hydrogel degraded entirely in a manner of a few hours, while the GelMA–AlgMA hydrogel showed a strong resistance to degradation as it maintained around 80% of its mass in the same amount of time. They also demonstrated that the composite materials did not have a noticeable effect in terms of the pore size or porosity as compared to GelMA alone. In terms of mechanical properties, the GelMA–AlgMA composite had a 2-fold higher compressive modulus than the GelMA hydrogel. Interestingly, the GelMA–CMCMA composite had a 2-fold lower modulus than GelMA, therefore it is important to ensure compatibility of the prepolymers otherwise the properties could diminish rather than improve by forming a composite.

Hyaluronic acid (HA) is an important and common ECM component found in many tissues such as the pancreas, central nervous system, and cardiovascular system.[298,299] HA has necessary cell-receptor domains for various cellular functions and lacks integrin-binding domains such that cells are unable to adhere and spread.[299] To address this, Camci-Unal et al. incorporated methacrylated HA (HAMA) with GelMA.[299] By adjusting the concentration ratio of HAMA to GelMA and the overall prepolymer concentration, they were able to tune the mass swelling ratio, degradation time, and compressive modulus. Interestingly, they showed that HUVECs proliferated the most within the composite 1% HAMA–3% GelMA hydrogel versus the single component 1% HAMA or 3% GelMA hydrogel or a stiffer 2% HAMA–3% GelMA composite.

7.2.2. Composite Synthetic-Natural Hydrogels.—

Synthetic polymers can be developed to match certain property requirements by controlling for a narrow molecular weight distribution, monomer composition, functional groups, and end groups. Therefore, synthetic polymers are a logical candidate to improve and tune the mechanical properties of natural polymer hydrogels. For light-based printing, PEGDA is a favored prepolymer material, as it is easy to print fine features due to its low swelling ratio as it has a high cross-linking density. Additionally, PEG is a highly studied biomaterial due to its relative bioinertness and ease in modification to increase functionality. The molecular weight of the PEGDA prepolymer is a strong determinant of the resulting hydrogel's mechanical and physical properties because a lower molecular weight increases the ratio of reactive acrylate end-groups to PEG-monomer units, which in turn leads to a higher cross-linking density. Therefore, it is not feasible to compare PEGDA hydrogels without knowing their prepolymer molecular weights. Garcia-Lizarribar et al. also investigated a PEGDA–GelMA composite hydrogels, however, they did not report the PEGDA molecular weight so, it is not possible to put their data into context.[297] The inclusion of 1% PEGDA resulted in poor encapsulation of C2C12 cells with viability of less than 40%, which indicates that the PEGDA used had a molecular weight of less than 1000 Da.[300] In other works, Zhu and Tringale et al. combined 700 Da PEGDA with GelMA to greatly increase the stiffness of the hydrogel to 2–4 MPa, 3 orders of magnitude higher than a typical GelMA hydrogel necessary to achieve stiffnesses matched to that of rat peripheral nerve tissue for a 3D printed nerve conduit.[162]

7.2.3. Interpenetrating Polymer Network Hydrogels.—

An interpenetrating polymer network (IPN) is a special composite where at least two polymer networks are formed without covalently cross-linking to each other such that the networks become physically interlocked.[301,302] The purpose of forming an IPN is to increase the mechanical properties of the hydrogel, especially the toughness, because breaking the hydrogel now requires breaking through two (or more) networks. An IPN can be formed either simultaneously or sequentially. An IPN can be formed simultaneous by using two different cross-linking mechanisms such as step-growth and chain-growth polymerization (see section 2 for detailed mechanism discussion). For light-based hydrogel formation, dual thiol–yne (similar mechanism to thiol–ene chemistry) and (meth)acrylate cross-linking mechanisms have been used to create IPNs of gelatin- and PEG-based materials.[303] Additionally, an IPN can be made of two networks of the same material by photo-cross-linking the prepolymer solution inside an already formed hydrogel.[304] For 3D printing, this strategy could be useful to strengthen a printed part by soaking it in the prepolymer solution, removing any excess material, and re-exposing it to the appropriate light source.

8. LIGHT-BASED 3D PRINTING MODALITIES

Light-based 3D printing systems function by enabling precise spatiotemporal control over localized photopolymerization of biomaterials to build a desired structure. In this section, various light-based 3D printing modalities will be highlighted ranging from serial, planar, and volumetric build formats (Figure 20) developed to form simple to complex geometries applicable for tissue engineering and regenerative medicine. A summary of the advantages and disadvantages of each light-based 3D printing modality is provided in Table 3.

8.1. Inkjet and Microextrusion Printing

In raster-like 3D printing platforms, materials and cells are deposited through a nozzle in a serial fashion either drop-by-drop as with inkjet printers or line-by-line as with extrusion printers (Figure 20Ai–ii). These setups typically involve a two-stage fabrication process: (1) a photopolymerizable bioink capable of rapid reversible cross-linking (e.g., ionic cross-linking or thermal gelation) is chosen to ensure it can be deposited appropriately into the desired structure, and (2) covalently photo-cross-linking the printed structure via light exposure to permanently stabilize the construct. For instance, to form micrometer-scale cell-laden structures, Xie et al. employed an inkjet printer fitted with an electro-assisted module to rapidly deposit low viscosity GelMA bioinks containing bone marrow stem cells into uniform microdroplets measuring 100 μm in diameter.[312] Upon collection and subsequent cross-linking of the microdroplets via exposure to 405 nm light, this group demonstrated this technique as a biocompatible method to encapsulate cells, produce microspheres for drug control release, as well as the printing of more intricate patterns onto a conductive membrane to ensure continuous printing of the droplets.[312] In similar work, Stratesteffen et al. utilized a custom air-pressure-driven drop-on-demand printing platform to produce droplets of GelMA–collagen hydrogels containing HUVECs and human mesenchymal stem cells (hMSCs).[308] They found that modulating UV-light exposure to their printed cellularized constructs could be tuned to mimic the rheological and mechanical properties to promote capillary network formation in vitro toward the goal of forming prevascularized tissues.[308]

In the case for extrusion bioprinting, Zhang et al. produced endothelialized myocardium tissues using a coaxial extrusion printer to deliver a bioink consisting of GelMA and alginate in the sheath while the core deposited $CaCl_2$ solution.[11] In this setup, physical cross-linking of the alginate component was first achieved via contact with the $CaCl_2$ solution, followed by chemical cross-linking of the GelMA component postprinting via UV exposure.[11] In another application, Jang et al. used a combination of vitamin B2-induced UVA cross-linking followed by thermal gelation to produce 3D printed heart dECM tissues.[150] Vitamin B2 (i.e., riboflavin), a naturally occurring and noncytotoxic photoinitiator, was mixed with solubilized porcine heart dECM bioink and extruded onto a low temperature platform to prevent gelation during printing.[150] Once the first layer was complete, it was exposed to UVA light to initiate covalent cross-linking of the heart dECM bioink and this process was repeated for all subsequent layers to form the final 3D structure.[150] The complete printed construct was then placed at 37 °C to induce thermal gelation of the heart dECM to provide additional mechanical strength to match that of native cardiac tissue.[150]

Overall, these methods enable tailoring of the bulk mechanical properties of the printed construct via light curing of the structure post printing. However, it is important to note that homogeneity of the local mechanical properties within the printed construct is limited by the light penetration depth, such that larger structures may exhibit less photopolymerization within the center of the construct using this approach and therefore result in a heterogeneous construct. Because these printers operate using a layer-by-layer approach, it is also critical that the chosen biomaterials possess rapid gelation kinetics to enable high aspect ratio of the 3D printed structures, prevent collapse during fabrication, and ensure the build is completed within a reasonable duration. Furthermore, surface artifacts between the interfaces of each successive layer may lead to weak points within the structure and resolution in the z-direction is highly dependent on the nozzle size and viscosity of the biomaterial. In most instances, depending on the application and desired build volume, inkjet and extrusion-based printers fabrication times can range from minutes to hours and are limited in design complexities because overhanging structures are often difficult to produce without supportive or sacrificial structures.

8.2. Laser-Based Stereolithography

Conventional stereolithography involves scanning a laser across the surface of a prepolymer resin vat (Figure 20Aiii). The laser beam can be either continuous or pulsed such as a femtosecond pulse. The latter is needed for two-photon polymerization (TPP).[313–316] Laser-based stereolithography has been widely utilized to produce precise tissue engineering scaffolds[317,318] and biomedical devices, especially in the field of dentistry.[319] In the area of bioprinting, Chan et al. were able to successfully encapsulate NIH/3T3 cells, a mouse fibroblast cell line, in PEGDA (700 Da–10 000 Da) using a modified SLA machine and demonstrated that the cells proliferated under certain conditions after 2 weeks based on a MTS assay.[300] This study was limited to only an assessment of viability and proliferation and did not assess any cellular function. To determine whether lower-frequency lasers may be more cell compatible, Wang et al. recently explored if a 405 nm laser can be used in 3D bioprinting with high cell viability.[320] They demonstrated that a 405 nm laser with a 150 mW laser diode setup can be used to print and encapsulate MCF-7 cells, a breast-cancer cell line, in PEGDA (700 Da) with 95% cell viability and up to 50 μm feature resolution.[320] As they only demonstrated their technique with a robust cancer cell line, future experiments are needed to determine the compatibility of visible light laser stereolithography with primary cells, which tend to be more sensitive to cytotoxic stimuli, such as HUVECs, which are common for in vitro vascularization studies.

In TPP, a high-powered femtosecond pulse laser is used to solidify regions within a photopolymerizable vat in a serial and contactless manner to produce structures with up to nanoscale resolutions. This direct 3D laser writing process enables submicrometer feature sizes due to the Gaussian nature of light absorption. By employing femtosecond pulsed lasers, two or more photons can be simultaneously absorbed to form active species to initialize the photopolymerization process.[313,321] Because absorption occurs only at the peak region of light intensity with highest energy, polymerization is confined within the volume of the focused laser beam to achieve submicrometer scale features (<100 nm) and nanoscale tolerances.[313,322] There are no topological constraints with direct laser writing, therefore overhanging structures can be readily fabricated without the need for supportive or sacrificial layers. Melissinaki et al. took advantage of TPP's capabilities to investigate the effects of the microscale topology of PLA scaffolds on neuronal guidance and regeneration.[316] They printed a PLA scaffold with 7 μm thick microgroove walls that were spaced 50 μm apart for axonal guidance. To ensure uniformity of the microstructures it is critical to have laser-synchronized motion such that laser firing is timed appropriately with the motion path, which can lead to very long fabrication times (i.e., hours) and is not scalable to accommodate the building of larger structures.

8.3. Digital Light Processing (DLP)-Based Printing

In recent years, digital light processing (DLP)-based 3D printing technologies have represented a paradigm shift in traditional 3D printing modalities, primarily by drastically increasing fabrication speeds and resolution. Rather than operating in a serial manner as with conventional inkjet and extrusion printers, an entire plane of the object is fabricated at once which substantially decreases the build time.[14] The general setup of these printers involves a light source, typically UV (i.e., 365 nm) or visible light (i.e., 405 nm), that illuminates a DMD chip programmed to project various digital patterns through a set of optics into a photopolymerizable vat along with a motorized build platform to control the height of the build (Figure 20B). Each micromirror on the DMD chip is representative of one pixel in the digital image and thus microscale resolutions as small as 3–5 μm feature sizes can be achieved given the appropriate optics. As such, highly complex biomimetic structures can be readily generated with physiologically relevant topological feature sizes.

The DLP-based 3D printing process can be classified into two approaches: layer-by-layer or continuous. In the layer-by-layer approach, the build regime operates in a sequential fashion where a layer is printed and then the build stage is moved to allow unpolymerized material to rewet the printing area prior to fabricating the next layer (Figure 20Bi). The structures formed using this technique are often not smooth, with limited resolution in the z-direction due to the layer-by-layer nature of the build. To circumvent these challenges, the concept of using a continuous approach in DLP-based printing systems was developed by Shaochen Chen's group in 2012, where a dynamic optical projection stereolithography (DOPsL) fabrication approach was first introduced.[14] By synchronizing the projection of digital patterns into a photopolymerizable vat with the movement of the build stage, a continuous print regime can be achieved to yield structures with smooth side walls and overhanging microstructures in seconds.[14] Arrays of various geometric shapes such as curved microwell structures, flower patterns, and spiral-like structures were demonstrated within a single printed chip measuring 4.6 mm × 3.5 mm.[14] The DOPsL noncontact fabrication approach is advantageous for the fabrication of soft biomaterials, as the printed part remains stationary within the prepolymer vat during the build to prevent collapse or delamination.[14] This method is ideal for bioprinting biomimetic microtissues that incorporate encapsulated cells within soft photopolymerizable hydrogel precursors (e.g., dilute solutions of e.g. PEGDA, GelMA, and GM-HA). Moreover, gradient stiffness can also be designed into the printed constructs by modulating the light exposure pattern or intensity corresponding to areas of lesser or greater cross-linking.[14]

To accommodate the build of larger complex structures, Joseph M. DeSimone’s group in 2015 introduced a layerless fabrication technique termed continuous liquid interface production (CLIP) as an alternative to additive manufacturing.[90] To eliminate the iterative layer-by-layer process, this new approach relies on the well-understood oxygen inhibition in free-radical polymerization by utilizing an oxygen-permeable window to ensure a thin layer of uncured prepolymer is always present at the fabrication window and printed part (Figure 20Bii).[90,323] Because of this continuous process, large centimeter scale structures can be produced while maintaining high feature resolution (i.e., <100 μm) without compromising fabrication speed to complete a print in minutes compared to conventional nozzle-based printing methods which would take hours.[323] For instance, this printing approach has been utilized in the tissue engineering field to generate highly intricate and complex constructs including perfusable multivascular network structures and implantable peripheral nerve conduits.[94,162] It is noteworthy that this printing approach is more feasible for producing stiffer structures (e.g., high concentration biomaterials such as PEGDA) to ensure structural integrity and resolution during the build sequence because softer biomaterials cannot support themselves and will exhibit collapse and deformation during the movement of the build probe. In the context of continuous large-scale fabrication, thermal accumulation at the print window in CLIP printing modalities due to the exothermic (often exceeding 120 °C) nature of polymerization reactions can result in thermal deformations of the printed material such as cracking, warping, and clouding, which when left unmitigated may limit the extent of scalability in build volume.[324] Thus, rather than utilizing an oxygen permeable window, Walker et al. developed a mobile liquid interface containing fluorinated oil that acts to reduce adhesion between the printed part and the interface as well as providing direct cooling to the entire printing area.[324] This technique is termed high-area rapid printing (HARP), whereby the photopolymerizable material is situated above a layer of flowing immiscible fluorinated oil which ultimately allows the scalable construction of very large objects. For instance, the group demonstrated the fabrication of a 38 cm × 61 cm × 76 cm object completed in 1 h and 45 min at 100 L/h volumetric throughput.[324] Because of the nonreliance of oxygen inhibition, this printing technique is also capable of accommodating oxygen-sensitive as well as oxygen-insensitive polymeric material systems.[324]

Until recently, DLP-based 3D printing modalities have been limited to planar printing regimes. The concept of implementing volumetric additive manufacturing in 3D printing technologies provides a novel strategy to overcome challenges in traditional layer-by-layer approaches such as poor surface quality, limited geometric complexity, and slow fabrication speeds. One of the first reports of volumetric build setups was reported by Shusteff et al., where complex 3D structures were fabricated via holographic (phase-controlled) beam shaping to produce targeted patterns within a prepolymer vat.[325] In particular, three orthogonally directed light beams intersect and superimpose to offset the limited axial resolution from each of the other beam directions.[325] As a result, a one-step volumetric print can be achieved to construct millimeter scale structures with high spatial resolutions in all three dimensions.[325] In 2019, Hayden Taylor's group introduced a volumetric additive manufacturing method using DLP technology termed computed axial lithography (CAL).[326] This novel technique enables the generation of various geometries via controlled volumetric photopolymerization and was inspired by CT imaging reconstruction technology (Figure 20C). Images are projected in synchrony with the rotation of a vat containing photopolymerizable materials such that the superposition of exposures from multiple angles provides sufficient energy to photo-polymerize a discrete voxel of the material into the desired geometry.[326] A key advantage of this platform is the ability to print using high viscosity fluids (up to approximately 90 000 cP) or solids, which are typically challenging with other DLP-based printing setups that involve the printed object to move during the printing process (e.g., CLIP and HARP).[326] Furthermore, the concentration of photoinitiator employed in the prepolymer solution must be low enough for light to penetrate the entire volume of the prepolymer vat while also being high enough to induce photopolymerization within the targeted region. It is also important to note that minimizing the relative motion of the object being printed and the prepolymer solution during the rotating process is critical to maintain appropriate print resolution, shape, and fidelity. As such, lower viscosity hydrogel materials such as GelMA will require thermal gelling prior to printing. With regard to bioprinting applications, volumetric printing techniques also provide several advantages for fabricating soft hydrogel structures of high geometric complexity rapidly. This is because most hydrogel biomaterials appropriate for producing cell-laden constructs are often of low modulus (i.e., 1–10 kPa) and therefore difficult to resolve because the forces exerted onto the printed object can cause collapse or deformation as with layer-by-layer printing processes. Volumetric 3D printing can overcome these challenges because the printed object remains stationary and suspended during the print, thus minimal forces are exerted on the object and intricate overhanging or hollow patterns can be fabricated in a scalable manner. Bernal et al. demonstrated this possibility by printing cellularized gelatin constructs by first thermogelling the chondroprogenitor cells and GelMA prepolymer mixture to prevent cell sedimentation and ensure positional stability of the printed object.[17] Following this, the projection of different patterns along multiple rotational angles using a visible (405 nm) light source enabled the materialization of a cellularized disc-shape construct such that when the unpolymerized material is washed away at 37 °C the recovered cellularized construct possessed greater than 85% cell viability.[17]

9. STRATEGIES FOR CONTROLLING LIGHT-BASED 3D PRINTING QUALITY

Light-based 3D printing and 3D printing in general has proven to be a challenge to standardize the end-part properties as it can vary depending on a multitude of material and process parameters. Material parameters such as the prepolymer and photoinitiator concentrations can be consistently set for synthetic prepolymers, however, naturally derived prepolymers are inherently susceptible to batch-to-batch variation which therefore require the end user to adjust the printing process per material batch. Additionally, encapsulating cells during light-based 3D printing adds additional variability to the printing process that requires a good understanding of how to modify print parameters to achieve a desired 3D construct with high cell viability. In this section, we will discuss how to determine and modify printing parameters based upon the field's current understanding of photopolymerization chemistry and optical engineering. A summary of troubleshooting strategies for controlling light-based 3D printing quality and resolution is listed in Table 4.

9.1. Determination of Material Composition

9.1.1. Sensitivity of Photoinitiator.—The quantum yield is a measurement of photons emitted in response to a light-absorbing molecule being activated via photon bombardment. It is a widely used quantification method for photoinduced reactions in spectroscopy, illumination, and analytical chemistry.[327] Physically, the quantum yield of a compound is defined as the fraction of molecules required to emit a photon after direct excitation by sources such heat, electrical current, and light. In many cases, it equals the total number of emitted photons from a bulk sample divided by the total number of absorbed photons except for reactions that generate photons intrinsically.

Quantum yield of a photoinitiator is an important assessment of its sensitivity and efficiency. In the context of laser-induced 3D printing, quantum yield is necessary for setting the thresholds for laser action and determining the suitability of materials for specific wavelengths. Particularly in biomedical applications, quantum yield of a photoinitiator is a critical judgment criterion due to the need to maintain a low irradiation energy for preserving cell viability.[29] A photoinitiator's absorption spectrum and its related extinction coefficient also affect the overall free radical generation. Even if the photoinitiator has a high quantum yield, if it does not have a sufficient absorbance at the irradiation wavelength this will result in poor free-radical production.[328] For bioprinting, it is especially important to use a light source with a non-DNA damaging, cytocompatible spectrum range, which are generally considered to be 365 nm and above.[29] Additionally, the cytocompatibility often requires the photoinitiator to be water-soluble and fully dispersed within a hydrogel system. Thus, most photoinitiators suitable for biological applications are limited to hydrophilic molecules such as benzylidene cyclanone dyes and eosin Y, which have high quantum yields at a low energy light wavelength (~800 nm), or salt-based photoinitiators such as LAP and Irgacure 2959, which have high quantum yields and fast conversion kinetics at a high energy light wavelength (~400 nm).[329]

9.1.2. Critical Energy and Penetration Depth.—Critical energy (E_c) and penetration depth (D_p) of a polymer are critical material parameters in choosing laser and resin composition for 3D printing. They are purely resin-dependent terms which govern photopolymerization assuming a Gaussian laser.[330,331] E_c and D_p are derived from a Beer–Lambert relationship describing the penetration of light in a resin as shown in eq 4:[332]

$$P_z = P_0 e^{-z/D_\mathrm{p}} \tag{4}$$

where P_z is the power of incident light at a certain depth z below the surface. P_0 denotes the power of light at the surface. D_p is the depth where the intensity of the penetrating light falls to 1/e of the surface intensity. D_p is related to the absorbance characteristics of resins, which are determined by their material compositions. Physically, the power terms can be converted to energy terms and the position z becomes the cure depth. After transformation the equation becomes

$$C_\mathrm{d} = D_\mathrm{p} \ln\left(\frac{E_0}{E_\mathrm{c}}\right) \tag{5}$$

Eq 5 is also called the working curve equation. C_d refer to the depth/thickness of cured resin, E_0 is the energy of incident light at surface, and E_c is the critical energy required to initiate polymerization. Practically, by log-plotting C_d against different E_0 values, a straight line should be produced with a slope of D_p and an x-intercept of E_c. Determining these parameters for a given prepolymer solution will help users to optimize the printing process such as laser intensity and exposure time to achieve desired resolutions. Particularly, for high resolution SLA and DLP-based printing with fine z resolutions, the users need E_c and D_p to minimize thickness of each layer and choosing the appropriate light intensity, scan speed, and z-axis motion speed to optimize the curing conditions.

9.2. Light Exposure Dose

The effective exposure dose is a product of the exposure time and energy density of the light source. The exposure time is controlled by setting how long the light exposure will project on the printing region. The energy density can be proportionally manipulated by adjusting the output light intensity. The exposure dose needs to be optimized for any change in material (see section 9.1.2). Once optimized for a material, it can be adjusted within an experimentally determined range to adjust cross-linking density for the photopolymerization of (meth)-acrylate-based mechanisms and thereby tune for mechanical and physical properties of the hydrogel.

9.2.1. Light Exposure Time.—Light exposure coupled with photoinitiator chemistry governs the kinetics of photopolymerization initiation. It is important to choose the correct wavelength of light to maximize the photoinitiator absorbance to decrease the exposure time for rapid printing. However, for bioprinting, it is necessary to also consider the effect of shorter wavelength light (i.e., deep UV) on cell viability and DNA damage.[29] The effective light exposure is a product of the total exposure time and energy density of light. For a given energy density of light (i.e., determined by the power of the light source), one can tune the exposure time to control the photoinitiation and production of free radicals, whose spatiotemporal concentration will determine the degree of photopolymerization and/or photo-cross-linking. This in turn will directly affect the resulting cross-link density, the average molecular weight between cross-links, the pore size and porosity, and mechanical properties such as stiffness.

9.2.2. Light Power.

9.2.2. Light Power.—The light power is dependent on the light or laser source. By controlling the voltage supplied to the light source, one can adjust the light intensity. For the same effective exposure dose, a lower light intensity would require a longer exposure time. Thus, sometimes it is advantageous to use a lower light intensity to have greater tunability of the hydrogel properties by having a larger exposure-time range for acellular prints. For bioprinting, using the highest cytocompatible light intensity allows one to use the minimum necessary exposure time to reduce prolonged cell exposure to free radicals.

9.2.3. Effects on Mechanical and Physical Properties.—By modifying the exposure dose, one can control the degree of photo-cross-linking that directly corresponds to the mechanical properties, which is typically characterized by measuring the stiffness and the physical properties (e.g., pore size) of a hydrogel. Zhu et al. were able to increase the modulus of a PEGDA–GelMA composite hydrogel by a factor of 2, from 2 MPa to over 4 MPa, by increasing the energy density of the irradiated light by a factor of ~2.5.[162] On the other hand, Garcia-Lizarribar et al. maintained the same light intensity but modified the exposure time from a minimum of 5 s exposure to 25 s, and the modulus of both GelMA and GelMA–AlgMA hydrogels increased by a slightly lower factor of ~1.5. Interestingly, the GelMA–PEGDA hydrogel stiffness did not appreciably increase upon the increased exposure time, though it is unclear why this occurred. Increasing the cross-linking density leads to a denser hydrogel and thus a lower average pore size. For cell seeding, the cells may be able to handle a lower pore size, but for bioprinting, an average pore size of less than the diameter of the cell (e.g., less than 20 μm) will have a negative effect on cell viability.[305] This highlights the key need to balance the appropriate stiffness of the hydrogel with the appropriate pore size and porosity because for most hydrogel formulations these factors interdependent.

9.3. Post-Cure Process

Providing a secondary cure step, either by thermal methods or UV irradiation, after printing is a common procedure for light-based 3D printing as the free-radical chain growth polymerization generally has a gel point of relatively low conversion.[333] Therefore, the printed material will solidify much sooner before the photopolymerization process is complete. In this case, the additive manufacturing field refers to the as-is printed part as a “green” part. If a biomaterial requires enhanced mechanical properties to function (e.g., for an orthopedic application), a postcure process will finish the photopolymerization reaction of the green part, resulting in the final part. Salmoria et al. has shown that for an epoxy resin, UV, microwave, and oven postcure processes all led to an increase in elastic modulus, ultimate tensile strength, and fracture strength.[334] The strain at break decreased by 1–2% as a stiffer structure is less capable of damping the energy of deformation as compared to the green part. For bioprinting, it is less common to include a postcure step as it may negatively affect the cell viability. However, some groups have implemented an enzymatic cross-linking step using microbial transglutaminase either before or after UV cross-linking as a way to modulate the mechanical properties of GelMA in a noncytotoxic manner.[335,336]

9.4. Factors Affecting Print Resolution

The fabrication resolution is a critical index to evaluate a 3D printing method. In this section, we will discuss critical factors affecting resolution relevant to DLP-based 3D printing modalities. Because of the propagating nature of light in a wide-field optical microscope, it is easier to achieve fine resolution in the lateral direction (i.e., perpendicular to the propagation direction of light) than in the axial direction (i.e., along the propagation direction of light). Similarly, plane-projecting methods also feature anisotropic fabrication resolution. As such, we can use the lateral resolution and the axial resolution to characterize the fabrication resolution of plane-projecting methods.

Lateral resolution determines the finest feature size on the $x-y$ plane (i.e., the plane perpendicular to the light propagation direction, which is also the horizontal plane in the real-world coordinates). Axial resolution determines the finest overhanging layer thickness in the z direction (i.e., along the light propagation direction, which is also the vertical direction in the real-world coordinate). Ideally, the lateral resolution is determined by the size of micromirror on the DMD chip and the magnification of the projecting optics, whereas the axial resolution is determined by the positioning resolution of the vertical stage. However, there are a few inherent physical factors that can also affect the lateral and axial resolution, including Abbe diffraction limit, aberration, material absorption, light scattering, and molecular diffusion. The influence of these factors can be negligible in macroscale 3D printing, yet they have substantial influence on microscale resolution.

9.4.1. Diffraction Limit.—Though an optical projection system with greater demagnification results in finer lateral resolution, infinitely fine resolution is not achievable. The diffraction limit is due to the wave nature of light and, consequently, is an inherent resolution limit. A light beam cannot be focused into an infinitely small point by an optical system. Instead, an Airy disk will be formed. According to Rayleigh’s criteria, the resolution limit of the optical system is half of the diameter of the Airy disk, which is around $0.61\lambda/\mathrm{NA}$, where λ is the wavelength of light and NA is the numerical aperture of the lens.[337]

Plane-projection 3D printers commonly use near-UV light. A small numerical aperture lens is used in order to have a sufficient field-of-view. Assuming that $\lambda = 405$ nm and NA = 0.05, then the resolution limit based on the Airy disk calculation is 4.05 μm. A finer diffraction resolution limit can be achieved by using a lens of higher numerical aperture or using a light source of shorter wavelength. By utilizing two-photon absorption phenomenon, two-photon photopolymerization laser direct writing method can achieve a lateral resolution down to 100 nm.[338] Inspired by stimulated emission depletion microscopy (STED),[339] super resolution laser direct writing methods that can bypass the diffraction limit are also reported.[85,340,341] These methods use a normal Airy disk to initiate photopolymerization, while a donut-shaped focal spot of another wavelength is used to inhibit photopolymerization, which reduces the effective photopolymerization area.

9.4.2. Optical Aberrations.—Optical aberration is an important factor that can affect the resolution. There are two classes of aberrations, including monochromatic aberrations and chromatic aberrations. Both aberrations result in imperfect imaging and leads to deteriorated resolution. A well-designed objective lens, which contains multiple lens elements, can reduce the influence of aberrations but also greatly increases the cost. Using a narrow-spectrum light source such as single-color LED or laser is another way to avoid chromatic aberrations. Applying a smaller aperture to the imaging lenses is a simple and low-cost method to reduce the aberrations, however, the Abbe diffraction limit worsens as the aperture gets smaller.

9.4.3. Light Penetration Depth.—

The light penetration depth plays an important role in deciding the axial resolution. Light decays exponentially along the propagation direction due to absorption according to the Beer–Lambert Law. The light penetration depth is defined as the inverse of the absorption coefficient. Prepolymer material subjected to exposure above the photopolymerization threshold will polymerize. As the light intensity decays along the propagation direction, photopolymerization only happens in the surface layer. Here we define the curing depth as the same as the light penetration depth, which is also the axial resolution of the 3D printer.

Material absorption can also affect the lateral resolution. Upon light exposure, a layer of a certain thickness is polymerized. If the curing depth is greater than the optical depth of focus, then the out-of-focus plane will also polymerize, resulting in a deteriorated lateral resolution. To improve the axial resolution, the absorption coefficient of the prepolymer material should be increased. This can be achieved by using high-absorption photoinitiators, increasing photoinitiator concentration, or doping light-absorbing additives such as tartrazine, HMBS, TINUVIN 234, and food dye.[94,162,342] Common prepolymer materials have a curing depth of around 100 μm ~ 1 mm. By doping absorptive additives, the curing depth can be reduced to tens of micrometers.

A recently reported technique by You et al. can further reduce the light penetration depth to submicrometer scale by projecting patterns onto the glass–air interface of a prism where total internal reflection occurs.[343] This technique utilizes the attenuation of evanescent wave instead of the attenuation caused by absorption to control the curing depth. To prevent lateral resolution deterioration caused by out-of-focus plane polymerization, the curing depth should be smaller than the depth of focus. The depth of focus can be calculated by $d_{\mathrm{DoF}} = \frac{\delta}{\mathrm{NA}}$, where δ is the required resolution and NA is the numerical aperture. If the projection optics has a numerical aperture of 0.05, and 5 μm lateral resolution is required, then the depth of focus d_{DoF} is 100 μm. Hence, the material absorption should be strong enough to ensure the curing depth $d_z < d_{\mathrm{DoF}} = 100$ μm.

9.4.4. Light Scattering.—

Light scattering can significantly deteriorate the fabrication resolution and fidelity. An optically clear media allows projecting a sharp pattern, however, an opaque media can scatter light and blur the projected pattern. Although optically clear materials are desirable for photopolymerization-based 3D printing, some optically scattering materials are widely used in making functional devices. For example, micro/nanoparticles can be added into a polymeric material to achieve certain physical, chemical, electrical, or mechanical properties, while cells can be incorporated to achieve biological activity. All of these particles can contribute strongly to light scattering effects and hinder printing resolution. Similarly, some pure polymeric materials themselves can also be intrinsically light scattering. The effect of light scattering is difficult to eliminate if an opaque material is used. A simple practice to mitigate is to increase the material absorption by doping with light-absorptive additives.[94]

Light scattering has a negative effect on the resolution when the projected light scatters due to the presence of the newly printed solid. To address this process-dependent scattering affect, it is necessary to understand the kinetics of photopolymerization, which can be divided into three distinct stages: initiation, propagation, and termination. However, viscous and vitrification effects in bulk polymerization often result in incomplete functional group conversion. Therefore, a more dynamic model than standard free-radical polymerization kinetics is necessary. In this case, it is worthwhile to study the diffusion-controlled free-volume dependence of both the propagation and termination from a single set of kinetic data both by mathematical simulation and experimental investigation. Goodner et. al elucidated the relation using a homopolymerization system composed of 2-hydroxyethyl methacrylate (HEMA) for linear polymerization and diethylene glycol dimethacrylate (DEGDMA) for cross-linked polymerization, both using 2,2-dimethoxy-2-phenylacetophenone (DMPA) as the photoinitiator.[344] The study revealed three regimes during linear polymerization: non-diffusion-limited propagation and termination, autoacceleration and autodeceleration, and an additional reaction-diffusion termination without propagation limitations between autoacceleration and autodeceleration steps in cross-linked polymerization. They found that postexposure curing occurred during the last three stages where the light source was off, yet the polymerization continued. These findings are important in defining 3D printing parameters as well as improving printing fidelity.[345]

A recent study by You et al. has shown that resolution deterioration caused by light scattering can be avoided by using flashing photopolymerization: if the prepolymer material is a homogeneous and optically clear solution before polymerization and only becomes opaque after polymerization.[345] This technique uses short (~10 ms) and intense flashes to induce photopolymerization. During the exposure period, free radicals are generated but the material is still barely polymerized and thus light scattering is absent. After the exposure, polymerization continuous to proceed in the dark and finally the material solidifies and opacifies.

The effect of light scattering can also be mitigated by optimizing the projected digital masks. By using masks that are not identical to the target structure, the effect of scattering can be compensated. A machine learning approach can be used to calculate the optimized masks.[346] Instead of using binary digital photomasks which are identical to the targeted printing structure, grayscale photomasks which are not identical to the target are used. These grayscale masks can compensate and counterbalance the effect of scattering and thus improve the fabrication fidelity and resolution. The convolutional neural network-based artificial intelligence (AI) is trained with randomly generated masks and their corresponding printed structure. After training, the AI could output the grayscale masks for a targeted printing structure.

9.4.5. Molecular Diffusion.—Although free radicals are only generated within the light illuminated region, the free radicals and propagating chains can diffuse out of the illuminated region and cause unwanted polymerization. According to Fick's laws of diffusion, the diffusion length can be estimated by $L = 2\sqrt{Dt}$, where D is the diffusivity and t is the free-radical lifetime. To reduce the diffusion length, we can either use high viscosity materials, which have lower diffusivity, or dope a free-radical quencher such as TEMPO to reduce the free radical lifetime.[342,347]

10. FUTURE OUTLOOK

It is envisioned that future 3D printing systems will continue to evolve as a fundamental instrument for advanced fabrication and the automation of these processes is necessary to drive scalable production in major areas such as the biomedical, automotive, robotics, and manufacturing industries. This brings an important innovative direction where neural network-based artificial intelligence (AI) is now beginning to be integrated into current workflows to improve precision and enable automated 3D printing. This is a particularly useful and powerful strategy, as current methods still rely on manual trial-and-error inputs of different parameters (e.g., light intensity, exposure time, power) to produce the desired print. As the biomaterials library expands and the incorporation of nanoparticles, cells, and other components are used, these factors will ultimately introduce difficulties and time delay in fabrication as users will need to optimize printing parameters for each unique formulation and for every chosen design. By applying machine learning approaches, AI can help solve these technical issues and alleviate much of the guessing work for users in the future as well as facilitate the throughput, consistency, and industrial application of 3D printing technologies.

Another area gaining attention is the concept of 4D printing in which time is integrated into 3D printing to enable responsive changes in shape or functionality of the printed objects over time due to an external stimulus (e.g., pH, temperature, magnetic field, water). This is particularly interesting in the context of biomedical applications as 3D bioprinted structures, especially in the case where cells or bioactive factors are incorporated, can be considered as a dynamic rather than static construct that will continue to change and evolve with time postprinting.[352] The ability to incorporate programmable functionality within complex systems provides a means to create higher level constructs capable of reacting to environmental changes such that they may be considered as pseudo "living" systems. For example, Gladman et al. fabricated composite hydrogel structures mimicking plant-like architectures which change shape upon immersion in water due to encoded localized anisotropic swelling.[353] This was accomplished by controlling the orientation of printed cellulose fibrils within the composite hydrogel to pattern regions of elastic and swelling anisotropies which allows for predictable shape memory properties. In addition to geometric changes, 4D printing can also be viewed as an approach to enable scaffolds to possess functional transformation and allow cell/tissue maturation over time postprinting. This concept extends from the fact that biomimetic constructs can be programmed to mimic constituents of the native extracellular matrix microenvironment to guide and promote the proliferation and differentiation of stem cells during culture. For instance, Miao et al. used a photolithographicstereolithographic tandem fabrication technique to form hierarchical biomimetic 4D micropatterned topographies to regulate cardiomyogenesis of seeded human MSCs using smart soybean oil epoxidized acrylate (SOEA) bioinks.[354] Furthermore, 4D bioprinting can also be useful to recapitulate the complexities of native tissues to produce models that accurately simulate in vivo processes for understanding developmental stages. Expanding this concept to the neural field, Esworthy et al. proposed that 4D bioprinting could be used to produce tissue models that mimic the in vivo cortical folding process by recapitulating physiologically relevant stresses through controlled timing and folding of the printed construct.[355] Despite these advances, a limitation in 4D printing technologies is the lack of stimuli-responsive biomaterials that are compatible with 3D printing processes and meet the requirements of having dynamic capabilities.

In general, a key bottleneck regarding the utility of 3D printing systems depend heavily on the availability of compatible biomaterials that suit the vast array of research applications. We believe that this review will help provide a useful framework for researchers in biology, chemistry, materials science, and bioengineering to rationally design novel biomaterials and expand the biomaterials library for 3D printing. We also highlighted methods to overcome commonly encountered fabrication challenges associated with light-based 3D printing from the perspective of biomaterial formulation and printer system parameters. With regard to the continued advancements in light-based 3D printing technologies, recent developments are trending toward voxel-based printing strategies to greatly improve upon the throughput, scalability, and resolution achieved with current light-based printing processes. In summary, the application of these next-generation systems to accommodate cell-based printing will involve a combination of ingenuity across multiple disciplines, including materials science, optical engineering, biology, and medicine, to further drive future innovative breakthroughs in tissue engineering and regenerative medicine.

11. CONCLUSIONS

Over the years, 3D printing technologies have quickly evolved into advanced systems for the fabrication of highly complex structures for biomedical applications. This new additive manufacturing approach for the development of novel scaffolds, tissue and organ substitutes, as well as medical implants has transformed many fields as an effective tool to facilitate innovative research directions not achievable with traditional biofabrication methods. A strong advantage of 3D printing is the ability to directly control the deposition of cells and supporting materials to fabricate geometrically intricate biomimetic structures in a rapid and scalable fashion. Presently, there are several different 3D printing modalities actively employed in tissue engineering and regenerative medicine that encompass nozzle-based as well as light-based platforms. Nozzle-based platforms, such as extrusion and inkjet 3D printers, remain a popular choice for biofabrication as the printing process is ideally suited to support living cells in addition to its ease of use, low cost, and compatibility with a wide range of biomaterials. Several pertinent reviews in literature have covered the application of nozzle-based printers in detail, however, there are few papers that comprehensively review the utilization of light-based 3D printing in biomedical engineering. As such, the aim of this article was to provide a detailed overview on the application and advancement of light-based 3D printing as well as the recent developments in photo-cross-linkable biomaterials to address the increasing adoption of light-based 3D printing technologies.

Considering the interdependent relationship between biomaterial formulation and 3D printing modality, both of which dictate the success of the intended printed part and feasibility of the printing process, we first provided an in-depth discussion on commonly used photoreactive biomaterials suited for light-based 3D bioprinting applications. These biomaterials all have the following in common: (a) they are optically clear (i.e., the prepolymer solution does not strongly scatter nor absorb light), (b) they are in solution at the operational temperature, and (c) the material can be functionalized (e.g., GelMA and PEGDA). The light-based 3D printing process involves photoinduced polymerization either by free-radical chain-growth or orthogonal step-growth mechanisms, thus gaining an understanding on how to control polymerization kinetics is critical in achieving high-shape fidelity and resolution in light-based 3D printing. Here, we summarized several photoinhibiting methods such as using dual-light wavelengths of activation to independently control photoactivation and photoinhibition, incorporation of photoinhibitor species like o-Cl-HABI and TETD, as well as the addition of free radical quenchers (e.g., TEMPO) to reduce photopolymerization rates. Similarly, photoabsorbing molecules can also be employed to attenuate light at specific wavelengths to improve pattern conformity. Examples include compounds such as food dyes (e.g., tartrazine), gold nanoparticles, and HMBS. Photolabile chemistries typically used in polymeric systems was also discussed as strategies to introduce photocontrolled activation of biomolecules to further expand the functionality polymers. These include the modification of the prepolymer with photolabile molecules such as *o*-nitrobenzyl and coumarin-4-yl ester moieties among others. Following this, we outlined the properties and utility of photo-cross-linkable natural, synthetic, and composite biomaterials that are well-suited for light-based 3D printing in tissue engineering and regenerative medicine applications.

Concurrent with development of photo-cross-linkable biomaterials, we next underlined the key developmental milestones of light-based 3D printer platforms. Namely, light-based 3D printers can be classified into hierarchal printing modalities ranging from serial to planar to volumetric build regimes. Here, we focused on the latter two modalities that are enabled by DLP-based technology as they have been most frequently employed in literature due to their superior micrometer-scale resolution, rapid fabrication speeds on the order of seconds to minutes, and scalability. Altogether, these features make it ideal for cell-based bioprinting applications. Primary examples of advanced light-based 3D printer modalities are dynamic optical projection stereolithography (DOPsL), continuous liquid interface production (CLIP), and computed axial lithography (CAL) were discussed. This review also provides a comprehensive guide for researchers looking to improve fabrication quality while also providing a basic understanding of the theoretical and practical aspects of light projection to enable standardized optimization of system parameters concerning these 3D printers. More specifically, several key variables that affect the outcome of the printed construct were discussed in detail. For instance, material composition (e.g., photoinitiator sensitivity, critical energy, and depth of penetration of the polymer), light exposure dosage (i.e., duration and power), postcuring processes, and optical properties (e.g., diffraction limit, optical aberrations, light penetration depth, scattering effects, and molecular diffusion) all contribute to the resulting quality of the printed structure. Recognition and understanding of the independent effects of each of these parameters is valuable in the future design and engineering of improved next-generation light-based 3D printers.

ACKNOWLEDGMENTS

This work was supported in part by grants from the National Institutes of Health (R21AR074763, R33HD090662, R01EB021857, R21HD100132) and the National Science Foundation (1937653, 1907434, 1903933). This manuscript is also based upon work supported by the National Science Foundation Graduate Research Fellowship Program under grant no. DGE-1650112.

Biographies

Claire Yu received her bachelor’s degree in Engineering Chemistry from Queen’s University in Kingston, Ontario, Canada. She also received her Ph.D. in Chemical Engineering with specialization in Biomedical Engineering at Queen’s University and was the recipient of the prestigious Natural Sciences and Engineering Research Council (NSERC) Alexander Graham Bell Canada Graduate Scholarship during her studies. In her dissertation, she focused on the development of tissue-specific bioscaffolds produced from human decellularized adipose tissue matrices and adipose-derived stem cells as a cell-based therapy for soft tissue regeneration. Upon graduation, she pursued postdoctoral studies at UCSD in Professor Shaochen Chen’s laboratory and was the recipient of the prestigious NSERC Postdoctoral Fellowship Scholarship. Here, she developed novel biomaterial bioinks for 3D bioprinting and worked on projects fabricating biomimetic tissues for drug testing, in vitro diagnostics, disease modeling, and regenerative medicine. Claire continues to pursue her passion and multidisciplinary experience in biomaterials, 3D bioprinting, and biofabrication, stem cell biology, and 3D cell/tissue culture for tissue engineering and regenerative medicine.

Jacob Schimelman received his B.S.E. degree in Polymer Science and Engineering at Case Western Reserve University. He recently completed his M.S. in NanoEngineering at UCSD and is currently a Ph.D. student in Dr. Shaochen Chen’s laboratory at UCSD. He is a recipient of the prestigious National Science Foundation Graduate Research Fellowship (GRFP) and the 2019 Department of NanoEngineering Graduate Student of the Year award. At UCSD, he is developing 3D-printed scaffolds for neural repair as well as novel biomaterials for bioprinting.

Pengrui Wang received his B.S. and M.S. in Materials Science and Engineering in 2013 and 2014 from University of Michigan, Ann Arbor. Recently, he earned his Ph.D. degree in Materials Science and Engineering from UCSD in 2019. His research was focused on polymer chemistry and establishing relationships between 3D printing process and resulted material properties. Currently, he is working at a plant-based food company to investigate food processing and texture.

Kathleen L. Miller graduated with her bachelor’s degree in Chemical Engineering from Tufts University in Medford, MA. Following her graduation, she worked at Massachusetts General Hospital in microfluidic device and cancer research, sparking her interest in tissue engineering. She received her master’s degree in NanoEngineering from UCSD and is currently working towards her Ph.D. in 3D printed cardiac tissues in Dr. Shaochen Chen's lab.

Xuanyi Ma received her bachelor's degree in Medical Engineering from the University of Hong Kong and Ph.D. in Bioengineering at UCSD in 2018. At UCSD, she worked in Professor Shaochen Chen's lab to establish biomimetic organ models using human iPSC-derived hepatic cells within a hydrogel-based 3D matrix and applying these models for in vitro drug screening and disease modeling. Xuanyi received the 3D Printing Life Science award by MilliporeSigma and was named as a 2018 Siebel Scholar.

Shangting You received his B.S. degree in Optical Engineering from Zhejiang University in 2015 and his Ph.D. degree in Nanoengineering from UCSD in 2019. His research is focused on microscopy, 3D printing, and their biomedical as well as tissue engineering applications.

Jiaao Guan received his B.E. degree in 2017 from McGill University and his M.S. degree in 2019 from UCSD. He is currently pursuing his Ph.D. at UCSD under the supervision of Prof. Shaochen Chen and cosupervised by Prof. Zhaowei Liu. His current research is focused on using machine learning to achieve high fidelity micro- to nanoscale 3D bioprinting and to discover 3D printed material structural properties.

Bingjie Sun received her B.S in Material Chemistry in 2005 and Ph.D. in Polymer Chemistry and Physics in 2010, both from Fudan University, China. During the period of pursuing her Ph.D., she worked two years at Harvard University in the School of Engineering and Applied Sciences. After graduation, she worked as an advisor in ExxonMobil Chemical Department of Product Stewardship & Regulatory Affairs for two and a half years, working on global polymer regulations and advocacy. Afterwards, she continued her research at Harvard University and later at UCSD. She has extensive knowledge on polymer material synthesis, processing, and characterization.

Wei Zhu received his Ph.D. and postdoctoral training in the Nanoengineering Department at UCSD. Prior to that, Dr. Zhu received his B.S. in Optical Engineering at Zhejiang University, China. In addition, he received his micro-MBA certificate from the UCSD Rady School of Management. Dr. Zhu has vast knowledge and expertise in 3D printing, biomaterials, micro/nanofabrication, and tissue engineering with publications in top journals. His work has been covered by numerous mainstream news media including the Wall Street Journal, Washington Post, Forbes, Fortune, etc. His current research focuses on the development of next-generation 3D bioprinters and their applications in tissue engineering and regenerative medicine.

Shaochen Chen is a Professor and Chairman of the Nanoengineering Department at the University of California, San Diego (UCSD). He is the founding director of the Biomaterials and Tissue Engineering Center at UCSD. He is also a faculty member of the Institute of Engineering in Medicine and the Clinical Translational Research Institute at UCSD. Before joining UCSD, Dr. Chen had been a Professor and a Pearlie D. Henderson Centennial Endowed Faculty Fellow in Engineering in the Mechanical Engineering Department at the University of Texas at Austin. From 2008 to 2010, Dr. Chen served as the Program Director for the Nanomanufacturing Program in the National Science Foundation (NSF).

REFERENCES

(1). Edmondson R; Broglie JJ; Adcock AF; Yang L Three-Dimensional Cell Culture Systems and Their Applications in Drug Discovery and Cell-Based Biosensors. Assay Drug Dev. Technol 2014, 12, 207–218. [PubMed: 24831787]

(2). Antoni D; Burckel H; Josset E; Noel G Three-Dimensional Cell Culture: A Breakthrough in Vivo. Int. J. Mol. Sci 2015, 16, 5517–5527. [PubMed: 25768338]

(3). Tibbitt MW; Anseth KS Hydrogels as Extracellular Matrix Mimics for 3D Cell Culture. Biotechnol. Bioeng 2009, 103, 655–663. [PubMed: 19472329]

(4). Frantz C; Stewart KM; Weaver VM The Extracellular Matrix at a Glance. J. Cell Sci 2010, 123, 4195–4200. [PubMed: 21123617]

(5). Ozbolat IT; Peng W; Ozbolat V Application Areas of 3D Bioprinting. Drug Discovery Today 2016, 21, 1257–1271. [PubMed: 27086009]

(6). Murphy SV; Atala A 3D Bioprinting of Tissues and Organs. Nat. Biotechnol 2014, 32, 773–785. [PubMed: 25093879]

(7). Ma X; Liu J; Zhu W; Tang M; Lawrence N; Yu C; Gou M; Chen S 3D Bioprinting of Functional Tissue Models for Personalized Drug Screening and in Vitro Disease Modeling. Adv. Drug Delivery Rev 2018, 132, 235–251.

(8). Yu C; Zhu W; Sun B; Mei D; Gou M; Chen S Modulating Physical, Chemical, and Biological Properties in 3D Printing for Tissue Engineering Applications. Appl. Phys. Rev 2018, 5, 041107. [PubMed: 31938080]

(9). Hull C Apparatus for Production of Three Dimensional Objects by Stereolithography. US US4,575,330A, 1986.

(10). Homan KA; Kolesky DB; Skylar-Scott MA; Herrmann J; Obuobi H; Moisan A; Lewis JA Bioprinting of 3D Convoluted Renal Proximal Tubules on Perfusable Chips. Sci. Rep 2016, 6, 34845. [PubMed: 27725720]

(11). Zhang YS; Arneri A; Bersini S; Shin SR; Zhu K; Goli-Malekabadi Z; Aleman J; Colosi C; Busignani F; Dell'Erba V; et al. Bioprinting 3D Microfibrous Scaffolds for Engineering Endothelialized Myocardium and Heart-on-a-Chip. Biomaterials 2016, 110, 45–59. [PubMed: 27710832]

(12). Hsieh FY; Lin HH; Hsu S-H 3D Bioprinting of Neural Stem Cell-Laden Thermoresponsive Biodegradable Polyurethane Hydrogel and Potential in Central Nervous System Repair. Biomaterials 2015, 71, 48–57. [PubMed: 26318816]

(13). Hornbeck LJ The DMD™ Projection Display Chip: A MEMS-Based Technology. MRS Bull. 2001, 26, 325–327.

(14). Zhang AP; Qu X; Soman P; Hribar KC; Lee JW; Chen S; He S Rapid Fabrication of Complex 3D Extracellular Microenvironments by Dynamic Optical Projection Stereolithography. Adv. Mater 2012, 24, 4266–4270. [PubMed: 22786787]

(15). Ma X; Qu X; Zhu W; Li YS; Yuan S; Zhang H; Liu J; Wang P; Lai CSE; Zanella F; et al. Deterministically Patterned Biomimetic Human IPSC-Derived Hepatic Model via Rapid 3D Bioprinting. Proc. Natl. Acad. Sci. U. S. A 2016, 113, 2206–2211. [PubMed: 26858399]

(16). Koffler J; Zhu W; Qu X; Platoshyn O; Dulin JN; Brock J; Graham L; Lu P; Sakamoto J; Marsala M; et al. Biomimetic 3D-Printed Scaffolds for Spinal Cord Injury Repair. Nat. Med 2019, 25, 263–269. [PubMed: 30643285]

(17). Bernal PN; Delrot P; Loterie D; Li Y; Malda J; Moser C; Levato R Volumetric Bioprinting of Complex Living-Tissue Constructs within Seconds. Adv. Mater 2019, 31, 1904209.

(18). Kannurpatti AR; Peiffer RW; Guymon CA; Bowman CN Photochemistry of Polymers: Photopolymerization Fundamentals and Applications; SPIE, 1996; Vol. 10285.

(19). Nguyen KT; West JL Photopolymerizable Hydrogels for Tissue Engineering Applications. Biomaterials 2002, 23, 4307–4314. [PubMed: 12219820]

(20). Ifkovits JL; Burdick JA Review: Photopolymerizable and Degradable Biomaterials for Tissue Engineering Applications. Tissue Eng. 2007, 13, 2369–2385. [PubMed: 17658993]

(21). Dhariwala B; Hunt E; Boland T Rapid Prototyping of Tissue-Engineering Constructs, Using Photopolymerizable Hydrogels and Stereolithography. Tissue Eng. 2004, 10, 1316–1322. [PubMed: 15588392]

(22). Mandrycky C; Wang Z; Kim K; Kim DH 3D Bioprinting for Engineering Complex Tissues In Biotechnology Advances; Elsevier, 2016; pp 422–434.

(23). Cowie JMG; Valeria A Polymers: Chemistry and Physics of Modern Materials, 3rd ed.; CRC Press, 2007.

(24). Odian G Principles of Polymerization, 4th ed.; John Wiley & Sons: Hoboken, NJ, 2004.

(25). Ma X; Dewan S; Liu J; Tang M; Miller KL; Yu C; Lawrence N; McCulloch AD; Chen S 3D Printed Micro-Scale Force Gauge Arrays to Improve Human Cardiac Tissue Maturation and Enable High Throughput Drug Testing. Acta Biomater. 2019, 95, 319–327. [PubMed: 30576862]

(26). Choi JR; Yong KW; Choi JY; Cowie AC Recent Advances in Photo-Crosslinkable Hydrogels for Biomedical Applications. BioTechniques 2019, 66, 40–53. [PubMed: 30730212]

(27). Zorlutuna P; Annabi N; Camci-unal G; Nikkhah M; Cha JM; Nichol JW; Manbachi A; Bae H; Chen S; Khademhosseini A Microfabricated Biomaterials for Engineering 3D Tissues. Adv. Mater 2012, 24, 1782–1804. [PubMed: 22410857]

(28). Fairbanks BD; Schwartz MP; Bowman CN; Anseth KS Photoinitiated Polymerization of PEG-Diacrylate with Lithium Phenyl-2,4,6-Trimethylbenzoylphosphinate: Polymerization Rate and Cytocompatibility. Biomaterials 2009, 30, 6702–6707. [PubMed: 19783300]

(29). Ruskowitz ER; Deforest CA Proteome-Wide Analysis of Cellular Response to Ultraviolet Light for Biomaterial Synthesis and Modification. ACS Biomater. Sci. Eng 2019, 5, 2111–2116.

(30). Shih H; Lin C Visible-Light-Mediated Thiol-Ene Hydrogelation Using Eosin-Y as the Only Photoinitiator. Macromol. Rapid Commun 2013, 34, 269–273. [PubMed: 23386583]

(31). DeForest CA; Anseth KS Photoreversible Patterning of Biomolecules within Click-Based Hydrogels. Angew. Chem., Int. Ed 2012, 51, 1816–1819.

(32). Seiffert S Origin of Nanostructural Inhomogeneity in Polymer-Network Gels. Polym. Chem 2017, 8, 4472–4487.

(33). Sunyer R; Jin AJ; Nossal R; Sackett DL Fabrication of Hydrogels with Steep Stiffness Gradients for Studying Cell Mechanical Response. PLoS One 2012, 7, e46107. [PubMed: 23056241]

(34). Kade MJ; Burke DJ; Hawker CJ The Power of Thiol-Ene Chemistry. J. Polym. Sci., Part A: Polym. Chem 2010, 48, 743–750.

(35). Massi A; Nanni D Thiol–Yne Coupling: Revisiting Old Concepts as a Breakthrough for up-to-Date Applications. Org. Biomol. Chem 2012, 10, 3791–3807. [PubMed: 22491759]

(36). Xu Y; Xiong X; Cai L; Tang Z; Ye Z Thiol-Ene Click Chemistry. Prog. Chem 2012, 24, 385–394.

(37). Nair DP; Podgórski M; Chatani S; Gong T; Xi W; Fenoli CR; Bowman CN The Thiol-Michael Addition Click Reaction: A Powerful and Widely Used Tool in Materials Chemistry. Chem. Mater 2014, 26, 724–744.

(38). Lowe AB Thiol-Ene “Click” Reactions and Recent Applications in Polymer and Materials Synthesis: A First Update. Polym. Chem 2014, 5, 4820–4870.

(39). Roppolo I; Frascella F; Gastaldi M; Castellino M; Ciubini B; Barolo C; Scaltrito L; Nicosia C; Zanetti M; Chiappone A Thiol–Yne Chemistry for 3D Printing: Exploiting an off-Stoichio-metric Route for Selective Functionalization of 3D Objects. Polym. Chem 2019, 10, 5950–5958.

(40). Herner A; Lin Q Photo-Triggered Click Chemistry for Biological Applications. Top. Curr. Chem 2016, 374, 1.

(41). Ramapanicker R; Chauhan P Click Chemistry: Mechanistic and Synthetic Perspectives In Click Reactions in Organic Synthesis; Chandrasekaran S, Ed.; Wiley-VCH, 2016; pp 1–24.

(42). Chen RT; Marchesan S; Evans RA; Styan KE; Such GK; Postma A; McLean KM; Muir BW; Caruso F Photoinitiated Alkyne–Azide Click and Radical Cross-Linking Reactions for the Patterning of PEG Hydrogels. Biomacromolecules 2012, 13, 889–895. [PubMed: 22332589]

(43). Kharasch MS; Read AT; Mayo FR The Peroxide Effect in the Addition of Reagents to Unsaturated Compounds. XVI. The Addition of Thioglycolic Acid to Styrene and Isobutylene. Chem. Ind 1938, 57, 752–754.

(44). Hoyle CE; Hensel RD; Grubb MB Laser-Initiated Polymerization of a Thiol-Ene System. Polym. Photochem 1984, 4, 69–80.

(45). Hoyle CE; Lee TY; Roper T Thiol-Enes: Chemistry of the Past with Promise for the Future. J. Polym. Sci., Part A: Polym. Chem 2004, 42, 5301–5338.

(46). Lee TY; Roper TM; Jonsson ES; Guymon CA; Hoyle CE Thiol-Ene Photopolymerization Kinetics of Vinyl Acrylate/Multi-functional Thiol Mixtures. Macromolecules 2004, 37, 3606–3613.

(47). Dondoni A The Emergence of Thiol-Ene Coupling as a Click Process for Materials and Bioorganic Chemistry. Angew. Chem., Int. Ed 2008, 47, 8995–8997.

(48). Schlaad H Thiol-X Chemistry in Polymer Science. Polymer 2014, 55, 5509–5510.

(49). Toepke MW; Impellitteri NA; Theisen JM; Murphy WL Characterization of Thiol-Ene Crosslinked PEG Hydrogels. Macromol. Mater. Eng 2013, 298, 699–703. [PubMed: 24883041]

(50). Azagarsamy MA; Anseth KS Bioorthogonal Click Chemistry: An Indispensable Tool to Create Multifaceted Cell Culture Scaffolds. ACS Macro Lett. 2013, 2, 5–9. [PubMed: 23336091]

(51). Yilmaz G; Yagci Y Light-Induced Step-Growth Polymerization. Prog. Polym. Sci 2020, 100, 101178.

(52). Wiley KL; Ovadia EM; Calo CJ; Huber RE; Kloxin AM Rate-Based Approach for Controlling the Mechanical Properties of ‘Thiol–Ene’ Hydrogels Formed with Visible Light. Polym. Chem 2019, 10, 4428–4440. [PubMed: 32405326]

(53). Khire VS; Lee TY; Bowman CN Surface Modification Using Thiol-Acrylate Conjugate Addition Reactions. Macromolecules 2007, 40, 5669–5677.

(54). Hoffmann A; Leonards H; Tobies N; Pongratz L; Kreuels K; Kreimendahl F; Apel C; Wehner M; Nottrodt N New Stereolithographic Resin Providing Functional Surfaces for Biocompatible Three-Dimensional Printing. J. Tissue Eng 2017, 8, 2041731417744485. [PubMed: 29318001]

(55). Hong T; Liu W; Li M; Chen C Click Chemistry at the Microscale. Analyst 2019, 144, 1492–1512. [PubMed: 30632547]

(56). Hillmering M; Pardon G; Vastesson A; Supekar O; Carlborg CF; Brandner BD; van der Wijngaart W; Haraldsson T Off-Stoichiometry Improves the Photostructuring of Thiol–Enes through Diffusion-Induced Monomer Depletion. Microsystems Nanoeng. 2016, 2, 15043.

(57). Xin S; Chimene D; Garza JE; Gaharwar AK; Alge DL Clickable PEG Hydrogel Microspheres as Building Blocks for 3D Bioprinting. Biomater. Sci 2019, 7, 1179–1187. [PubMed: 30656307]

(58). Carlborg CF; Haraldsson T; Öberg K; Malkoch M; Van Der Wijngaart W Beyond PDMS: Off-Stochiometry Thiol-Ene Based Soft Lithography for Rapid Prototyping of Microfluidic Devices. Lab Chip 2011, 11, 136.

(59). Kharasch MS; Nudenberg W; Mantell GJ Reactions of Atoms and Free Radicals in Solution. XXV. the Reactions of Olefins with Mercaptans in the Presence of Oxygen. J. Org. Chem 1951, 16, 524–532.

(60). Machado TO; Sayer C; Araujo PHH Thiol-Ene Polymerisation: A Promising Technique to Obtain Novel Biomaterials. Eur. Polym. J 2017, 86, 200–215.

(61). Cole MA; Jankousky KC; Bowman CN Redox Initiation of Bulk Thiol-Ene Polymerizations. Polym. Chem 2013, 4, 1167–1175. [PubMed: 23565125]

(62). Cramer NB; Reddy SK; O’Brien AK; Bowman CN Thiol–Ene Photopolymerization Mechanism and Rate Limiting Step Changes for Various Vinyl Functional Group Chemistries. Macromolecules 2003, 36, 7964–7969.

(63). Fairbanks BD; Schwartz MP; Halevi AE; Nuttelman CR; Bowman CN; Anseth KS A Versatile Synthetic Extracellular Matrix Mimic via Thiol-Norbornene Photopolymerization. Adv. Mater 2009, 21, 5005–5010. [PubMed: 25377720]

(64). Hoyle CE; Bowman CN Thiol-Ene Click Chemistry. Angew. Chem., Int. Ed 2010, 49, 1540–1573.

(65). O’Brien AK; Cramer NB; Bowman CN Oxygen Inhibition in Thiol–Acrylate Photopolymerizations. J. Polym. Sci., Part A: Polym. Chem 2006, 44, 2007–2014.

(66). Rydholm AE; Bowman CN; Anseth KS Degradable Thiol-Acrylate Photopolymers: Polymerization and Degradation Behavior of an in Situ Forming Biomaterial. Biomaterials 2005, 26, 4495–4506. [PubMed: 15722118]

(67). Northrop BH; Coffey RN Thiol–Ene Click Chemistry: Computational and Kinetic Analysis of the Influence of Alkene Functionality. J. Am. Chem. Soc 2012, 134, 13804–13817. [PubMed: 22853003]

(68). Cramer NB; Davies T; O'Brien AK; Bowman CN Mechanism and Modeling of a Thiol–Ene Photopolymerization. Macromolecules 2003, 36, 4631–4636.

(69). Ramapanicker R; Chauhan P Click Chemistry: Mechanistic and Synthetic Perspectives In Click Reactions in Organic Synthesis; Chandrasekaran S, Ed.; Wiley-VCH, 2016; pp 1–24.

(70). Rehmann MS; Skeens KM; Kharkar PM; Ford EM; Maverakis E; Lee KH; Kloxin AM Tuning and Predicting Mesh Size and Protein Release from Step Growth Hydrogels. Biomacromolecules 2017, 18, 3131–3142. [PubMed: 28850788]

(71). Jivan F; Fabela N; Davis Z; Alge DL Orthogonal Click Reactions Enable the Synthesis of ECM-Mimetic PEG Hydrogels without Multi-Arm Precursors. J. Mater. Chem. B 2018, 6, 4929–4936. [PubMed: 30746148]

(72). Ooi HW; Mota C; ten Cate AT; Calore A; Moroni L; Baker MB Thiol-Ene Alginate Hydrogels as Versatile Bioinks for Bioprinting. Biomacromolecules 2018, 19, 3390–3400. [PubMed: 29939754]

(73). Tigner TJ; Rajput S; Gaharwar AK; Alge DL Comparison of Photocrosslinkable Gelatin Derivatives and Initiators for Three-Dimensional Extrusion Bioprinting. Biomacromolecules 2020, 21, 454–463.

(74). Mũnoz Z; Shih H; Lin CC Gelatin Hydrogels Formed by Orthogonal Thiol-Norbornene Photochemistry for Cell Encapsulation. Biomater. Sci 2014, 2, 1063–1072. [PubMed: 32482001]

(75). Dobos A; Van Hoorick J; Steiger W; Gruber P; Markovic M; Andriotis OG; Rohatschek A; Dubruel P; Thurner PJ; Van Vlierberghe S; et al. Thiol–Gelatin–Norbornene Bioink for Laser-Based High-Definition Bioprinting. Adv. Healthcare Mater 2019, 1900752.

(76). Van Hoorick J; Gruber P; Markovic M; Rollot M; Graulus GJ; Vagenende M; Tromayer M; Van Erps J; Thienpont H; Martins JC; et al. Highly Reactive Thiol-Norbornene Photo-Click Hydrogels: Toward Improved Processability. Macromol. Rapid Commun 2018, 39, 1800181.

(77). Greene T; Lin C-C Modular Cross-Linking of Gelatin-Based Thiol–Norbornene Hydrogels for in Vitro 3D Culture of Hepatocellular Carcinoma Cells. ACS Biomater. Sci. Eng 2015, 1, 1314–1323.

(78). Seiffert S Scattering Perspectives on Nanostructural Inhomogeneity in Polymer Network Gels. Prog. Polym. Sci 2017, 66, 1–21.

(79). Hillmering M; Pardon G; Vastesson A; Supekar O; Carlborg CF; Brandner BD; van der Wijngaart W; Haraldsson T Off-Stoichiometry Improves the Photostructuring of Thiol–Enes through Diffusion-Induced Monomer Depletion. Microsystems Nanoeng. 2016, 2, 15043–7.

(80). Fredrik CF; Haraldsson T; Öberg K; Malkoch M; van der Wijngaart W Beyond PDMS: Off-Stoichiometry Thiol – Ene (OSTE) Based Soft Lithography for Rapid Prototyping of Microfluidic Devices. Lab Chip 2011, 11, 3136–3147. [PubMed: 21804987]

(81). Hoffmann A; Leonards H; Tobies N; Pongratz L; Kreuels K; Kreimendahl F; Apel C; Wehner M; Nottrodt N New Stereolithographic Resin Providing Functional Surfaces for Biocompatible Three-Dimensional Printing. J. Tissue Eng 2017, 8, 2041731417744485. [PubMed: 29318001]

(82). Xin S; Chimene D; Garza JE; Gaharwar AK; Alge DL Clickable PEG Hydrogel Microspheres as Building Blocks for 3D Bioprinting. Biomater. Sci 2019, 7, 1179–1187. [PubMed: 30656307]

(83). Grim JC; Brown TE; Aguado BA; Chapnick DA; Viert AL; Liu X; Anseth KS A Reversible and Repeatable Thiol–Ene Bioconjugation for Dynamic Patterning of Signaling Proteins in Hydrogels. ACS Cent. Sci 2018, 4, 909–916. [PubMed: 30062120]

(84). Wu DC; Loh XJ; Wu YL; Lay CL; Liu Y Living" Controlled in Situ Gelling Systems: Thiol-Disulfide Exchange Method toward Tailor-Made Biodegradable Hydrogels. J. Am. Chem. Soc 2010, 132, 15140–15143. [PubMed: 20929223]

(85). Scott TF; Kowalski BA; Sullivan AC; Bowman CN; McLeod RR Two-Color Single-Photon Photoinitiation and Photoinhibition for Subdiffraction Photolithography. Science (Washington, DC, U. S.) 2009, 324, 913–917.

(86). Lovell LG; Elliott BJ; Brown JR; Bowman CN The Effect of Wavelength on the Polymerization of Multi(Meth)Acrylates with Disulfide/Benzilketal Combinations. Polymer 2001, 42, 421–429.

(87). van der Laan HL; Burns MA; Scott TF Volumetric Photopolymerization Confinement through Dual-Wavelength Photoinitiation and Photoinhibition. ACS Macro Lett. 2019, 8, 899–904.

(88). Kabasakalian P; Townley ER Photolysis of Nitrite Esters in Solution. I. Photochemistry of n-Octyl Nitrite. J. Am. Chem. Soc 1962, 84, 2711–2716.

(89). De Beer MP; Van Der Laan HL; Cole MA; Whelan RJ; Burns MA; Scott TF Rapid, Continuous Additive Manufacturing by Volumetric Polymerization Inhibition Patterning. Sci. Adv 2019, 5, No. eaau8723. [PubMed: 30746465]

(90). Tumbleston JR; Shirvanyants D; Ermoshkin N; Janusziewicz R; Johnson AR; Kelly D; Chen K; Pinschmidt R; Rolland JP; Ermoshkin A; et al. Continuous Liquid Interface Production of 3D Objects. Science (Washington, DC, U. S.) 2015, 347, 1349–1352.

(91). Siegenthaler KO; Studer A Nitroxide-Mediated Radical Polymerization/Increase of Steric Demand in Nitroxides. How Much Is Too Much? Macromolecules 2006, 39, 1347–1352.

(92). Ouyang X; Zhang K; Wu J; Wong DSH; Feng Q; Bian L; Zhang AP Optical μ-Printing of Cellular-Scale Microscaffold Arrays for 3D Cell Culture. Sci. Rep 2017, 7, 8880. [PubMed: 28827528]

(93). Stevens LJ; Burgess JR; Stochelski MA; Kuczek T Amounts of Artificial Food Dyes and Added Sugars in Foods and Sweets Commonly Consumed by Children. Clin. Pediatr. (Philadelphia) 2015, 54, 309–321.

(94). Grigoryan B; Paulsen SJ; Corbett DC; Sazer DW; Fortin CL; Zaita AJ; Greenfield PT; Calafat NJ; Gounley JP; Ta AH; et al. Multivascular Networks and Functional Intravascular Topologies within Biocompatible Hydrogels. Science (Washington, DC, U. S.) 2019, 364, 458–464.

(95). Nong HV; Hung LX; Thang PN; Chinh VD; Vu LV; Dung PT; Van Trung T; Nga PT Fabrication and Vibration Characterization of Curcumin Extracted from Turmeric (Curcuma Longa) Rhizomes of the Northern Vietnam. SpringerPlus 2016, 5, 1147. [PubMed: 27504245]

(96). Desai N; Finosh GT; Panicker NG; Ramachandran R; Varghese A Cytotoxic Effects of Curcumin At Various Concentrations and Role of Curcumin on Lipid Peroxidation and Activities of Antioxidant Enzymes of the Rat Peripheral Blood Lymphocytes. Blood 2011, 118, 4933–4933a.

(97). Merzlyak MN; Chivkunova OB; Solovchenko AE; Naqvi KR Light Absorption by Anthocyanins in Juvenile, Stressed, and Senescing Leaves. J. Exp. Bot 2008, 59, 3903–3911. [PubMed: 18796701]

(98). Simon U; Dimartino S Direct 3D Printing of Monolithic Ion Exchange Adsorbers. J. Chromatogr. A 2019, 1587, 119–128. [PubMed: 30579643]

(99). Obaid MK; Abdullah LC; Idan IJ Removal of Reactive Orange 16 Dye from Aqueous Solution by Using Modified Kenaf Core Fiber. J. Chem 2016, 2016, 1–7.

(100). Kumar S; Aaron J; Sokolov K Directional Conjugation of Antibodies to Nanoparticles for Synthesis of Multiplexed Optical Contrast Agents with Both Delivery and Targeting Moieties. Nat. Protoc 2008, 3, 314–320. [PubMed: 18274533]

(101). Brüning A; Kast RE Oxidizing to Death: Disulfiram for Cancer Cell Killing. Cell Cycle 2014, 13, 1513–1514. [PubMed: 24759086]

(102). Hu K; An J; Yoon YJ Two-Wavelength, Photo-Initiation and Photo-Inhibition Competing for Selective Photo-Patterning of Hydrogel Porous Microstructures. Int. J. Precis. Eng. Manuf 2018, 19, 729–735.

(103). Wang E; Liu Y; Xu C; Liu J Antiproliferative and Proapoptotic Activities of Anthocyanin and Anthocyanidin Extracts from Blueberry Fruits on B16-F10 Melanoma Cells. Food Nutr. Res 2017, 61, 1325308. [PubMed: 28680383]

(104). Yu H; Li J; Wu D; Qiu Z; Zhang Y Chemistry and Biological Applications of Photo-Labile Organic Molecules. Chem. Soc. Rev 2010, 39, 464–473. [PubMed: 20111771]

(105). Klán P; Šolomek T; Bochet CG; Blanc A; Givens R; Rubina M; Popik V; Kostikov A; Wirz J Photoremovable Protecting Groups in Chemistry and Biology: Reaction Mechanisms and Efficacy. Chem. Rev 2013, 113, 119–191. [PubMed: 23256727]

(106). Schwörer M; Wirz J Photochemical Reaction Mechanisms of 2-Nitrobenzyl Compounds in Solution, I. 2-Nitrotoluene: Thermodynamic and Kinetic Parameters of Theaci-Nitro Tautomer. Helv. Chim. Acta 2001, 84, 1441–1458.

(107). Adams SR; Kao JPY; Tsien RY Biologically Useful Chelators That Take up Calcium(2+) upon Illumination. J. Am. Chem. Soc 1989, 111, 7957–7968.

(108). Wieboldt R; Gee KR; Niu L; Ramesh D; Carpenter BK; Hess GP Photolabile Precursors of Glutamate: Synthesis, Photochemical Properties, and Activation of Glutamate Receptors on a Microsecond Time Scale. Proc. Natl. Acad. Sci. U. S. A 1994, 91, 8752–8756. [PubMed: 8090718]

(109). Momotake A; Lindegger N; Niggli E; Barsotti RJ; Ellis-Davies GCR The Nitrodibenzofuran Chromophore: A New Caging Group for Ultra-Efficient Photolysis in Living Cells. Nat. Methods 2006, 3, 35–40. [PubMed: 16369551]

(110). Schade B; Hagen V; Schmidt R; Herbrich R; Krause E; Eckardt T; Bendig J Deactivation Behavior and Excited-State Properties of (Coumarin-4-Yl)Methyl Derivatives. 1. Photocleavage of (7-Methoxycoumarin-4-Yl)Methyl-Caged Acids with Fluorescence Enhancement. J. Org. Chem 1999, 64, 9109–9117.

(111). Furuta T; Takeuchi H; Isozaki M; Takahashi Y; Kanehara M; Sugimoto M; Watanabe T; Noguchi K; Dore TM; Kurahashi T; et al. Bhc-CNMPs as Either Water-Soluble or Membrane-Permeant Photoreleasable Cyclic Nucleotides for Both One- and Two-Photon Excitation. ChemBioChem 2004, 5, 1119–1128. [PubMed: 15300837]

(112). Givens RS; Jung A; Park C-H; Weber J; Bartlett W New Photoactivated Protecting Groups. 7. p-Hydroxyphenacyl: A Photo-trigger for Excitatory Amino Acids and Peptides 1. J. Am. Chem. Soc 1997, 119, 8369–8370.

(113). Matsuzaki M; Honkura N; Ellis-Davies GCR; Kasai H Structural Basis of Long-Term Potentiation in Single Dendritic Spines. Nature 2004, 429, 761–766. [PubMed: 15190253]

(114). Wang X; Ao Q; Tian X; Fan J; Tong H; Hou W; Bai S Gelatin-Based Hydrogels for Organ 3D Bioprinting. Polymers (Basel, Switz.) 2017, 9, 401.

(115). Van Den Bulcke AI; Bogdanov B; De Rooze N; Schacht EH; Cornelissen M; Berghmans H Structural and Rheological Properties of Methacrylamide Modified Gelatin Hydrogels. Biomacromolecules 2000, 1, 31–38. [PubMed: 11709840]

(116). Zhu W; Ma X; Gou M; Mei D; Zhang K; Chen S 3D Printing of Functional Biomaterials for Tissue Engineering. Curr. Opin. Biotechnol 2016, 40, 103–112. [PubMed: 27043763]

(117). Liu J; He J; Liu J; Ma X; Chen Q; Lawrence N; Zhu W; Xu Y; Chen S Rapid 3D Bioprinting of in Vitro Cardiac Tissue Models Using Human Embryonic Stem Cell-Derived Cardiomyocytes. Bioprinting 2019, 13, e00040. [PubMed: 31572807]

(118). Lee BH; Shirahama H; Cho NJ; Tan LP Efficient and Controllable Synthesis of Highly Substituted Gelatin Methacrylamide for Mechanically Stiff Hydrogels. RSC Adv. 2015, 5, 106094–106097.

(119). Shirahama H; Lee BH; Tan LP; Cho NJ Precise Tuning of Facile One-Pot Gelatin Methacryloyl (GelMA) Synthesis. Sci. Rep 2016, 6, 31036. [PubMed: 27503340]

(120). Zhu M; Wang Y; Ferracci G; Zheng J; Cho NJ; Lee BH Gelatin Methacryloyl and Its Hydrogels with an Exceptional Degree of Controllability and Batch-to-Batch Consistency. Sci. Rep 2019, 9, 6863. [PubMed: 31053756]

(121). Klotz BJ; Gawlitta D; Rosenberg AJWP; Malda J; Melchels FPW Gelatin-Methacryloyl Hydrogels: Towards Biofabrication-Based Tissue Repair. Trends Biotechnol. 2016, 34, 394–407. [PubMed: 26867787]

(122). Vining KH; Mooney DJ Mechanical Forces Direct Stem Cell Behaviour in Development and Regeneration. Nat. Rev. Mol. Cell Biol 2017, 18, 728–742. [PubMed: 29115301]

(123). Ma X; Yu C; Wang P; Xu W; Wan X; Lai CSE; Liu J; Koroleva-Maharajh A; Chen S Rapid 3D Bioprinting of Decellularized Extracellular Matrix with Regionally Varied Mechanical Properties and Biomimetic Microarchitecture. Biomaterials 2018, 185, 310–321. [PubMed: 30265900]

(124). Huang TQ; Qu X; Liu J; Chen S 3D Printing of Biomimetic Microstructures for Cancer Cell Migration. Biomed. Microdevices 2014, 16, 127–132. [PubMed: 24150602]

(125). Ren J; Han P; Ma X; Farah EN; Bloomekatz J; Zeng X-XI; Zhang R; Swim MM; Witty AD; Knight HG; Deshpande R; Xu W; Yelon D; Chen S; Chi NC Canonical Wnt5b Signaling Directs Outlying Nkx2.5+ Mesoderm into Pacemaker Cardiomyocytes. Dev. Cell 2019, 50, 729. [PubMed: 31402282]

(126). Lin CC; Raza A; Shih H PEG Hydrogels Formed by Thiol-Ene Photo-Click Chemistry and Their Effect on the Formation and Recovery of Insulin-Secreting Cell Spheroids. Biomaterials 2011, 32, 9685–9695. [PubMed: 21924490]

(127). Greene T; Lin C-C Modular Cross-Linking of Gelatin-Based Thiol–Norbornene Hydrogels for in Vitro 3D Culture of Hepatocellular Carcinoma Cells. ACS Biomater. Sci. Eng 2015, 1, 1314.

(128). Bertlein S; Brown G; Lim KS; Jungst T; Boeck T; Blunk T; Tessmar J; Hooper GJ; Woodfield TBF; Groll J Thiol–Ene Clickable Gelatin: A Platform Bioink for Multiple 3D Biofabrication Technologies. Adv. Mater 2017, 29, 1703404.

(129). Chattopadhyay S; Raines RT Review: Collagen-Based Biomaterials for Wound Healing Biopolymers. John Wiley and Sons: Hoboken, NJ, 2014; pp 821–833.

(130). Ricard-Blum S The Collagen Family. Cold Spring Harbor Perspect. Biol 2011, 3, a004978.

(131). Parenteau-Bareil R; Gauvin R; Berthod F Collagen-Based Biomaterials for Tissue Engineering Applications. Materials 2010, 3, 1863–1887.

(132). Shoulders MD; Raines RT Collagen Structure and Stability. Annu. Rev. Biochem 2009, 78, 929–958. [PubMed: 19344236]

(133). Gough JE; Scotchford CA; Downes S Cytotoxicity of Glutaraldehyde Crosslinked Collagen/Poly(Vinyl Alcohol) Films Is by the Mechanism of Apoptosis. J. Biomed. Mater. Res 2002, 61, 121–130. [PubMed: 12001254]

(134). Sundararaghavan HG; Monteiro GA; Lapin NA; Chabal YJ; Miksan JR; Shreiber DI Genipin-Induced Changes in Collagen Gels: Correlation of Mechanical Properties to Fluorescence. J. Biomed. Mater. Res., Part A 2008, 87A, 308–320.

(135). Orban JM; Wilson LB; Kofroth JA; El-Kurdi MS; Maul TM; Vorp DA Crosslinking of Collagen Gels by Transglutaminase. J. Biomed. Mater. Res 2004, 68A, 756–762.

(136). Hinton TJ; Jallerat Q; Palchesko RN; Park JH; Grodzicki MS; Shue H-J; Ramadan MH; Hudson AR; Feinberg AW Three-Dimensional Printing of Complex Biological Structures by Freeform Reversible Embedding of Suspended Hydrogels. Sci. Adv 2015, 1, No. e1500758. [PubMed: 26601312]

(137). Lee A; Hudson AR; Shiwarski DJ; Tashman JW; Hinton TJ; Yerneni S; Bliley JM; Campbell PG; Feinberg AW 3D Bioprinting of Collagen to Rebuild Components of the Human Heart. Science (Washington, DC, U. S.) 2019, 365, 482–487.

(138). Gaudet ID; Shreiber DI Characterization of Methacrylated Type-I Collagen as a Dynamic, Photoactive Hydrogel. Biointerphases 2012, 7, 25. [PubMed: 22589068]

(139). Drzewiecki KE; Malavade JN; Ahmed I; Lowe CJ; Shreiber DI A Thermoreversible, Photocrosslinkable Collagen BioInk for Free-Form Fabrication of Scaffolds for Regenerative Medicine. Technology 2017, 05, 185–195.

(140). Bell A; Kofron M; Nistor V Multiphoton Crosslinking for Biocompatible 3D Printing of Type I Collagen. Biofabrication 2015, 7, 035007. [PubMed: 26335389]

(141). Frischknecht R; Seidenbecher CI The Crosstalk of Hyaluronan-Based Extracellular Matrix and Synapses. Neuron Glia Biology 2008, 4, 249–257. [PubMed: 19811705]

(142). Park D; Kim Y; Kim H; Kim K; Lee YS; Choe J; Hahn JH; Lee H; Jeon J; Choi C; et al. Hyaluronic Acid Promotes Angiogenesis by Inducing RHAMM-TGFβ Receptor Interaction via CD44-PKCδ. Mol. Cells 2012, 33, 563–574. [PubMed: 22610405]

(143). Toole BP Hyaluronan: From Extracellular Glue to Pericellular Cue. Nat. Rev. Cancer 2004, 4, 528–539. [PubMed: 15229478]

(144). Xu X; Jha AK; Harrington DA; Farach-Carson MC; Jia X Hyaluronic Acid-Based Hydrogels: From a Natural Polysaccharide to Complex Networks. Soft Matter 2012, 8, 3280–3294. [PubMed: 22419946]

(145). Badylak SF The Extracellular Matrix as a Biologic Scaffold Material. Biomaterials 2007, 28, 3587–3593. [PubMed: 17524477]

(146). Garreta E; Oria R; Tarantino C; Pla-Roca M; Prado P; Fernández-Avilés F; Campistol JM; Samitier J; Montserrat N Tissue Engineering by Decellularization and 3D Bioprinting. Mater. Today 2017, 20, 166–178.

(147). Crapo PM; Gilbert TW; Badylak SF An Overview of Tissue and Whole Organ Decellularization Processes. Biomaterials 2011, 32, 3233–3243. [PubMed: 21296410]

(148). Pati F; Jang J; Ha D-H; Won Kim S; Rhie J-W; Shim J-H; Kim D-H; Cho D-W Printing Three-Dimensional Tissue Analogues with Decellularized Extracellular Matrix Bioink. Nat. Commun 2014, 5, 3935. [PubMed: 24887553]

(149). Skardal A; Devarasetty M; Kang HW; Mead I; Bishop C; Shupe T; Lee SJ; Jackson J; Yoo J; Soker S; et al. A Hydrogel Bioink Toolkit for Mimicking Native Tissue Biochemical and Mechanical Properties in Bioprinted Tissue Constructs. Acta Biomater. 2015, 25, 24–34. [PubMed: 26210285]

(150). Jang J; Kim TG; Kim BS; Kim S-W; Kwon S-M; Cho D-W Tailoring Mechanical Properties of Decellularized Extracellular Matrix Bioink by Vitamin B2-Induced Photo-Crosslinking. Acta Biomater. 2016, 33, 88–95. [PubMed: 26774760]

(151). Panwar A; Tan L Current Status of Bioinks for Micro-Extrusion-Based 3D Bioprinting. Molecules 2016, 21, 685.

(152). Yu C; Ma X; Zhu W; Wang P; Miller KL; Stupin J; Koroleva-Maharajh A; Hairabedian A; Chen S Scanningless and Continuous 3D Bioprinting of Human Tissues with Decellularized Extracellular Matrix. Biomaterials 2019, 194, 1–13. [PubMed: 30562651]

(153). Axpe E; Oyen M Applications of Alginate-Based Bioinks in 3D Bioprinting. Int. J. Mol. Sci 2016, 17, 1976.

(154). Freeman FE; Kelly DJ Tuning Alginate Bioink Stiffness and Composition for Controlled Growth Factor Delivery and to Spatially Direct MSC Fate within Bioprinted Tissues. Sci. Rep 2017, 7, 17042. [PubMed: 29213126]

(155). Jeon O; Bouhadir KH; Mansour JM; Alsberg E Photocrosslinked Alginate Hydrogels with Tunable Biodegradation Rates and Mechanical Properties. Biomaterials 2009, 30, 2724–2734. [PubMed: 19201462]

(156). Chou AI; Nicoll SB Characterization of Photocrosslinked Alginate Hydrogels for Nucleus Pulposus Cell Encapsulation. J. Biomed. Mater. Res., Part A 2009, 91A, 187–194.

(157). Chou AI; Akintoye SO; Nicoll SB Photo-Crosslinked Alginate Hydrogels Support Enhanced Matrix Accumulation by Nucleus Pulposus Cells in Vivo. Osteoarthr. Cartil 2009, 17, 1377–1384.

(158). Omobono MA; Zhao X; Furlong MA; Kwon CH; Gill TJ; Randolph MA; Redmond RW Enhancing the Stiffness of Collagen Hydrogels for Delivery of Encapsulated Chondrocytes to Articular Lesions for Cartilage Regeneration. J. Biomed. Mater. Res., Part A 2015, 103, 1332–1338.

(159). Borzacchiello A; Russo L; Malle BM; Schwach-Abdellaoui K; Ambrosio L Hyaluronic Acid Based Hydrogels for Regenerative Medicine Applications. BioMed Res. Int 2015, 2015, 871218. [PubMed: 26090451]

(160). West ER; Xu M; Woodruff TK; Shea LD Physical Properties of Alginate Hydrogels and Their Effects on in Vitro Follicle Development. Biomaterials 2007, 28, 4439–4448. [PubMed: 17643486]

(161). Tabriz AG; Hermida MA; Leslie NR; Shu W Three-Dimensional Bioprinting of Complex Cell Laden Alginate Hydrogel Structures. Biofabrication 2015, 7, 045012. [PubMed: 26689257]

(162). Zhu W; Tringale KR; Woller SA; You S; Johnson S; Shen H; Schimelman J; Whitney M; Steinauer J; Xu W; et al. Rapid Continuous 3D Printing of Customizable Peripheral Nerve Guidance Conduits. Mater. Today 2018, 21, 951–959.

(163). Wolf K; Te Lindert M; Krause M; Alexander S; Te Riet J; Willis AL; Hoffman RM; Figdor CG; Weiss SJ; Friedl P Physical Limits of Cell Migration: Control by ECM Space and Nuclear Deformation and Tuning by Proteolysis and Traction Force. J. Cell Biol 2013, 201, 1069–1084. [PubMed: 23798731]

(164). Yang Y; Motte S; Kaufman LJ Pore Size Variable Type I Collagen Gels and Their Interaction with Glioma Cells. Biomaterials 2010, 31, 5678–5688. [PubMed: 20430434]

(165). Wang Y; Ma M; Wang J; Zhang W; Lu W; Gao Y; Zhang B; Guo Y Development of a Photo-Crosslinking, Biodegradable GelMA/PEGDA Hydrogel for Guided Bone Regeneration Materials. Materials 2018, 11, 1345.

(166). Noh I; Kim N; Tran HN; Lee J; Lee C 3D Printable Hyaluronic Acid-Based Hydrogel for Its Potential Application as a Bioink in Tissue Engineering. Biomater. Res 2019, 23, 3. [PubMed: 30774971]

(167). Zhu W; Qu X; Zhu J; Ma X; Patel S; Liu J; Wang P; Lai CSE; Gou M; Xu Y; et al. Direct 3D Bioprinting of Prevascularized Tissue Constructs with Complex Microarchitecture. Biomaterials 2017, 124, 106–115. [PubMed: 28192772]

(168). Escudero-Castellanos A; Ocampo-García BE; Domínguez-García MV; Flores-Estrada J; Flores-Merino MV Hydrogels Based on Poly(Ethylene Glycol) as Scaffolds for Tissue Engineering Application: Biocompatibility Assessment and Effect of the Sterilization Process. J. Mater. Sci.: Mater. Med 2016, 27, 176. [PubMed: 27752974]

(169). Alconcel SNS; Baas AS; Maynard HD FDA-Approved Poly(Ethylene Glycol)-Protein Conjugate Drugs. Polym. Chem 2011, 2, 1442–1448.

(170). Cha C; Soman P; Zhu W; Nikkhah M; Camci-Unal G; Chen S; Khademhosseini A Structural Reinforcement of Cell-Laden Hydrogels with Microfabricated Three Dimensional Scaffolds. Biomater. Sci 2014, 2, 703–709. [PubMed: 24778793]

(171). Qu X; Zhu W; Huang S; Li Y-S; Chien S; Zhang K; Chen S Relative Impact of Uniaxial Alignment vs. Form-Induced Stress on Differentiation of Human Adipose Derived Stem Cells. Biomaterials 2013, 34, 9812–9818. [PubMed: 24060419]

(172). Qu X; Zhu W; Huang S; Li Y-S; Chien S; Zhang K; Chen S Relative Impact of Uniaxial Alignment vs. Form-Induced Stress on Differentiation of Human Adipose Derived Stem Cells. Biomaterials 2013, 34, 9812–9818. [PubMed: 24060419]

(173). Skardal A; Atala A Biomaterials for Integration with 3-D Bioprinting. Ann. Biomed. Eng 2015, 43, 730–746. [PubMed: 25476164]

(174). Skardal A; Zhang J; Prestwich GD Bioprinting Vessel-like Constructs Using Hyaluronan Hydrogels Crosslinked with Tetrahedral Polyethylene Glycol Tetracrylates. Biomaterials 2010, 31, 6173–6181. [PubMed: 20546891]

(175). Stanton MM; Samitier J; Sánchez S Bioprinting of 3D Hydrogels. Lab Chip 2015, 15, 3111–3115. [PubMed: 26066320]

(176). Hribar KC; Finlay D; Ma X; Qu X; Ondeck MG; Chung PH; Zanella F; Engler AJ; Sheikh F; Vuori K; et al. Nonlinear 3D Projection Printing of Concave Hydrogel Microstructures for Long-Term Multicellular Spheroid and Embryoid Body Culture. Lab Chip 2015, 15, 2412–2418. [PubMed: 25900329]

(177). Warner J; Soman P; Zhu W; Tom M; Chen S Design and 3D Printing of Hydrogel Scaffolds with Fractal Geometries. ACS Biomater. Sci. Eng 2016, 2, 1763–1770.

(178). Zhang W; Soman P; Meggs K; Qu X; Chen S Tuning the Poisson's Ratio of Biomaterials for Investigating Cellular Response. Adv. Funct. Mater 2013, 23, 3226–3232.

(179). Zhang W; Soman P; Meggs K; Qu X; Chen S Tuning the Poisson's Ratio of Biomaterials for Investigating Cellular Response. Adv. Funct. Mater 2013, 23, 3226–3232.

(180). Wang Y; Ameer GA; Sheppard BJ; Langer R A Tough Biodegradable Elastomer. Nat. Biotechnol 2002, 20, 602–606. [PubMed: 12042865]

(181). Nijst CLE; Bruggeman JP; Karp JM; Ferreira L; Zumbuehl A; Bettinger CJ; Langer R Synthesis and Characterization of Photocurable Elastomers from Poly(Glycerol-Co-Sebacate). Biomacromolecules 2007, 8, 3067–3073. [PubMed: 17725319]

(182). Manzanedo D; Gibson LJ; Allen SM Table of Contents. Clin. Transl. Sci 2012, 5, iii–iv.

(183). Rai R; Tallawi M; Grigore A; Boccaccini AR Synthesis, Properties and Biomedical Applications of Poly(Glycerol Sebacate) (PGS): A Review. Prog. Polym. Sci 2012, 37, 1051–1078.

(184). Loh XJ; Abdul Karim A; Owh C Poly(Glycerol Sebacate) Biomaterial: Synthesis and Biomedical Applications. J. Mater. Chem. B 2015, 3, 7641–7652. [PubMed: 32264574]

(185). Ravichandran R Cardiogenic Differentiation of Mesenchymal Stem Cells on Elastomeric Poly (Glycerol Sebacate)/Collagen Core/Shell Fibers. World J. Cardiol 2013, 5, 28. [PubMed: 23539543]

(186). Rai R; Tallawi M; Frati C; Falco A; Gervasi A; Quaini F; Roether JA; Hochburger T; Schubert DW; Seik L; et al. Bioactive Electrospun Fibers of Poly(Glycerol Sebacate) and Poly(ε-Caprolactone) for Cardiac Patch Application. Adv. Healthcare Mater 2015, 4, 2012–2025.

(187). Rai R; Tallawi M; Barbani N; Frati C; Madeddu D; Cavalli S; Graiani G; Quaini F; Roether JA; Schubert DW; et al. Biomimetic Poly(Glycerol Sebacate) (PGS) Membranes for Cardiac Patch Application. Mater. Sci. Eng., C 2013, 33, 3677–3687.

(188). Masoumi N; Jean A; Zugates JT; Johnson KL; Engelmayr GC Laser Microfabricated Poly(Glycerol Sebacate) Scaffolds for Heart Valve Tissue Engineering. J. Biomed. Mater. Res., Part A 2013, 101A, 104–114.

(189). Kharaziha M; Nikkhah M; Shin S-R; Annabi N; Masoumi N; Gaharwar AK; Camci-Unal G; Khademhosseini A PGS:Gelatin Nanofibrous Scaffolds with Tunable Mechanical and Structural Properties for Engineering Cardiac Tissues. Biomaterials 2013, 34, 6355–6366. [PubMed: 23747008]

(190). Ravichandran R; Venugopal JR; Sundarrajan S; Mukherjee S; Sridhar R; Ramakrishna S Minimally Invasive Injectable Short Nanofibers of Poly(Glycerol Sebacate) for Cardiac Tissue Engineering. Nanotechnology 2012, 23, 385102. [PubMed: 22947662]

(191). Hu T; Wu Y; Zhao X; Wang L; Bi L; Ma PX; Guo B Micropatterned, Electroactive, and Biodegradable Poly(Glycerol Sebacate)-Aniline Trimer Elastomer for Cardiac Tissue Engineering. Chem. Eng. J 2019, 366, 208–222.

(192). Vogt L; Rivera LR; Liverani L; Piegat A; El Fray M; Boccaccini AR Poly(ε-Caprolactone)/Poly(Glycerol Sebacate) Electrospun Scaffolds for Cardiac Tissue Engineering Using Benign Solvents. Mater. Sci. Eng., C 2019, 103, 109712.

(193). Chen Q-Z; Bismarck A; Hansen U; Junaid S; Tran MQ; Harding SE; Ali NN; Boccaccini AR Characterisation of a Soft Elastomer Poly(Glycerol Sebacate) Designed to Match the Mechanical Properties of Myocardial Tissue. Biomaterials 2008, 29, 47–57. [PubMed: 17915309]

(194). Chen Q-Z; Ishii H; Thouas GA; Lyon AR; Wright JS; Blaker JJ; Chrzanowski W; Boccaccini AR; Ali NN; Knowles JC; et al. An Elastomeric Patch Derived from Poly(Glycerol Sebacate) for Delivery of Embryonic Stem Cells to the Heart. Biomaterials 2010, 31, 3885–3893. [PubMed: 20153041]

(195). Ravichandran R; Venugopal JR; Sundarrajan S; Mukherjee S; Ramakrishna S Poly(Glycerol Sebacate)/Gelatin Core/Shell Fibrous Structure for Regeneration of Myocardial Infarction. Tissue Eng., Part A 2011, 17, 1363–1373. [PubMed: 21247338]

(196). Motlagh D; Yang J; Lui KY; Webb AR; Ameer GA Hemocompatibility Evaluation of Poly(Glycerol-Sebacate) in Vitro for Vascular Tissue Engineering. Biomaterials 2006, 27, 4315–4324. [PubMed: 16675010]

(197). Gao J; Ensley AE; Nerem RM; Wang Y Poly(Glycerol Sebacate) Supports the Proliferation and Phenotypic Protein Expression of Primary Baboon Vascular Cells. J. Biomed. Mater. Res., Part A 2007, 83A, 1070–1075.

(198). Redenti S; Neeley WL; Rompani S; Saigal S; Yang J; Klassen H; Langer R; Young MJ Engineering Retinal Progenitor Cell and Scrollable Poly(Glycerol-Sebacate) Composites for Expansion and Subretinal Transplantation. Biomaterials 2009, 30, 3405–3414. [PubMed: 19361860]

(199). Keirouz A; Fortunato G; Zhang M; Callanan A; Radacsi N Nozzle-Free Electrospinning of Polyvinylpyrrolidone/Poly(Glycerol Sebacate) Fibrous Scaffolds for Skin Tissue Engineering Applications. Med. Eng. Phys 2019, 71, 56–67. [PubMed: 31257053]

(200). Sundback C; Shyu J; Wang Y; Faquin W; Langer R; Vacanti J; Hadlock T Biocompatibility Analysis of Poly(Glycerol Sebacate) as a Nerve Guide Material. Biomaterials 2005, 26, 5454–5464. [PubMed: 15860202]

(201). Hu J; Kai D; Ye H; Tian L; Ding X; Ramakrishna S; Loh XJ Electrospinning of Poly(Glycerol Sebacate)-Based Nanofibers for Nerve Tissue Engineering. Mater. Sci. Eng., C 2017, 70, 1089–1094.

(202). Saudi A; Rafienia M; Zargar Kharazi A; Salehi H; Zarrabi A; Karevan M Design and Fabrication of Poly (Glycerol Sebacate)-based Fibers for Neural Tissue Engineering: Synthesis, Electrospinning, and Characterization. Polym. Adv. Technol 2019, 30, 1427–1440.

(203). Saravani S; Ebrahimian-Hosseinabadi M; Mohebbi-Kalhori D Polyglycerol Sebacate/Chitosan/Gelatin Nano-Composite Scaffolds for Engineering Neural Construct. Mater. Chem. Phys 2019, 222, 147–151.

(204). Jiang L; Jiang Y; Stiadle J; Wang X; Wang L; Li Q; Shen C; Thibeault SL; Turng L-S Electrospun Nanofibrous Thermoplastic Polyurethane/Poly(Glycerol Sebacate) Hybrid Scaffolds for Vocal Fold Tissue Engineering Applications. Mater. Sci. Eng., C 2019, 94, 740–749.

(205). Kemppainen JM; Hollister SJ Tailoring the Mechanical Properties of 3D-Designed Poly(Glycerol Sebacate) Scaffolds for Cartilage Applications. J. Biomed. Mater. Res., Part A 2010, 94A, 9–18.

(206). Jeong CG; Hollister SJ A Comparison of the Influence of Material on in Vitro Cartilage Tissue Engineering with PCL, PGS, and POC 3D Scaffold Architecture Seeded with Chondrocytes. Biomaterials 2010, 31, 4304–4312. [PubMed: 20219243]

(207). Liu Y; Tian K; Hao J; Yang T; Geng X; Zhang W Biomimetic Poly(Glycerol Sebacate)/Polycaprolactone Blend Scaffolds for Cartilage Tissue Engineering. J. Mater. Sci.: Mater. Med 2019, 30, 53. [PubMed: 31037512]

(208). Yang K; Zhang J; Ma X; Ma Y; Kan C; Ma H; Li Y; Yuan Y; Liu C β-Tricalcium Phosphate/Poly(Glycerol Sebacate) Scaffolds with Robust Mechanical Property for Bone Tissue Engineering. Mater. Sci. Eng., C 2015, 56, 37–47.

(209). Zaky SH; Lee K-W; Gao J; Jensen A; Close J; Wang Y; Almarza AJ; Sfeir C Poly(Glycerol Sebacate) Elastomer: A Novel Material for Mechanically Loaded Bone Regeneration. Tissue Eng., Part A 2014, 20, 45–53. [PubMed: 24020497]

(210). Yu S; Shi J; Liu Y; Si J; Yuan Y; Liu C A Mechanically Robust and Flexible PEGylated Poly(Glycerol Sebacate)/β-TCP Nanoparticle Composite Membrane for Guided Bone Regeneration. J. Mater. Chem. B 2019, 7, 3279–3290.

(211). Jian B; Wu W; Song Y; Tan N; Ma C Microporous Elastomeric Membranes Fabricated with Polyglycerol Sebacate Improved Guided Bone Regeneration in a Rabbit Model. Int. J. Nanomed 2019, 14, 2683–2692.

(212). Tallá Ferrer C; Vilariño-Feltrer G; Rizk M; Sydow HG; Vallés-Lluch A Nanocomposites Based on Poly(Glycerol Sebacate) with Silica Nanoparticles with Potential Application in Dental Tissue Engineering. Int. J. Polym. Mater 2019, 1–12.

(213). Hagandora CK; Gao J; Wang Y; Almarza AJ Poly (Glycerol Sebacate): A Novel Scaffold Material for Temporomandibular Joint Disc Engineering. Tissue Eng., Part A 2013, 19, 729–737. [PubMed: 23157344]

(214). Jaafar IH; Ammar MM; Jedlicka SS; Pearson RA; Coulter JP Spectroscopic Evaluation, Thermal, and Thermomechanical Characterization of Poly(Glycerol-Sebacate) with Variations in Curing Temperatures and Durations. J. Mater. Sci 2010, 45, 2525–2529.

(215). Engelmayr GC; Cheng M; Bettinger CJ; Borenstein JT; Langer R; Freed LE Accordion-like Honeycombs for Tissue Engineering of Cardiac Anisotropy. Nat. Mater 2008, 7, 1003–1010. [PubMed: 18978786]

(216). Chen J-Y; Hwang J; Ao-Ieong W-S; Lin Y-C; Hsieh Y-K; Cheng Y-L; Wang J Study of Physical and Degradation Properties of 3D-Printed Biodegradable, Photocurable Copolymers, PGSA-Co-PEGDA and PGSA-Co-PCLDA. Polymers (Basel, Switz.) 2018, 10, 1263.

(217). Gerecht S; Townsend SA; Pressler H; Zhu H; Nijst CLE; Bruggeman JP; Nichol JW; Langer R A Porous Photocurable Elastomer for Cell Encapsulation and Culture. Biomaterials 2007, 28, 4826–4835. [PubMed: 17692371]

(218). Lang N; Pereira MJ; Lee Y; Friehs I; Vasilyev NV; Feins EN; Ablasser K; O'Cearbhaill ED; Xu C; Fabozzo A; et al. A Blood-Resistant Surgical Glue for Minimally Invasive Repair of Vessels and Heart Defects. Sci. Transl. Med 2014, 6, 218ra6–218ra6a.

(219). Mahdavi A; Ferreira L; Sundback C; Nichol JW; Chan EP; Carter DJD; Bettinger CJ; Patanavanich S; Chignozha L; Ben-Joseph E; et al. A Biodegradable and Biocompatible Gecko-

Inspired Tissue Adhesive. Proc. Natl. Acad. Sci. U. S. A 2008, 105, 2307–2312. [PubMed: 18287082]

(220). Yeh Y-CC; Highley CB; Ouyang L; Burdick JA 3D Printing of Photocurable Poly(Glycerol Sebacate) Elastomers. Biofabrication 2016, 8, 045004. [PubMed: 27716633]

(221). Singh D; Harding AJ; Albadawi E; Boissonade FM; Haycock JW; Claeyssens F Additive Manufactured Biodegradable Poly(Glycerol Sebacate Methacrylate) Nerve Guidance Conduits. Acta Biomater. 2018, 78, 48–63. [PubMed: 30075322]

(222). Pashneh-Tala S; Owen R; Bahmaee H; Rekštytė S; Malinauskas M; Claeyssens F Synthesis, Characterization and 3D Micro-Structuring via 2-Photon Polymerization of Poly(Glycerol Sebacate)-Methacrylate–An Elastomeric Degradable Polymer. Front. Phys 2018, 6, 41.

(223). Yeh YC; Ouyang L; Highley CB; Burdick JA Norbornene-Modified Poly(Glycerol Sebacate) as a Photocurable and Biodegradable Elastomer. Polym. Chem 2017, 8, 5091–5099.

(224). Wang M; Lei D; Liu Z; Chen S; Sun L; Lv Z; Huang P; Jiang Z; You Z A Poly(Glycerol Sebacate) Based Photo/Thermo Dual Curable Biodegradable and Biocompatible Polymer for Biomedical Applications. J. Biomater. Sci., Polym. Ed 2017, 28, 1728–1739. [PubMed: 28657862]

(225). Zhu C; Kustra SR; Bettinger CJ Photocrosslinkable Biodegradable Elastomers Based on Cinnamate-Functionalized Polyesters. Acta Biomater. 2013, 9, 7362–7370. [PubMed: 23567941]

(226). Bodakhe S; Verma S; Garkhal K; Samal SK; Sharma SS; Kumar N Injectable Photocrosslinkable Nanocomposite Based on Poly(Glycerol Sebacate) Fumarate and Hydroxyapatite: Development, Biocompatibility and Bone Regeneration in a Rat Calvarial Bone Defect Model. Nanomedicine 2013, 8, 1777–1795. [PubMed: 23384697]

(227). Liu Q; Tian M; Shi R; Zhang L; Chen D; Tian W Structure and Properties of Thermoplastic Poly(Glycerol Sebacate) Elastomers Originating from Prepolymers with Different Molecular Weights. J. Appl. Polym. Sci 2007, 104, 1131–1137.

(228). Li Y; Cook WD; Moorhoff C; Huang W-C; Chen Q-Z Synthesis, Characterization and Properties of Biocompatible Poly(Glycerol Sebacate) Pre-Polymer and Gel. Polym. Int 2013, 62, 534–547.

(229). Wang Y; Kim YM; Langer R In Vivo Degradation Characteristics of Poly(Glycerol Sebacate). J. Biomed. Mater. Res 2003, 66A, 192–197.

(230). Ifkovits JL; Devlin JJ; Eng G; Martens TP; Vunjak-Novakovic G; Burdick JA Biodegradable Fibrous Scaffolds with Tunable Properties Formed from Photo-Cross-Linkable Poly(Glycerol Sebacate). ACS Appl. Mater. Interfaces 2009, 1, 1878–1886. [PubMed: 20160937]

(231). Liang S-L; Yang X-Y; Fang X-Y; Cook WD; Thouas GA; Chen Q-Z In Vitro Enzymatic Degradation of Poly (Glycerol Sebacate)-Based Materials. Biomaterials 2011, 32, 8486–8496. [PubMed: 21855132]

(232). Li X; Hong AT-L; Naskar N; Chung H-J Criteria for Quick and Consistent Synthesis of Poly(Glycerol Sebacate) for Tailored Mechanical Properties. Biomacromolecules 2015, 16, 1525–1533. [PubMed: 25857651]

(233). Frydrych M; Chen B Large Three-Dimensional Poly(Glycerol Sebacate)-Based Scaffolds-a Freeze-Drying Preparation Approach. J. Mater. Chem. B 2013, 1, 6650–6661. [PubMed: 32261274]

(234). Rydevik BL; Kwan MK; Myers RR; Brown RA; Triggs KJ; Woo SL; Garfin SR An in Vitro Mechanical and Histological Study of Acute Stretching on Rabbit Tibial Nerve. J. Orthop. Res 1990, 8, 694–701. [PubMed: 2388109]

(235). Lizarraga-Valderrama LR; Nigmatullin R; Taylor C; Haycock JW; Claeyssens F; Knowles JC; Roy I Nerve Tissue Engineering Using Blends of Poly(3-Hydroxyalkanoates) for Peripheral Nerve Regeneration. Eng. Life Sci 2015, 15, 612–621.

(236). Young RC; Terenghi G; Wiberg M Poly-3-Hydroxybuty-rate (PHB): A Resorbable Conduit for Long-Gap Repair in Peripheral Nerves. Br. J. Plast. Surg 2002, 55, 235–240. [PubMed: 12041978]

(237). Weir NA; Buchanan FJ; Orr JF; Dickson GR Degradation of Poly-L-Lactide. Part 1: In Vitro and in Vivo Physiological Temperature Degradation. Proc. Inst. Mech. Eng., Part H 2004, 218, 307–319.

(238). Bayer O Das Di-Isocyanat-Polyadditionsverfahren (Polyurethane). Angew. Chem 1947, 59, 257–272.

(239). Lövenich C; Albers R; Brassat L; Chrisochoou A; Ehbing H; Hättig J Polyurethanes (PU). Kunststoffe Int 2017, 107, 46–51.

(240). Stokes K; McVenes R; Anderson JM Polyurethane Elastomer Biostability. J. Biomater. Appl 1995, 9, 321–354. [PubMed: 9309503]

(241). Špírková M; Pavličević J; Strachota A; Poreba R; Bera O; Kaprálková L; Baldrian J; Šlouf M; Lazić N; Budinski-Simendić J Novel Polycarbonate-Based Polyurethane Elastomers: Composition-Property Relationship. Eur. Polym. J 2011, 47, 959–972.

(242). Liu Y; Zwingmann B; Schlaich M Carbon Fiber Reinforced Polymer for Cable Structures—A Review. Polymers (Basel, Switz.) 2015, 7, 2078–2099.

(243). Kausar A Polyurethane/Epoxy Interpenetrating Polymer Network In Aspects of Polyurethanes; InTech, 2017.

(244). Liu Y; Zwingmann B; Schlaich M Carbon Fiber Reinforced Polymer for Cable Structures—A Review. Polymers (Basel, Switz.) 2015, 7, 2078–2099.

(245). Liu X; Xu K; Liu H; Cai H; Su J; Fu Z; Guo Y; Chen M Preparation and Properties of Waterborne Polyurethanes with Natural Dimer Fatty Acids Based Polyester Polyol as Soft Segment. Prog. Org. Coat 2011, 72, 612–620.

(246). Rus D; Tolley MT Design, Fabrication and Control of Soft Robots. Nature 2015, 521, 467–475. [PubMed: 26017446]

(247). Patel DK; Sakhaei AH; Layani M; Zhang B; Ge Q; Magdassi S Highly Stretchable and UV Curable Elastomers for Digital Light Processing Based 3D Printing. Adv. Mater 2017, 29, 1606000.

(248). Gul JZ; Sajid M; Rehman MM; Siddiqui GU; Shah I; Kim K-H; Lee J-W; Choi KH 3D Printing for Soft Robotics – a Review. Sci. Technol. Adv. Mater 2018, 19, 243–262. [PubMed: 29707065]

(249). Yang Y; Chen Y 3D Printing of Smart Materials for Robotics with Variable Stiffness and Position Feedback In IEEE/ASME International Conference on Advanced Intelligent Mechatronics, AIM; IEEE, 2017; pp 418–423.

(250). Guelcher SA Biodegradable Polyurethanes: Synthesis and Applications in Regenerative Medicine7. Tissue Eng., Part B 2008, 14, 3–17.

(251). Whatley BR; Kuo J; Shuai C; Damon BJ; Wen X Fabrication of a Biomimetic Elastic Intervertebral Disk Scaffold Using Additive Manufacturing. Biofabrication 2011, 3, 015004. [PubMed: 21343634]

(252). Xu W; Wang X; Yan Y; Zhang R Rapid Prototyping of Polyurethane for the Creation of Vascular Systems. J. Bioact. Compat. Polym 2008, 23, 103–114.

(253). Hung K; Tseng C; Hsu S Synthesis and 3D Printing of Biodegradable Polyurethane Elastomer by a Water-Based Process for Cartilage Tissue Engineering Applications. Adv. Healthcare Mater 2014, 3, 1578–1587.

(254). Hsieh FY; Lin HH; Hsu S-H 3D Bioprinting of Neural Stem Cell-Laden Thermoresponsive Biodegradable Polyurethane Hydrogel and Potential in Central Nervous System Repair. Biomaterials 2015, 71, 48–57. [PubMed: 26318816]

(255). Huang CT; Kumar Shrestha L; Ariga K; Hsu SH A Graphene-Polyurethane Composite Hydrogel as a Potential Bioink for 3D Bioprinting and Differentiation of Neural Stem Cells. J. Mater. Chem. B 2017, 5, 8854–8864. [PubMed: 32264279]

(256). Robinson SS; Aubin CA; Wallin TJ; Gharaie S; Xu PA; Wang K; Dunham SN; Mosadegh B; Shepherd RF Stereolithography for Personalized Left Atrial Appendage Occluders. Adv. Mater. Technol 2018, 3, 1800233. [PubMed: 31803824]

(257). Holzapfel BM; Pilge H; Prodinger PM; Toepfer A; Mayer-Wagner S; Hutmacher DW; Von Eisenhart-Rothe R; Rudert M; Gradinger R; Rechl H Customised Osteotomy Guides and Endoprosthetic Reconstruction for Periacetabular Tumours. Int. Orthopaed 2014, 38, 1435–1442.

(258). Balani K; Verma V; Agarwal A; Narayan R Physical, Thermal, and Mechanical Properties of Polymers In Biosurfaces; John Wiley & Sons: Hoboken, NJ, 2015; pp 329–344.

(259). Saini M Implant Biomaterials: A Comprehensive Review. World J. Clin. Cases 2015, 3, 52. [PubMed: 25610850]

(260). von Burkersroda F; Schedl L; Göpferich A Why Degradable Polymers Undergo Surface Erosion or Bulk Erosion. Biomaterials 2002, 23, 4221–4231. [PubMed: 12194525]

(261). Göpferich A Polymer Bulk Erosion. Macromolecules 1997, 30, 2598–2604.

(262). Lyu SP; Untereker D Degradability of Polymers for Implantable Biomedical Devices. Int. J. Mol. Sci 2009, 10, 4033–4065. [PubMed: 19865531]

(263). Williams DF On the Mechanisms of Biocompatibility. Biomaterials 2008, 29, 2941–2953. [PubMed: 18440630]

(264). de Moraes Porto IC C. Polymer Biocompatibility In Polymerization; InTech, 2012.

(265). Gaharwar AK; Peppas NA; Khademhosseini A Nanocomposite Hydrogels for Biomedical Applications. Biotechnol. Bioeng 2014, 111, 441–453. [PubMed: 24264728]

(266). Memic A; Alhadrami HA; Hussain MA; Aldhahri M; Al Nowaiser F; Al-Hazmi F; Oklu R; Khademhosseini A Hydrogels 2.0: Improved Properties with Nanomaterial Composites for Biomedical Applications. Biomed. Mater 2016, 11, 014104.

(267). Shin SR; Aghaei-Ghareh-Bolagh B; Dang TT; Topkaya SN; Gao X; Yang SY; Jung SM; Oh JH; Dokmeci MR; Tang X; Khademhosseini A Cell-Laden Microengineered and Mechanically Tunable Hybrid Hydrogels of Gelatin and Graphene Oxide. Adv. Mater 2013, 25, 6385–6391. [PubMed: 23996513]

(268). Shin SR; Bae H; Cha JM; Mun JY; Chen YC; Tekin H; Shin H; Farshchi S; Dokmeci MR; Tang S; et al. Carbon Nanotube Reinforced Hybrid Microgels as Scaffold Materials for Cell Encapsulation. ACS Nano 2012, 6, 362–372. [PubMed: 22117858]

(269). Shin SR; Jung SM; Zalabany M; Kim K; Zorlutuna P; Kim SB; Nikkhah M; Khabiry M; Azize M; Kong J; et al. Carbon-Nanotube-Embedded Hydrogel Sheets for Engineering Cardiac Constructs and Bioactuators. ACS Nano 2013, 7, 2369–2380. [PubMed: 23363247]

(270). Zheng T; Pour Shahid Saeed Abadi P; Seo J; Cha BH; Miccoli B; Li YC; Park K; Park S; Choi SJ; Bayaniahangar R; et al. Biocompatible Carbon Nanotube-Based Hybrid Microfiber for Implantable Electrochemical Actuator and Flexible Electronic Applications. ACS Appl. Mater. Interfaces 2019, 11, 20615–20627. [PubMed: 31050404]

(271). Chiappone A; Roppolo I; Naretto E; Fantino E; Calignano F; Sangermano M; Pirri F Study of Graphene Oxide-Based 3D Printable Composites: Effect of the in Situ Reduction. Composites, Part B 2017, 124, 9–15.

(272). Janovák L; Dékány I Optical Properties and Electric Conductivity of Gold Nanoparticle-Containing, Hydrogel-Based Thin Layer Composite Films Obtained by Photopolymerization. Appl. Surf. Sci 2010, 256, 2809–2817.

(273). Han D; Lu Z; Chester SA; Lee H Micro 3D Printing of a Temperature-Responsive Hydrogel Using Projection Micro-Stereolithography. Sci. Rep 2018, 8, 1963. [PubMed: 29386555]

(274). Liu H; Wang S Poly(N-Isopropylacrylamide)-Based Thermo-Responsive Surfaces with Controllable Cell Adhesion. Sci. China: Chem 2014, 57, 552–557.

(275). Lee SW; Tettey KE; Kim IL; Burdick JA; Lee D Controlling the Cell-Adhesion Properties of Poly(Acrylic Acid)/Polyacrylamide Hydrogen-Bonded Multilayers. Macromolecules 2012, 45, 6120–6126.

(276). Lu Y; Sun J; Shen J Cell Adhesion Properties of Patterned Poly(Acrylic Acid)/Poly(Allylamine Hydrochloride) Multilayer Films Created by Room-Temperature Imprinting Technique. Langmuir 2008, 24, 8050–8055. [PubMed: 18572930]

(277). Zhao X; Ding X; Deng Z; Zheng Z; Peng Y; Long X Thermoswitchable Electronic Properties of a Gold Nanoparticle/Hydrogel Composite. Macromol. Rapid Commun 2005, 26, 1784–1787.

(278). Abdel-Halim ES; Al-Deyab SS Electrically Conducting Silver/Guar Gum/Poly(Acrylic Acid) Nanocomposite. Int. J. Biol. Macromol 2014, 69, 456–463. [PubMed: 24928058]

(279). Jalili NA; Muscarello M; Gaharwar AK Nanoengineered Thermoresponsive Magnetic Hydrogels for Biomedical Applications. Bioeng. Transl. Med 2016, 1, 297–305. [PubMed: 29313018]

(280). Zhu W; Li J; Leong YJ; Rozen I; Qu X; Dong R; Wu Z; Gao W; Chung PH; Wang J; et al. 3D-Printed Artificial Microfish. Adv. Mater 2015, 27, 4411–4417. [PubMed: 26121113]

(281). Xu F; Inci F; Mullick O; Gurkan UA; Sung Y; Kavaz D; Li B; Denkbas EB; Demirci U Release of Magnetic Nanoparticles from Cell-Encapsulating Biodegradable Nanobiomaterials. ACS Nano 2012, 6, 6640–6649. [PubMed: 22680777]

(282). Xu F; Wu CAM; Rengarajan V; Finley TD; Keles HO; Sung Y; Li B; Gurkan UA; Demirci U Three-Dimensional Magnetic Assembly of Microscale Hydrogels. Adv. Mater 2011, 23, 4254–4260. [PubMed: 21830240]

(283). Gaharwar AK; Rivera C; Wu CJ; Chan BK; Schmidt G Photocrosslinked Nanocomposite Hydrogels from PEG and Silica Nanospheres: Structural, Mechanical and Cell Adhesion Characteristics. Mater. Sci. Eng., C 2013, 33, 1800–1807.

(284). Gaharwar AK; Rivera CP; Wu CJ; Schmidt G Transparent, Elastomeric and Tough Hydrogels from Poly(Ethylene Glycol) and Silicate Nanoparticles. Acta Biomater. 2011, 7, 4139–4148. [PubMed: 21839864]

(285). Zuo Y; Liu X; Wei D; Sun J; Xiao W; Zhao H; Guo L; Wei Q; Fan H; Zhang X Photo-Cross-Linkable Methacrylated Gelatin and Hydroxyapatite Hybrid Hydrogel for Modularly Engineering Biomimetic Osteon. ACS Appl. Mater. Interfaces 2015, 7, 10386–10394. [PubMed: 25928732]

(286). Gaharwar AK; Dammu SA; Canter JM; Wu CJ; Schmidt G Highly Extensible, Tough, and Elastomeric Nanocomposite Hydrogels from Poly(Ethylene Glycol) and Hydroxyapatite Nanoparticles. Biomacromolecules 2011, 12, 1641–1650. [PubMed: 21413708]

(287). Gao W; Zhang Y; Zhang Q; Zhang L Nanoparticle-Hydrogel: A Hybrid Biomaterial System for Localized Drug Delivery. Ann. Biomed. Eng 2016, 44, 2049–2061. [PubMed: 26951462]

(288). Desai PN; Yuan Q; Yang H Synthesis and Characterization of Photocurable Polyamidoamine Dendrimer Hydrogels as a Versatile Platform for Tissue Engineering and Drug Delivery Pooja. Biomacromolecules 2010, 11, 666–673. [PubMed: 20108892]

(289). Zhang H; Patel A; Gaharwar AK; Mihaila SM; Iviglia G; Mukundan S; Bae H; Yang H; Khademhosseini A Hyperbranched Polyester Hydrogels with Controlled Drug Release and Cell Adhesion Properties Hongbin. Biomacromolecules 2013, 14, 1299–1310. [PubMed: 23394067]

(290). Gou M; Qu X; Zhu W; Xiang M; Yang J; Zhang K; Wei Y; Chen S Bio-Inspired Detoxification Using 3d-Printed Hydrogel Nanocomposites. Nat. Commun 2014, 5, 3774. [PubMed: 24805923]

(291). Sheffield C; Meyers K; Johnson E; Rajachar RM Application of Composite Hydrogels to Control Physical Properties in Tissue Engineering and Regenerative Medicine. Gels 2018, 4, 51.

(292). Goktas M; Cinar G; Orujalipoor I; Ide S; Tekinay AB; Guler MO Self-Assembled Peptide Amphiphile Nanofibers and PEG Composite Hydrogels as Tunable ECM Mimetic Microenvironment. Biomacromolecules 2015, 16, 1247–1258. [PubMed: 25751623]

(293). Barczyk M; Carracedo S; Gullberg D Integrins. Cell Tissue Res. 2010, 339, 269. [PubMed: 19693543]

(294). Chaudhuri O; Gu L; Klumpers D; Darnell M; Bencherif SA; Weaver JC; Huebsch N; Lee HP; Lippens E; Duda GN; et al. Hydrogels with Tunable Stress Relaxation Regulate Stem Cell Fate and Activity. Nat. Mater 2016, 15, 326–334. [PubMed: 26618884]

(295). Burdick JA; Prestwich GD Hyaluronic Acid Hydrogels for Biomedical Applications. Adv. Mater 2011, 23, H41–H56. [PubMed: 21394792]

(296). Levett PA; Hutmacher DW; Malda J; Klein TJ Hyaluronic Acid Enhances the Mechanical Properties of Tissue-Engineered Cartilage Constructs. PLoS One 2014, 9, No. e113216. [PubMed: 25438040]

(297). García-Lizarribar A; Fernández-Garibay X; Velasco-Mallorquí F; Castaño AG; Samitier J; Ramon-Azcon J Composite Biomaterials as Long-Lasting Scaffolds for 3D Bioprinting of Highly Aligned Muscle Tissue. Macromol. Biosci 2018, 18, 1800167.

(298). Hudnut AW; Lash-rosenberg L; Xin A; Leal Doblado JA; Zurita-lopez C; Wang Q; Armani AM Role of Extracellular Matrix in the Biomechanical Behavior of Pancreatic Tissue. ACS Biomater. Sci. Eng 2018, 4, 1916–1923. [PubMed: 31828218]

(299). Camci-Unal G; Cuttica D; Annabi N; Demarchi D; Khademhosseini A Synthesis and Characterization of Hybrid Hyaluronic Acid-Gelatin Hydrogels. Biomacromolecules 2013, 14, 1085–1092. [PubMed: 23419055]

(300). Chan V; Zorlutuna P; Jeong JH; Kong H; Bashir R Three-Dimensional Photopatterning of Hydrogels Using Stereolithography for Long-Term Cell Encapsulation. Lab Chip 2010, 10, 2062–2070. [PubMed: 20603661]

(301). Dragan ES Design and Applications of Interpenetrating Polymer Network Hydrogels. A Review. Chem. Eng. J 2014, 243, 572–590.

(302). Myung D; Waters D; Wiseman M; Duhamel P-E; Noolandi J; Ta CN; Frank CW Progress in the Development of Interpenetrating Polymer Network Hydrogels. Polym. Adv. Technol 2008, 19, 647–657. [PubMed: 19763189]

(303). Daniele MA; Adams AA; Naciri J; North SH; Ligler FS Interpenetrating Networks Based on Gelatin Methacrylamide and PEG Formed Using Concurrent Thiol Click Chemistries for Hydrogel Tissue Engineering Scaffolds. Biomaterials 2014, 35, 1845–1856. [PubMed: 24314597]

(304). Yang T; Malkoch M; Hult A Sequential Interpenetrating Poly(Ethylene Glycol) Hydrogels Prepared by UV-Initiated Thiol–Ene Coupling Chemistry. J. Polym. Sci., Part A: Polym. Chem 2013, 51, 363–371.

(305). Pepelanova I; Kruppa K; Scheper T; Lavrentieva A Gelatin-Methacryloyl (GelMA) Hydrogels with Defined Degree of Functionalization as a Versatile Toolkit for 3D Cell Culture and Extrusion Bioprinting. Bioengineering 2018, 5, 55.

(306). Bertlein S; Brown G; Lim KS; Jungst T; Boeck T; Blunk T; Tessmar J; Hooper GJ; Woodfield TBF; Groll J Thiol–Ene Clickable Gelatin: A Platform Bioink for Multiple 3D Biofabrication Technologies. Adv. Mater 2017, 29, 1703404.

(307). Sarapas JM; Tew GN Thiol-Ene Step-Growth as a Versatile Route to Functional Polymers. Angew. Chem 2016, 128, 16092–16095.

(308). Stratesteffen H; Köpf M; Kreimendahl F; Blaeser A; Jockenhoevel S; Fischer H GelMA-Collagen Blends Enable Drop-on-Demand 3D Printablility and Promote Angiogenesis. Biofabrication 2017, 9, 045002. [PubMed: 28795951]

(309). Xue D; Zhang J; Wang Y; Mei D Digital Light Processing-Based 3D Printing of Cell-Seeding Hydrogel Scaffolds with Regionally Varied Stiffness. ACS Biomater. Sci. Eng 2019, 5, 4825–4833.

(310). Pryor HI; O'Doherty E; Hart A; Owens G; Hoganson D; Vacanti JP; Masiakos PT; Sundback CA Poly(Glycerol Sebacate) Films Prevent Postoperative Adhesions and Allow Laparoscopic Placement. Surgery 2009, 146, 490–497. [PubMed: 19715806]

(311). Daniele MA; Adams AA; Naciri J; North SH; Ligler FS Interpenetrating Networks Based on Gelatin Methacrylamide and PEG Formed Using Concurrent Thiol Click Chemistries for Hydrogel Tissue Engineering Scaffolds. Biomaterials 2014, 35, 1845–1856. [PubMed: 24314597]

(312). Xie M; Gao Q; Zhao H; Nie J; Fu Z; Wang H; Chen L; Shao L; Fu J; Chen Z; et al. Electro-Assisted Bioprinting of Low-Concentration GelMA Microdroplets. Small 2019, 15, 1804216.

(313). Zhang W; Chen S Femtosecond Laser Nanofabrication of Hydrogel Biomaterial. MRS Bull. 2011, 36, 1028–1033.

(314). Stichler S; Jungst T; Schamel M; Zilkowski I; Kuhlmann M; Böck T; Blunk T; Teßmar J; Groll J Thiol-Ene Clickable Poly(Glycidol) Hydrogels for Biofabrication. Ann. Biomed. Eng 2017, 45, 273–285. [PubMed: 27177637]

(315). Claeyssens F; Hasan EA; Gaidukeviciute A; Achilleos DS; Ranella A; Reinhardt C; Ovsianikov A; Shizhou X; Fotakis C; Vamvakaki M; et al. Three-Dimensional Biodegradable Structures Fabricated by Two-Photon Polymerization. Langmuir 2009, 25, 3219–3223. [PubMed: 19437724]

(316). Melissinaki V; Gill AA; Ortega I; Vamvakaki M; Ranella A; Haycock JW; Fotakis C; Farsari M; Claeyssens F Direct Laser Writing of 3D Scaffolds for Neural Tissue Engineering Applications. Biofabrication 2011, 3, 045005. [PubMed: 21931197]

(317). Cui H; Esworthy T; Zhou X; Hann SY; Glazer RI; Li R; Zhang LG Engineering a Novel 3D Printed Vascularized Tissue Model for Investigating Breast Cancer Metastasis to Bone. Adv. Healthcare Mater 2019, 1900924.

(318). Magalhães LSSM; Eroni Paz Santos F; de Maria Vas Elias C; Afewerki S; Sousa GF; Furtado ASA; Marciano FR; Oliveira Lobo A Printing 3D Hydrogel Structures Employing Low-Cost Stereolithography Technology. J. Funct. Biomater 2020, 11, 12.

(319). Jockusch J; Özcan M Additive Manufacturing of Dental Polymers: An Overview on Processes, Materials and Applications. Dent. Mater. J 2020, 2019–123.

(320). Wang Z; Jin X; Tian Z; Menard F; Holzman JF; Kim K A Novel, Well-Resolved Direct Laser Bioprinting System for Rapid Cell Encapsulation and Microwell Fabrication. Adv. Healthcare Mater 2018, 7, 1701249.

(321). Paz VF; Emons M; Obata K; Ovsianikov A; Peterhänsel S; Frenner K; Reinhardt C; Chichkov B; Morgner U; Osten W Development of Functional Sub-100 Nm Structures with 3D Two-Photon Polymerization Technique and Optical Methods for Characterization. J. Laser Appl 2012, 24, 042004.

(322). Nguyen AK; Narayan RJ Two-Photon Polymerization for Biological Applications. Mater. Today 2017, 20, 314–322.

(323). Janusziewicz R; Tumbleston JR; Quintanilla AL; Mecham SJ; DeSimone JM Layerless Fabrication with Continuous Liquid Interface Production. Proc. Natl. Acad. Sci. U. S. A 2016, 113, 11703–11708. [PubMed: 27671641]

(324). Walker DA; Hedrick JL; Mirkin CA Rapid, Large-Volume, Thermally Controlled 3D Printing Using a Mobile Liquid Interface. Science 2019, 366, 360–364. [PubMed: 31624211]

(325). Shusteff M; Browar AEM; Kelly BE; Henriksson J; Weisgraber TH; Panas RM; Fang NX; Spadaccini CM One-Step Volumetric Additive Manufacturing of Complex Polymer Structures. Sci. Adv 2017, 3, No. eaao5496. [PubMed: 29230437]

(326). Kelly BE; Bhattacharya I; Heidari H; Shusteff M; Spadaccini CM; Taylor HK Volumetric Additive Manufacturing via Tomographic Reconstruction. Science 2019, 363, 1075–1079. [PubMed: 30705152]

(327). Demas JN; Crosby GA The Measurement of Photo-lumineseence Quantum. J. Phys. Chem 1971, 75, 991–1024.

(328). Eibel A; Fast DE; Gescheidt G Choosing the Ideal Photoinitiator for Free Radical Photopolymerizations: Predictions Based on Simulations Using Established Data. Polym. Chem 2018, 9, 5107–5115.

(329). Huang X; Wang X; Zhao Y Study on a Series of Water-Soluble Photoinitiators for Fabrication of 3D Hydrogels by Two-Photon Polymerization; Elsevier, 2017; Vol. 141.

(330). Rapid Prototyping & Manufacturing-Fundamentals of Stereolithography: Paul F. Jacobs, principal author, 1992 Society of Manufacturing Engineers xiv + 434 pp. $76.00 ($65.00 to SME members). J. Manuf. Syst 1993, 12, 430–433.

(331). Bennett J Measuring UV Curing Parameters of Commercial Photopolymers Used in Additive Manufacturing. Addit. Manuf 2017, 18, 203–212. [PubMed: 29503807]

(332). Benjamin AD; Abbasi R; Owens M; Olsen RJ; Walsh DJ; LeFevre TB; Wilking JN Light-Based 3D Printing of Hydrogels with High-Resolution Channels. Biomed. Phys. Eng. Express 2019, 5, 025035.

(333). Steyrer B; Neubauer P; Liska R; Stampfl J Visible Light Photoinitiator for 3D-Printing of Tough Methacrylate Resins. Materials 2017, 10, 1445.

(334). Salmoria GV; Ahrens CH; Beal VE; Pires ATN; Soldi V Evaluation of Post-Curing and Laser Manufacturing Parameters on the Properties of SOMOS 7110 Photosensitive Resin Used in Stereolithography. Mater. Eng 2009, 30, 758–763.

(335). Zhou M; Lee BH; Tan YJ; Tan LP Microbial Transglutaminase Induced Controlled Crosslinking of Gelatin Methacryloyl to Tailor Rheological Properties for 3D Printing. Biofabrication 2019, 11, 025011. [PubMed: 30743259]

(336). Basara G; Yue X; Zorlutuna P Dual Crosslinked Gelatin Methacryloyl Hydrogels for Photolithography and 3D Printing. Gels 2019, 5, 34.

(337). Born M; Wolf E; Bhatia AB; Clemmow PC; Gabor D; Stokes AR; Taylor AM; Wayman PA; Wilcock WL Principles of Optics; Cambridge University Press: Cambridge, UK, 1999.

(338). You S; Li J; Zhu W; Yu C; Mei D; Chen S Nanoscale 3D Printing of Hydrogels for Cellular Tissue Engineering. J. Mater. Chem. B 2018, 6, 2187–2197. [PubMed: 30319779]

(339). Hell SW; Wichmann J Breaking the Diffraction Resolution Limit by Stimulated Emission: Stimulated-Emission-Depletion Fluorescence Microscopy. Opt. Lett 1994, 19, 780. [PubMed: 19844443]

(340). Li L; Gattass RR; Gershgoren E; Hwang H; Fourkas JT Achieving/20 Resolution by One-Color Initiation and Deactivation of Polymerization. Science (Washington, DC, U. S.) 2009, 324, 910–913.

(341). Andrew TL; Tsai H-Y; Menon R Confining Light to Deep Subwavelength Dimensions to Enable Optical Nanopatterning. Science (Washington, DC, U. S.) 2009, 324, 917–921.

(342). Zhang AP; Qu X; Soman P; Hribar KC; Lee JW; Chen S; He S Rapid Fabrication of Complex 3D Extracellular Microenvironments by Dynamic Optical Projection Stereolithography. Adv. Mater 2012, 24, 4266–4270. [PubMed: 22786787]

(343). You S; Zhu W; Wang P; Chen S Projection Printing of Ultrathin Structures with Nanoscale Thickness Control. ACS Appl. Mater. Interfaces 2019, 11, 16059–16064. [PubMed: 30964636]

(344). Goodner MD; Lee HR; Bowman CN Method for Determining the Kinetic Parameters in Diffusion-Controlled Free-Radical Homopolymerizations. Ind. Eng. Chem. Res 1997, 36, 1247–1252.

(345). You S; Wang P; Schimelman J; Hwang HH; Chen S High-Fidelity 3D Printing Using Flashing Photopolymerization. Addit. Manuf 2019, 30, 100834. [PubMed: 32832382]

(346). You S; Guan J; Alido J; Hwang HH; Yu R; Kwe L; Su H; Chen S Mitigating Scattering Effects in Light-Based 3D Printing Using Machine Learning. J. Manuf. Sci. Eng 2020.

(347). Berry DB; You S; Warner J; Frank LR; Chen S; Ward SR * A 3D Tissue-Printing Approach for Validation of Diffusion Tensor Imaging in Skeletal Muscle. Tissue Eng., Part A 2017, 23, 980–988. [PubMed: 28338417]

(348). Zhang AP; Qu X; Soman P; Hribar KC; Lee JW; Chen S; He S Rapid Fabrication of Complex 3D Extracellular Microenvironments by Dynamic Optical Projection Stereolithography. Adv. Mater 2012, 24, 4266–4270. [PubMed: 22786787]

(349). Liu W; Deng T; Sun D; Jia Z; Li M; Tang A A Study of Mask Planning in Projection-Based Stereolithography Using Digital Image Correlation. Int. J. Adv. Manuf. Technol 2019, 104, 451–461.

(350). Su J; Su J Thiol-Mediated Chemoselective Strategies for In Situ Formation of Hydrogels. Gels 2018, 4, 72.

(351). Xue D; Wang Y; Mei D Multi-Step Exposure Method for Improving Structure Flatness in Digital Light Processing-Based Printing. J. Manuf. Process 2019, 39, 106–113.

(352). Miao S; Castro N; Nowicki M; Xia L; Cui H; Zhou X; Zhu W; Lee S-J; Sarkar K; Vozzi G; Tabata Y; Fisher J; Zhang LG 4D Printing of Polymeric Materials for Tissue and Organ Regeneration. Mater. Today 2017, 20, 577–591.

(353). Sydney Gladman A; Matsumoto EA; Nuzzo RG; Mahadevan L; Lewis JA Biomimetic 4D Printing. Nat. Mater 2016, 15, 413–418. [PubMed: 26808461]

(354). Miao S; Cui H; Nowicki M; Lee S; Almeida J; Zhou X; Zhu W; Yao X; Masood F; Plesniak MW; et al. Photolithographic-Stereolithographic-Tandem Fabrication of 4D Smart Scaffolds for Improved Stem Cell Cardiomyogenic Differentiation. Biofabrication 2018, 10, 035007. [PubMed: 29651999]

(355). Esworthy TJ; Miao S; Lee SJ; Zhou X; Cui H; Zuo YY; Zhang LG Advanced 4D-Bioprinting Technologies for Brain Tissue Modeling and Study. Int. J. Smart Nano Mater 2019, 10, 177–204. [PubMed: 32864037]

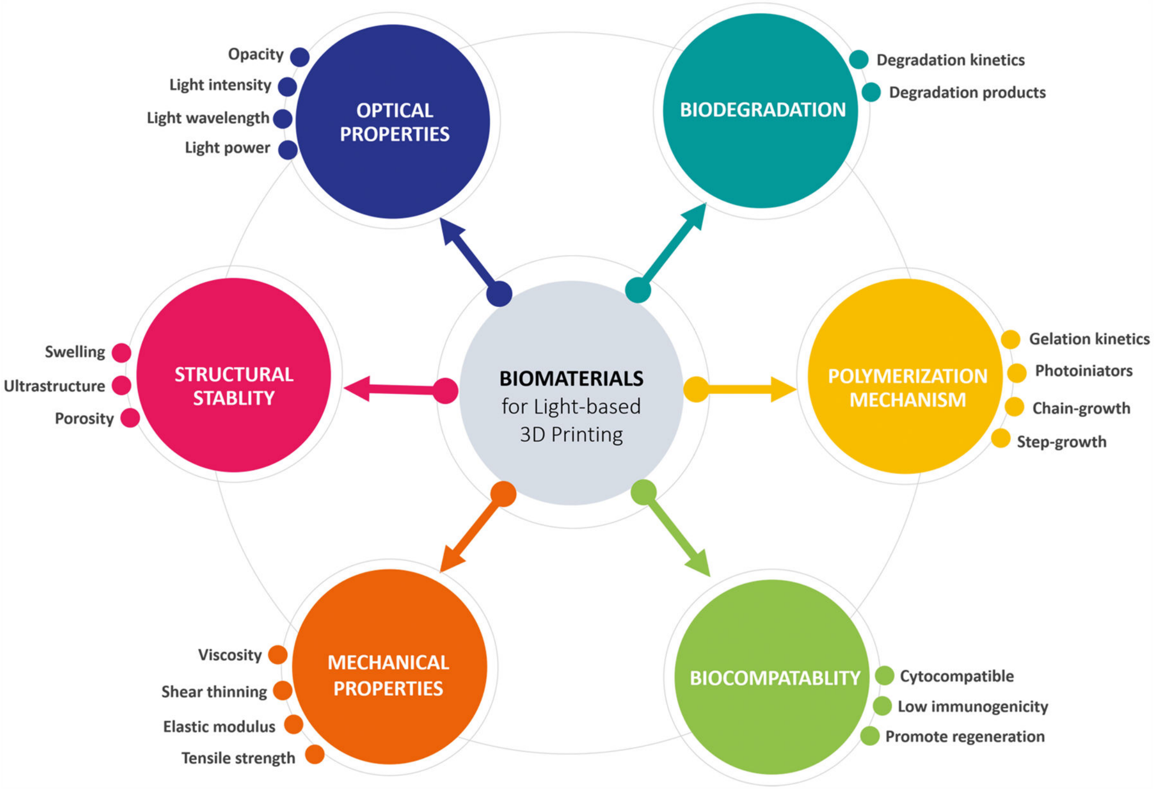

Figure 1.

Overview of biomaterials selection criteria for light-based 3D printing in tissue engineering and regenerative medicine applications.

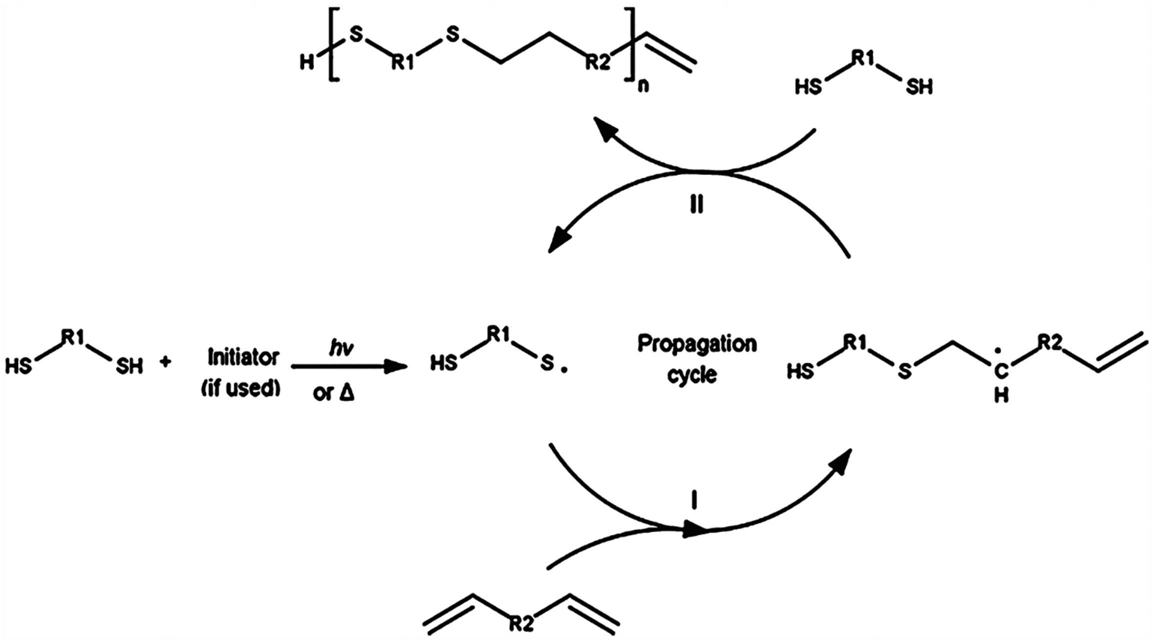

Figure 2.

Free radical initiated thiol–ene click chemistry reaction mechanism. Propagation occurs in mechanism I. The initiator free radical abstracts the thiol hydrogen, producing a thiyl radical that attacks the alkene double bond. Chain transfer occurs in mechanism II. The thiyl radical is regenerated by the alkyl radical abstracting a free thiol hydrogen, which under the right reaction conditions will occur much more often than attacking another alkene double bond. The thiyl radical can now continue to propagate the thiol–ene reaction. Reproduced with permission from ref 60. Copyright 2017 Elsevier.

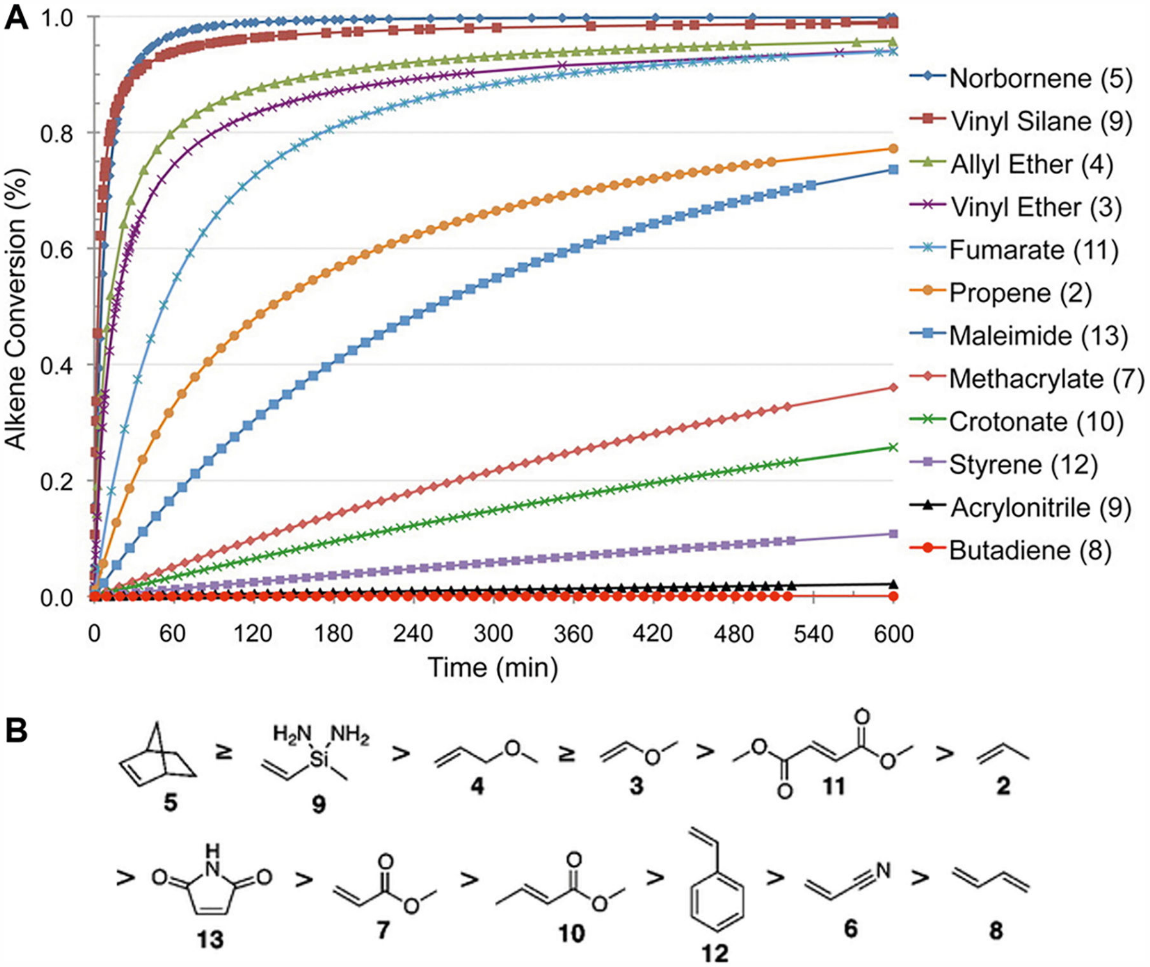

Figure 3.

Effect of alkene group selection on thiol–ene reaction kinetics. (A) Theoretical computation of the kinetics of the thiol–ene reaction dependent on the reactivity of the chosen alkene group. Norbornene is a popular alkene candidate for thiol–ene reactions due to its superior reaction rate. Methacrylate, the common reactive group for chain-growth photopolymerization, has a starkly slow thiol–ene kinetics, with the alkene conversion well below 50% even after a 10 h reaction time. (B) Descending list of alkene group reactivity based on the theoretical kinetics model. Reprinted with permission from ref 67. Copyright 2012 American Chemical Society.

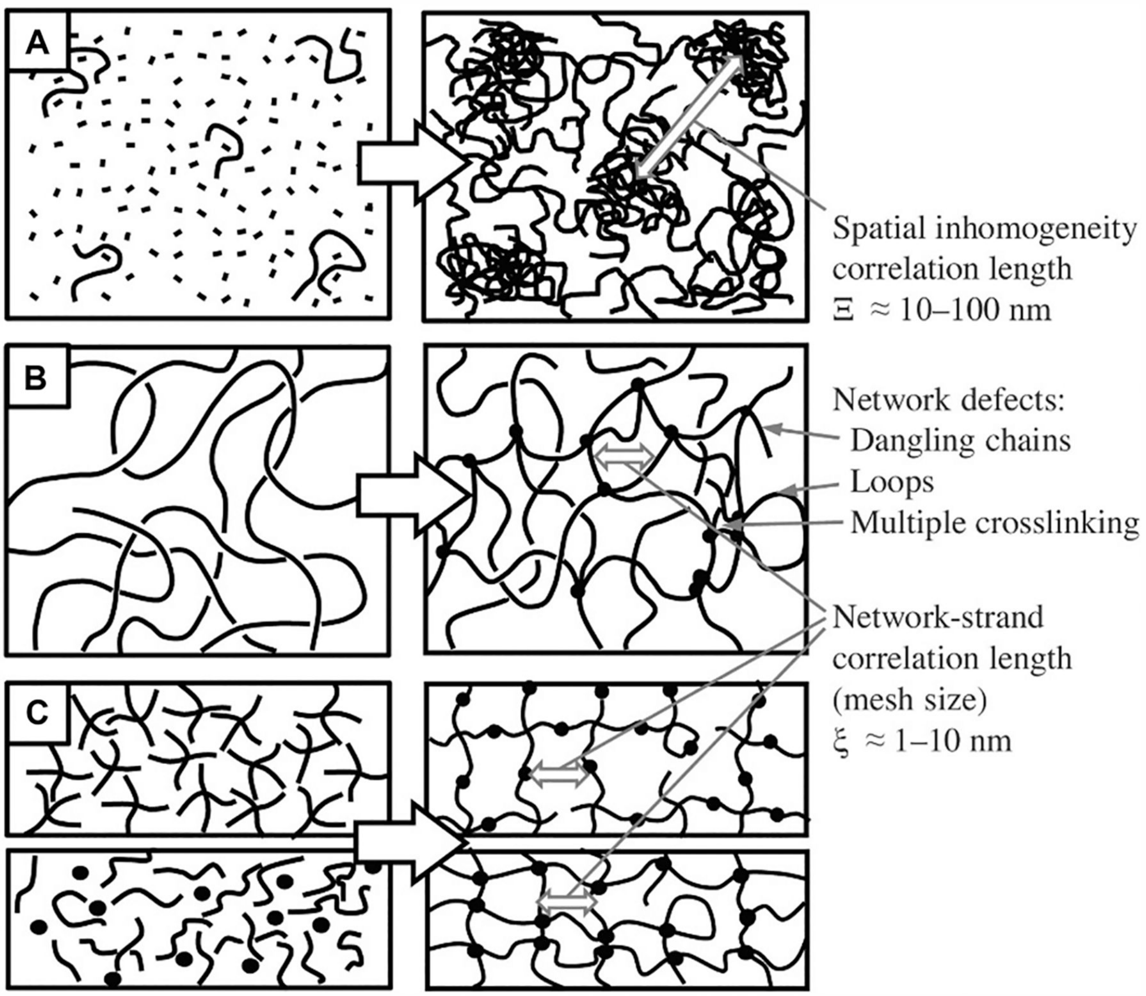

Figure 4.

Depiction of hydrogel network formation depending on cross-linking mechanism and the resulting degree of inhomogeneity. (A) Free-radical chain growth polymerization of monomers and cross-linkers leading to spatial inhomogeneity within the network architecture. (B) Network formation via cross-linking of reactive functional side groups of the polymer chains in a semidilute solution, leading to local inhomogeneity. (C) Orthogonal step-growth polymerization resulting in a mostly ordered, homogeneous network. Reproduced with permission from ref 78. Copyright 2017 Elsevier.

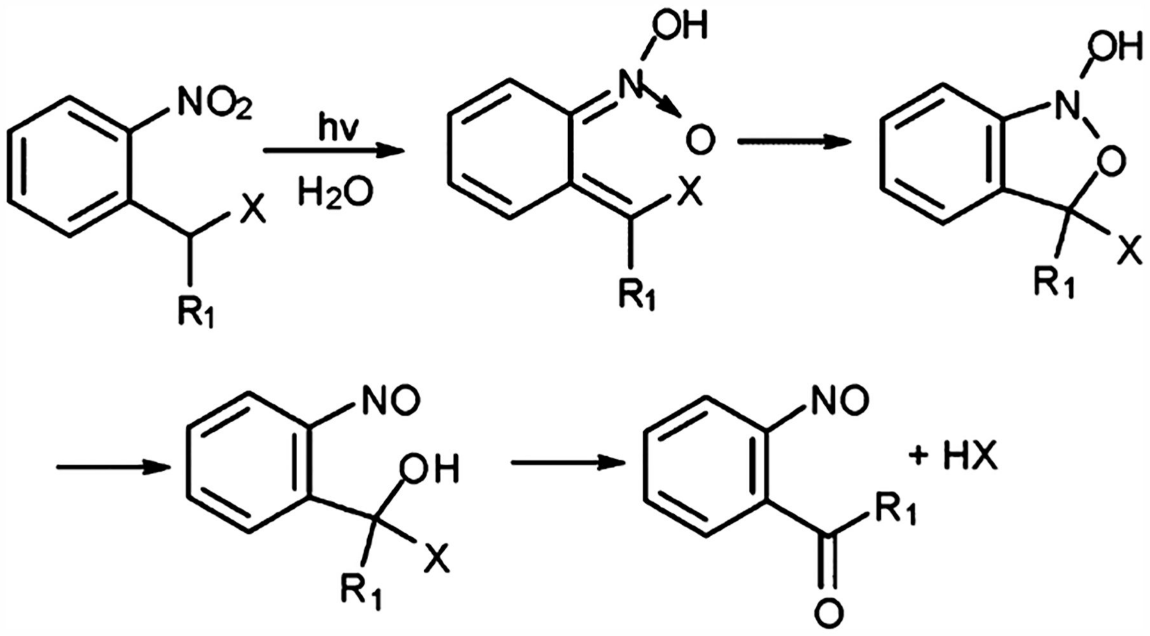

Figure 5.
Photolysis mechanism of *o*-nitrobenzyl (R1 = H) and nitrophenylethyl (R1 = methyl).

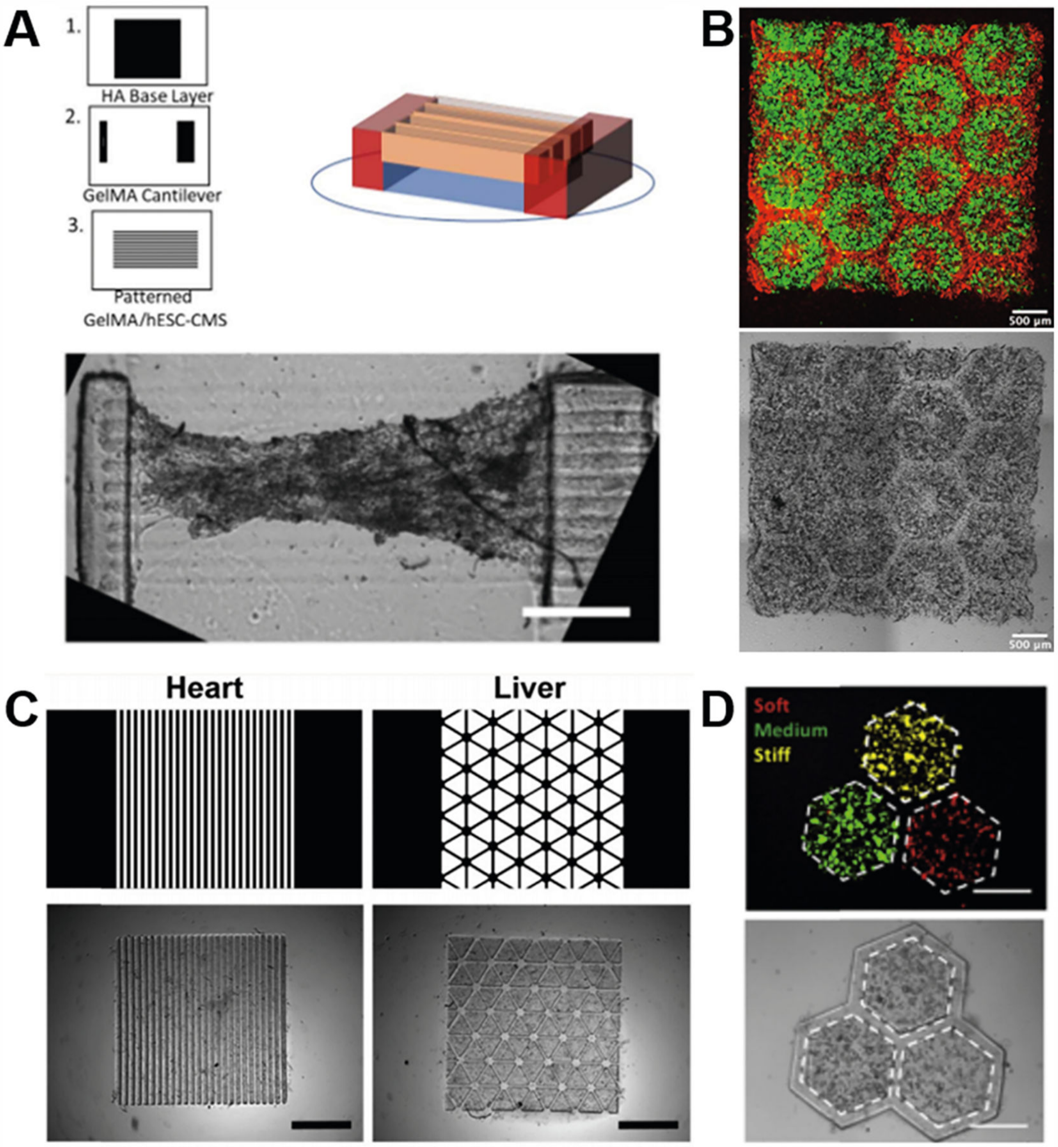

Figure 6.

Various tissue constructs bioprinted with naturally derived biomaterials. (A) Schematic and bright-field image of a cantilever cardiac tissue model bioprinted with GelMA for measuring the cardiac contraction force. Scale bar: 500 μm. Reproduced with permission from ref 117. Copyright 2019 Elsevier. (B) Fluorescence and bright field images of a biomimetic multicellular liver tissue model bioprinted with GelMA and GM-HA for drug testing. Scale bars: 500 μm. Reproduced with permission from ref 15. Copyright 2016 National Academy of Sciences. (C) Digital designs and bright field images of biomimetic heart and liver tissues bioprinted with tissue-specific dECM bioinks. Scale bar: 1 mm. Reproduced with permission from ref 152. Copyright 2019 Elsevier. (D) Fluorescence and bright field images of a hepatic cancer model bioprinted with liver dECM bioink to recapitulate various stages of fibrotic liver disease. Scale bars: 500 μm. Reproduced with permission from ref 123. Copyright 2018 Elsevier.

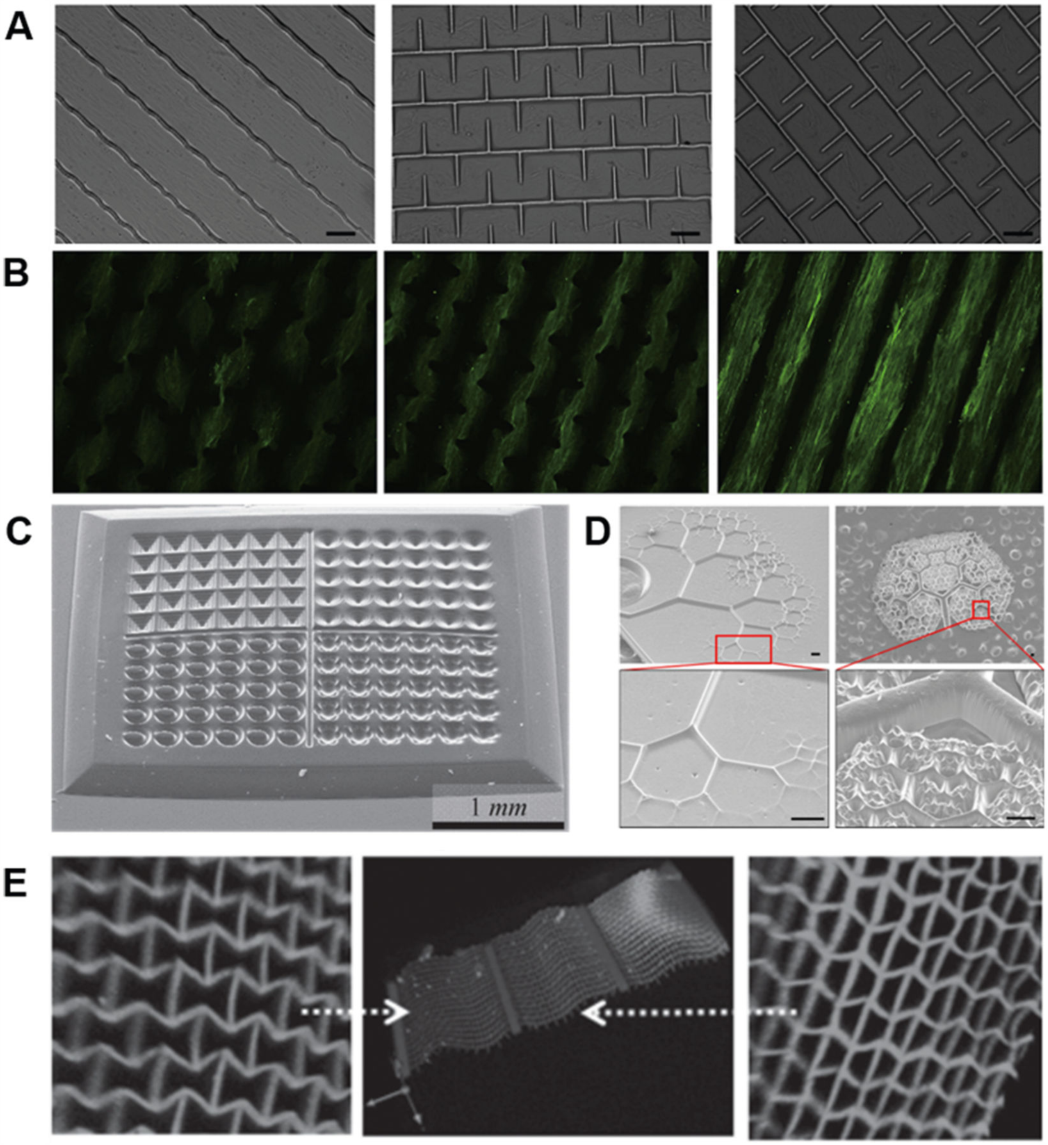

Figure 7.

Various 3D printed PEG-based hydrogel structures for cell biology. (A) 3D printed PEGDA patterns (from left to right: stripes, symmetric forks, and asymmetric forks) for investigating the impact of cellular alignment and stress on ADSC differentiation. Scale bars: 100 μm. (B) Immunofluorescent staining of smooth muscle α-actin revealing the cell alignment and myogenesis on the three PEGDA patterns. (A,B) Reproduced with permission from ref 172. Copyright 2013 Elsevier. (C) 3D printed microwells with various shapes for multicellular spheroid and embryoid body culture. Reproduced with permission from ref 14. Copyright 2012 Wiley-VCH. (D) Nature-inspired fractal patterns for investigating cell organization behaviors. Reproduced with permission from ref 177. Copyright 2016 American Chemical Society. (E) 3D printed web structures with microscale units featuring positive and negative Poisson's ratios. Reproduced with permission from ref 179. Copyright 2013 Wiley-VCH.

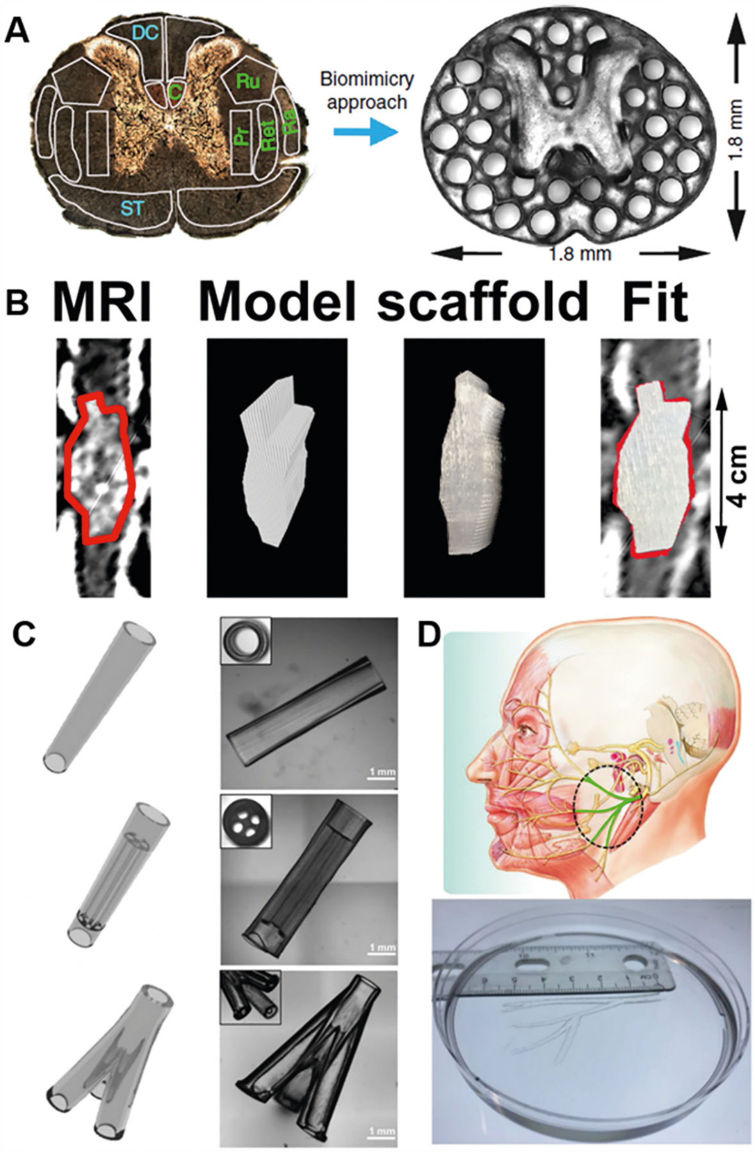

Figure 8.

Various 3D printed PEG-based hydrogel structures for tissue engineering and regenerative medicine. (A) 3D printed biomimetic spinal cord scaffold with microchannels for complete rat spinal cord transection. (B) 3D printed spinal cord scaffold based on MRI of human spinal cord injury. (A,B) Reprinted with permission from ref 16. Copyright 2019 Springer Nature. (C) Various 3D printed nerve guidance conduits (NGCs) for peripheral nerve regeneration. (D) 3D printed human life-size facial NGC. (C,D) Reproduced with permission from ref 162. Copyright 2018 Elsevier.

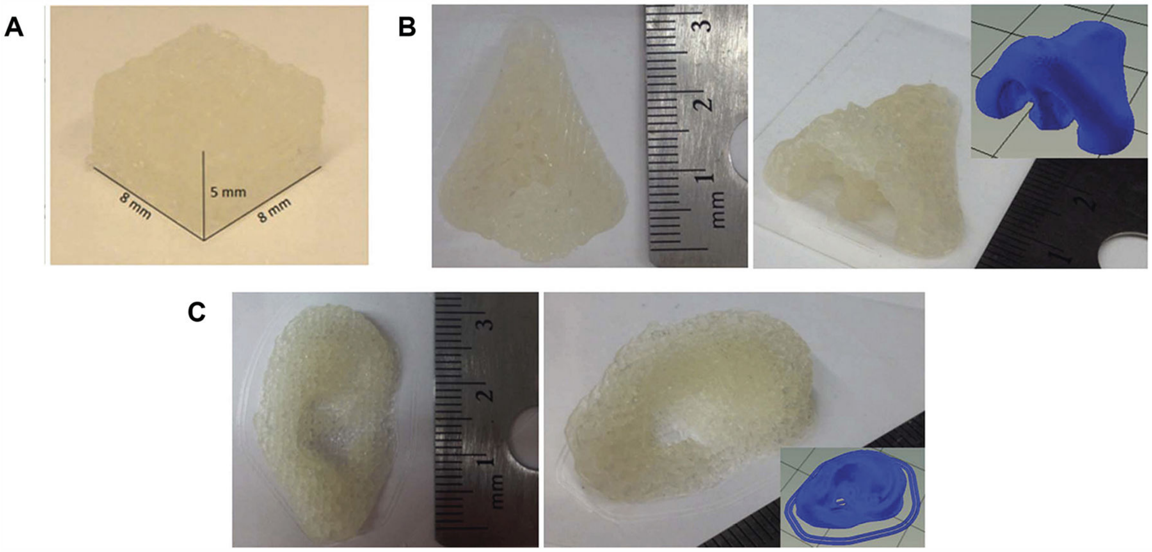

Figure 9.

3D printed Nor-PGS as (A) open-lattice cube, (B) nose, and (C) ear shaped structures. Reproduced with permission from ref 223. Copyright 2017 Royal Society of Chemistry.

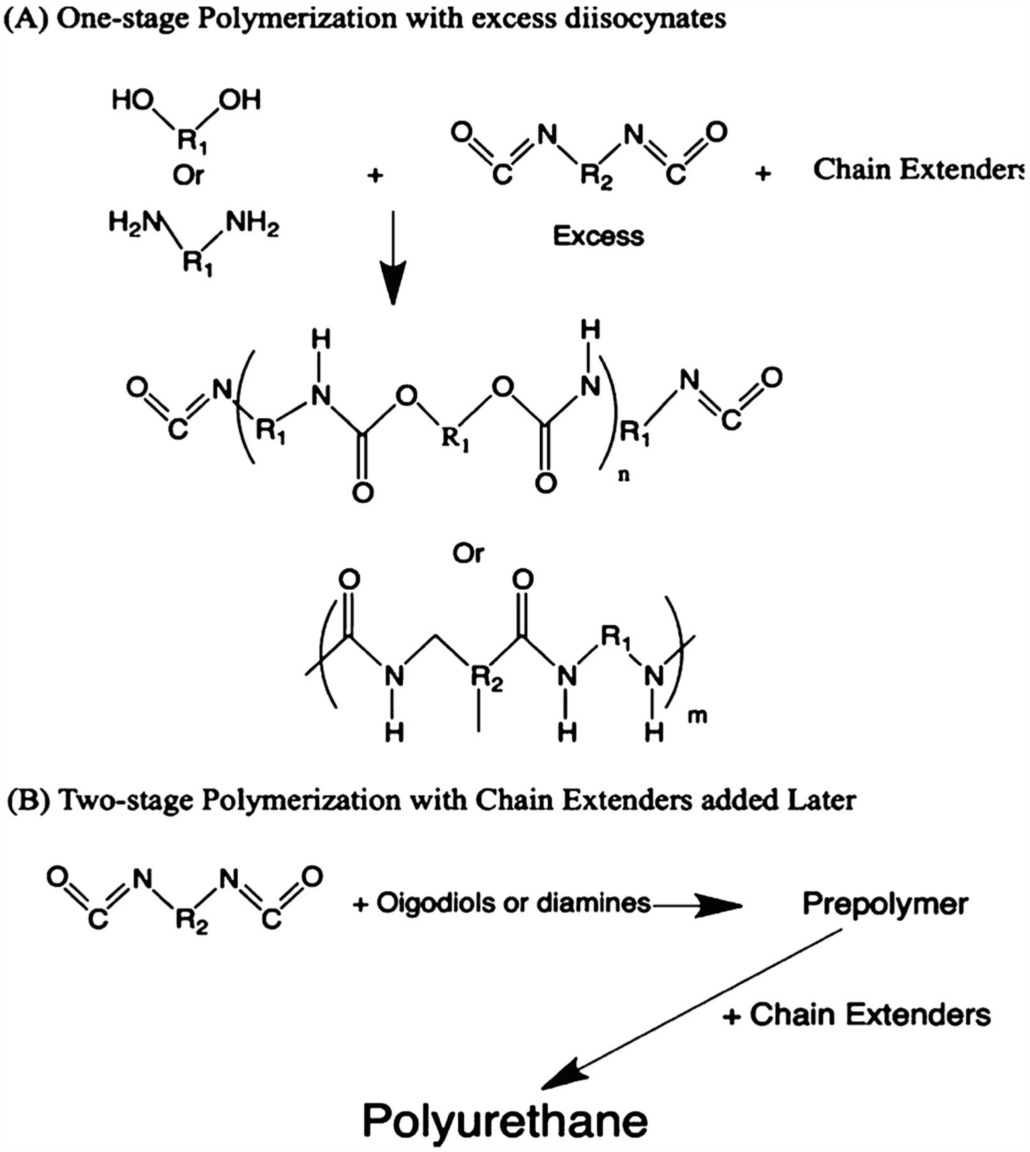

Figure 10.

Polymerization mechanism of polyurethanes. (A) One-stage polymerization where polyols/polyamines and chain extenders react with excess diisocyanates simultaneously. (B) Two-stage polymerization where polyols/polyamines react with diisocyanates first, followed by an additional reaction with the chain extenders.

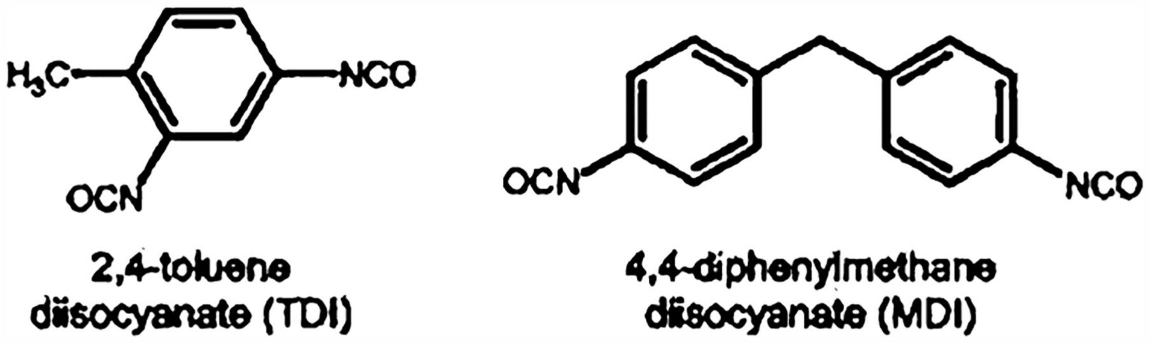

Figure 11.

Common diisocyanates used in large-scale polyurethane productions.

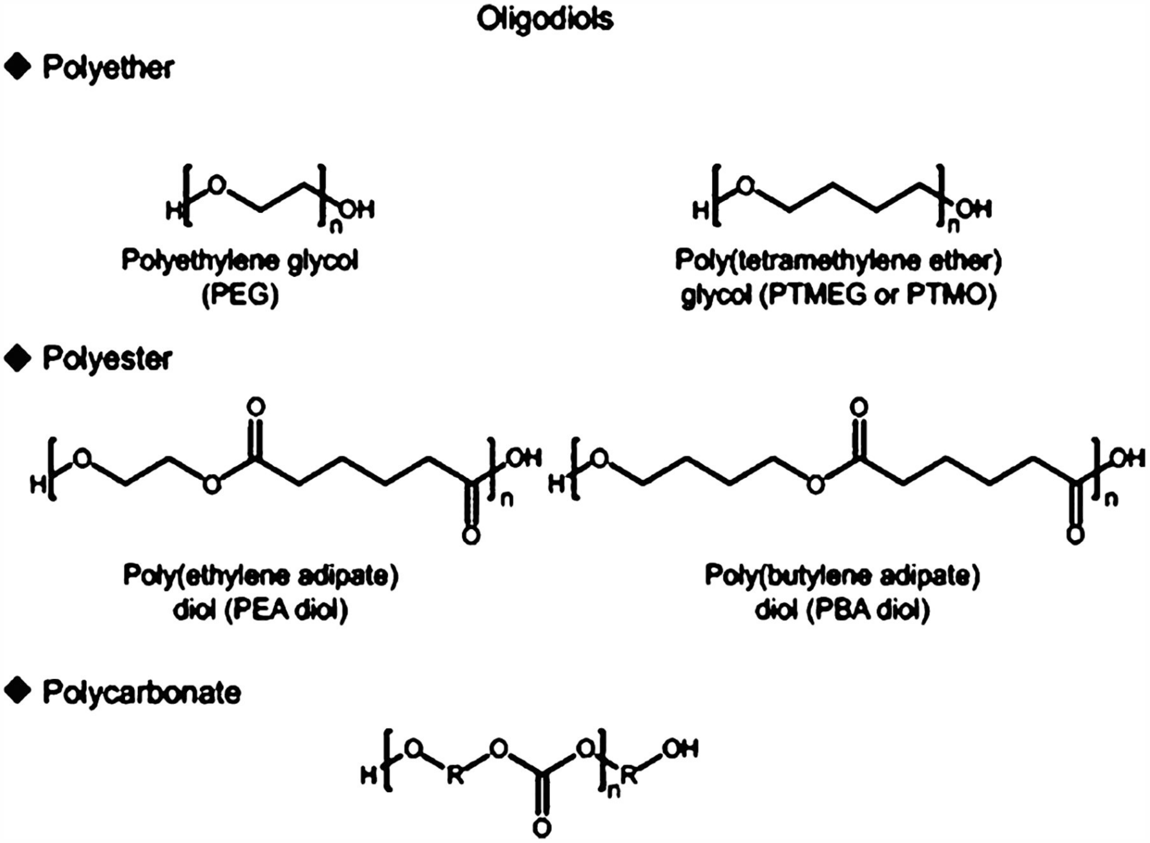

Figure 12.

Common oligodiols used in polyurethane production, including polyether, polyester, and polycarbonate-based oligodiols. The nature of oligodiols used will determine the properties of polyurethane synthesized.

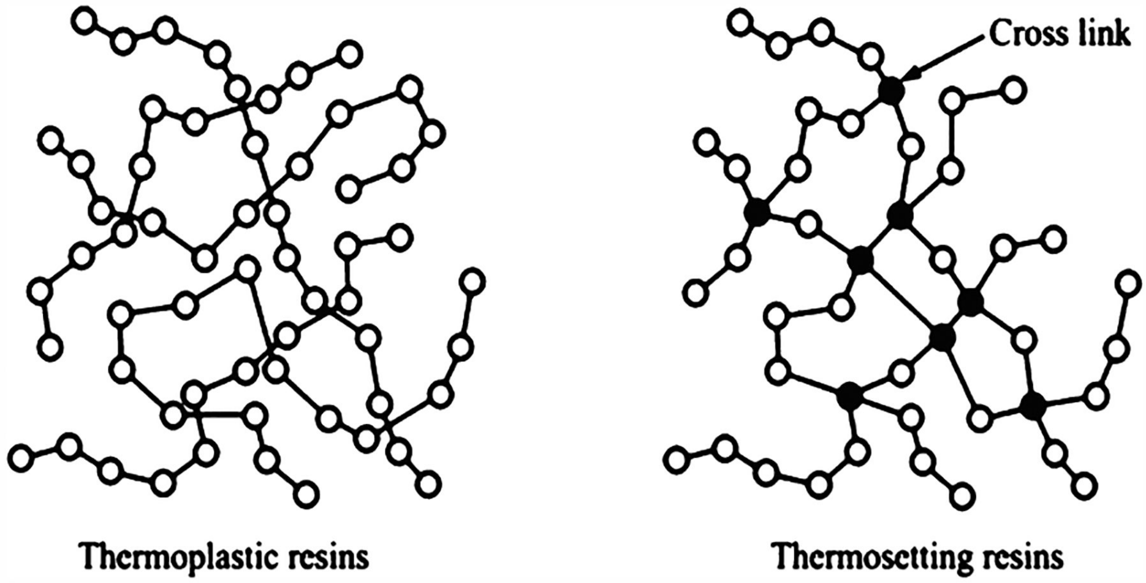

Figure 13.

Schematic drawings explaining the difference in polymer chain structures between thermoplastic and thermosetting polyurethanes. Thermoplastic polyurethanes will have higher backbone flexibilities, whereas thermosetting polyurethanes are generally more rigid. Reproduced with permission from ref 244. Copyright 2015 Multidisciplinary Digital Publishing Institute (MDPI).

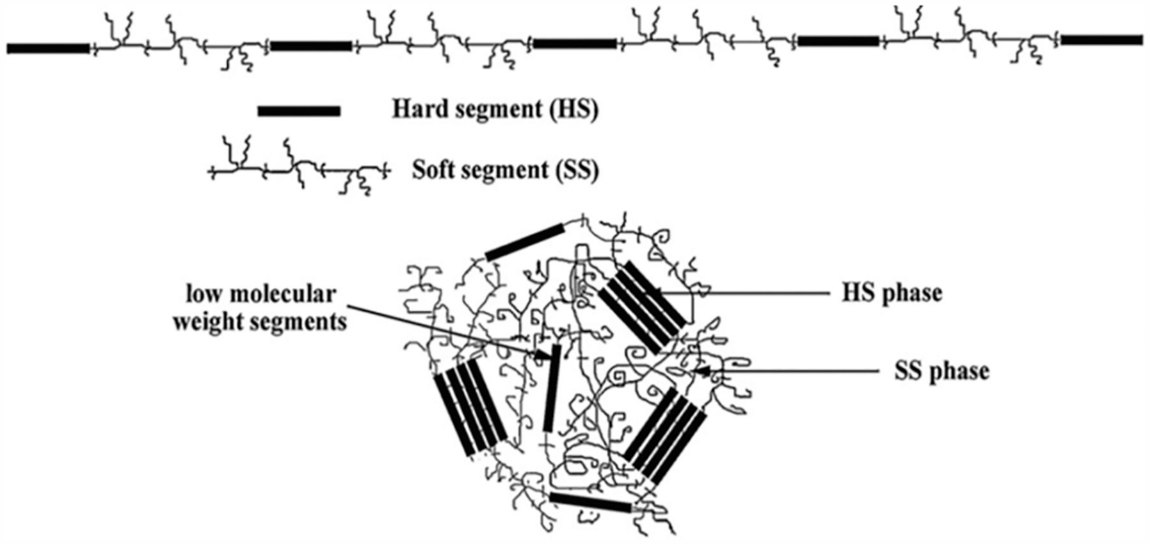

Figure 14.
Hard and soft segment distribution in PU. Reproduced with permission from ref 245. Copyright 2011 Elsevier.

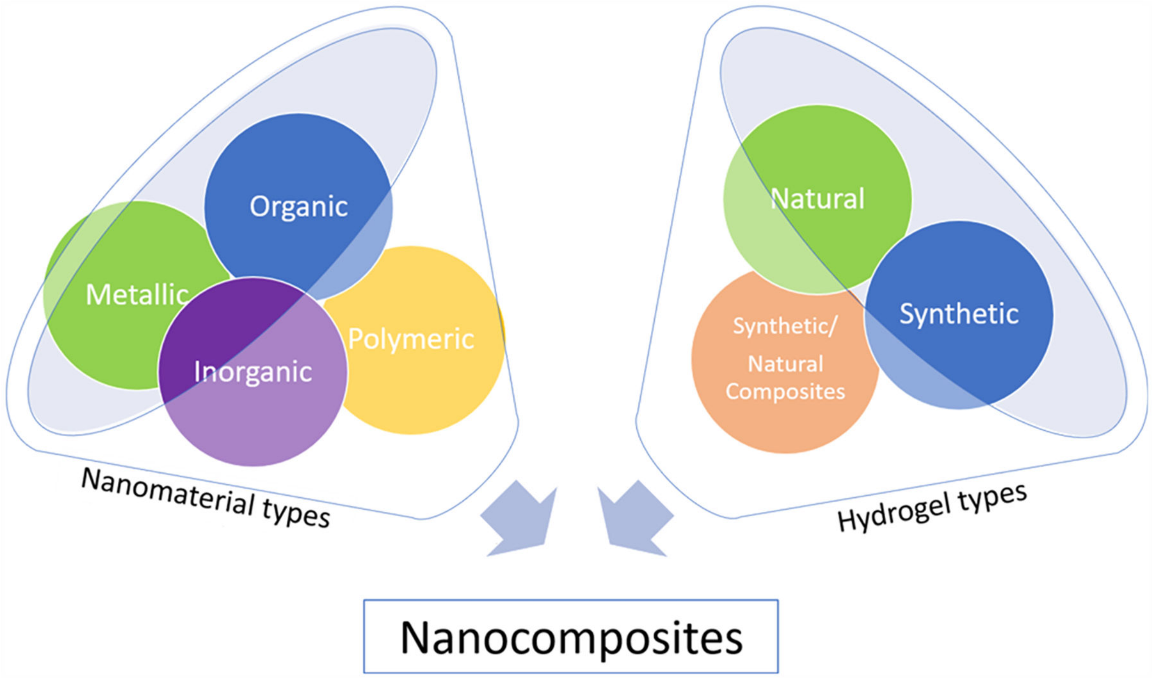

Figure 15.

Schematic of different types of nanomaterials that can be used to form nanocomposite hydrogels.

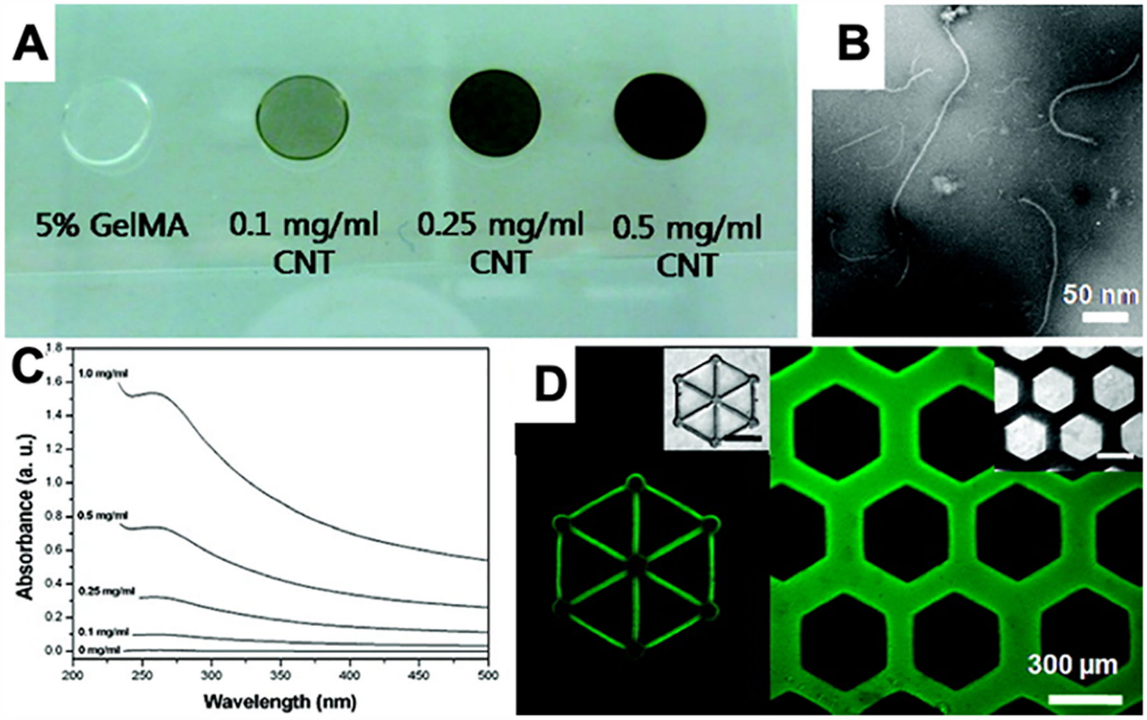

Figure 16.

(A) Optical images of CNT/GelMA prepolymer solutions showing increasing optical density with increasing CNT concentration. (B) High resolution transmission electron microscopy image of well-dispersed 0.5 mg/mL CNT/GelMA prepolymer solution. (C) UV–vis adsorption spectra of prepolymer solutions. Absorption at 365 nm increases with increasing CNT concentration. (D) Fluorescence images of micropatterned CNT/GelMA hydrogels. CNTs functionalized with FITC for visualization. Scale bar: 300 μm. Reproduced with permission from ref 268. Copyright 2012 American Chemical Society.

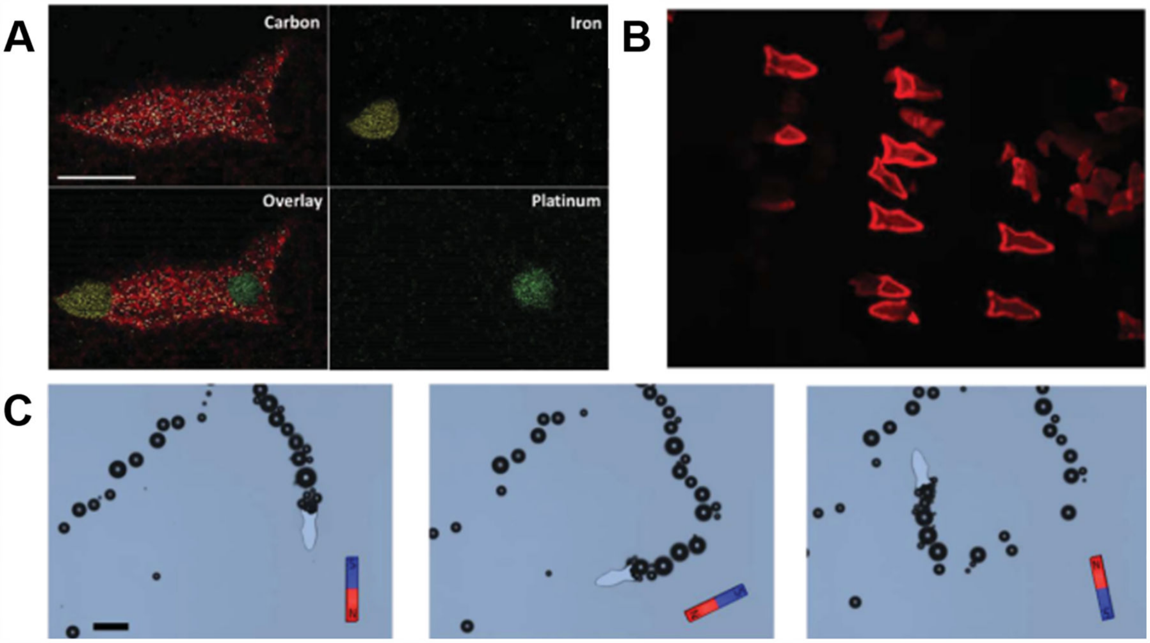

Figure 17.

3D printed microfish. (A) Energy-dispersive X-ray spectroscopy showing 3D microfish with different nanoparticles localized at the head, tail, and body. (B) Fluorescent image of the microfish after detoxification of a melittin solution. (C) Time-lapse images of the microfish performing sharp turns with magnetic guidance. (A–C) Reproduced with permission from ref 280. Copyright 2015 Wiley-VCH.

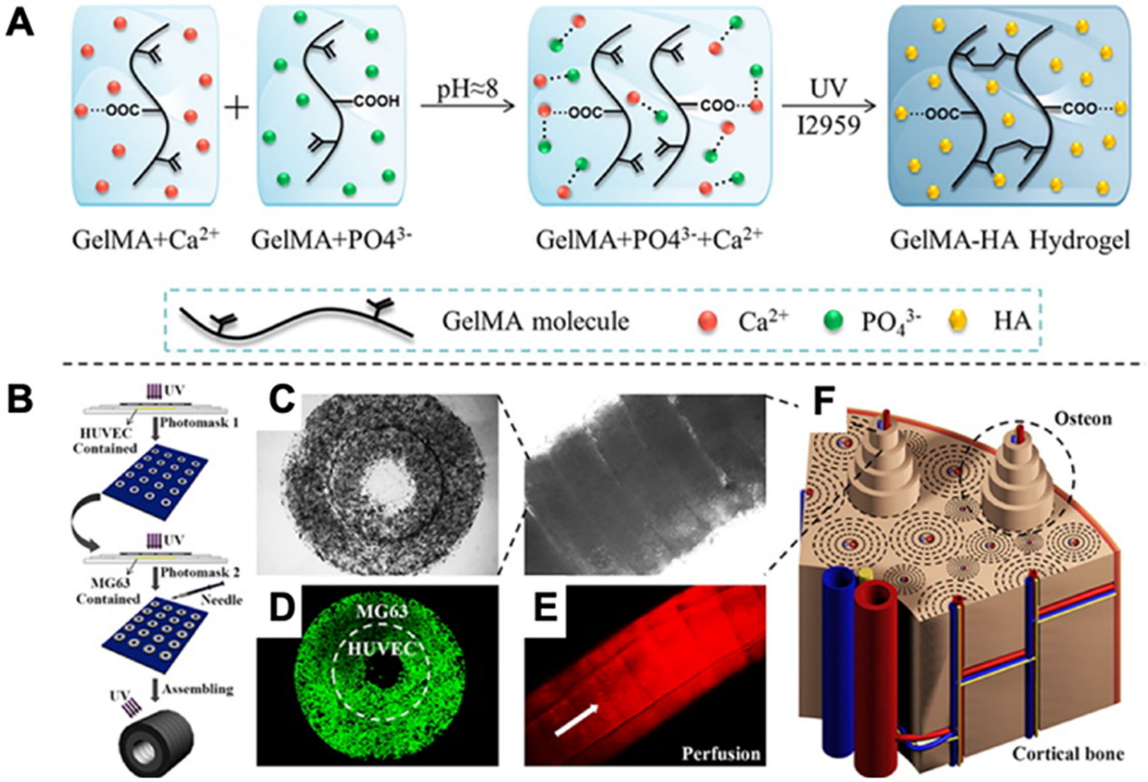

Figure 18.

(A) Schematic of the mechanism of hydroxyapatite (HA) formation in the GelMA network. (B) Schematic of printing setup. HUVECs encapsulated in the prepolymer system were first micropatterned, followed by MG63 cells encapsulated into the prepolymer system. The printed rings are then assembled in a modular fashion into tubes. (C) Characterization of osteon-like double-ring modules. Phase-contrast images of micropatterned print of single unit as well as a full tube assembly. (D) Confocal image of cells in the structure at day 7. (E) Fluorescent image of the tube under rhodamine (red) perfusion. (F) Schematic of the cortical bone used as inspiration for print. Reproduced with permission from ref 285. Copyright 2015 American Chemical Society.

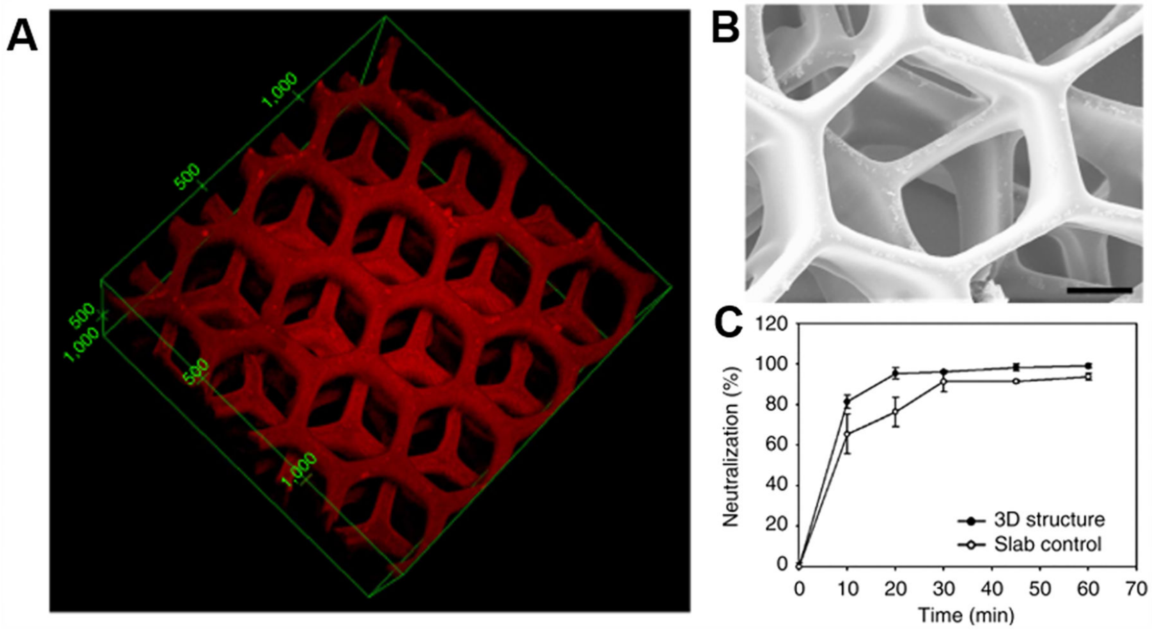

Figure 19.

3D printed liver detoxification device. (A) Fluorescent image of 3D printed liver-inspired detoxification device with polydiacetylene nanoparticles encapsulated in PEGDA. (B) Scanning electron microscope image of this detoxification device. Scale bar: 50 mm. (C) The liver-inspired detoxification device demonstrated higher neutralization efficiency than the slab control. (A–C) Reproduced with permission from ref 290. Copyright 2014 Springer Nature.

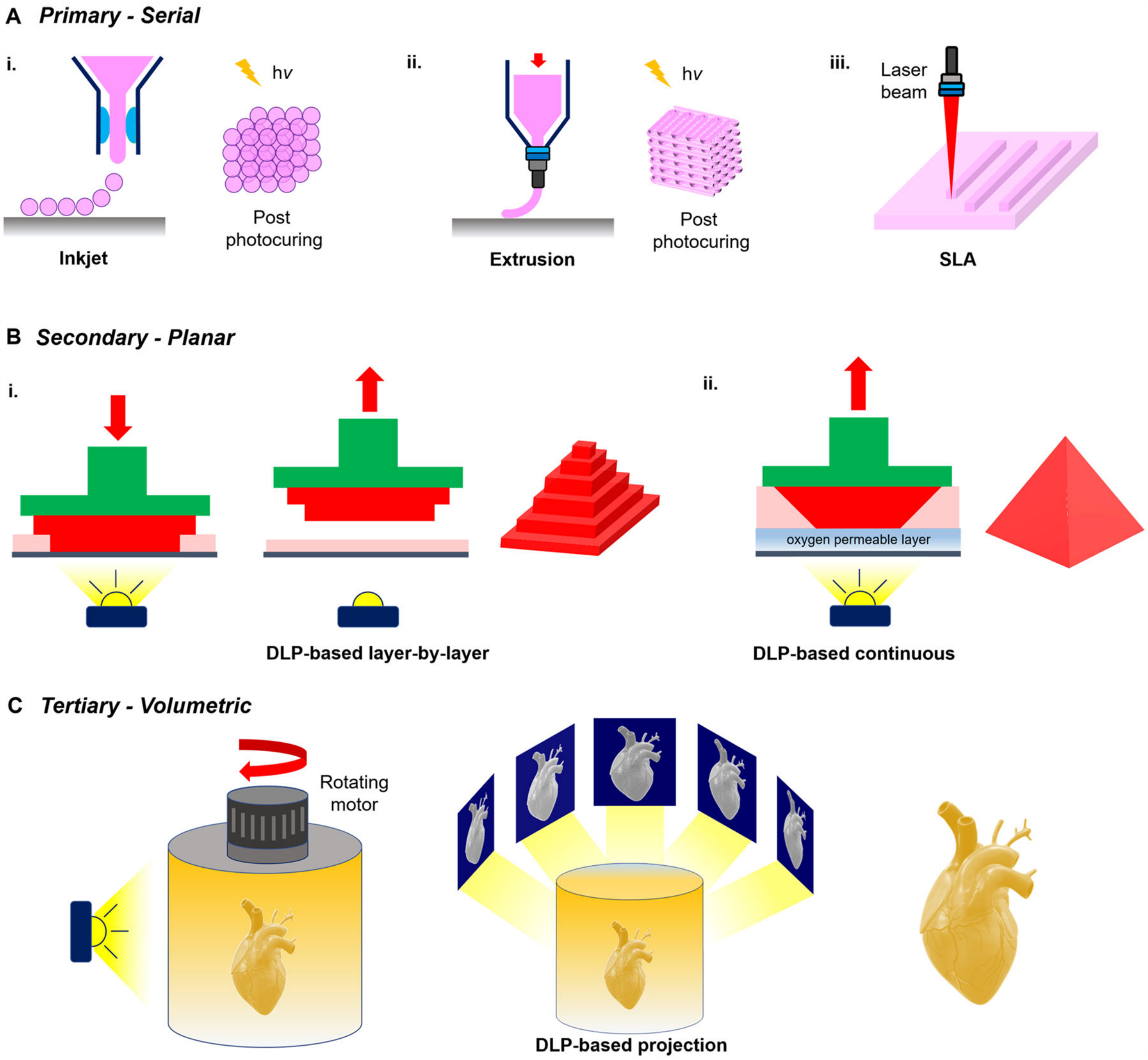

Figure 20.

Classification of light-based 3D printing modalities. (A) Primary configuration involves serial deposition of biomaterials in dot-by-dot or line-by-line fashion. (B) Secondary configuration involves planar build via digital light processing (DLP)-based projection of patterns into a biomaterial vat. (C) Tertiary configuration involves volumetric build via DLP-based projection of patterns into a rotating biomaterial vat.

(A) $\mathrm{I} \rightarrow 2\mathrm{R}^{\bullet}$

(B) $\mathrm{R}^{\bullet} + \mathrm{H_2C{=}CHR_1} \rightarrow \mathrm{RCH_2CHR}_1^{\bullet}$

(C) $\mathrm{RM}_1^{\bullet} + \mathrm{M}_1 \rightarrow \mathrm{RM}_2^{\bullet}$

(D) $\mathrm{RM}_n^{\bullet} + \mathrm{M}_1 \rightarrow \mathrm{RM}_{n+1}^{\bullet}$

(E) $\mathrm{RM}_x^{\bullet} + \mathrm{RM}_y^{\bullet} \rightarrow \mathrm{RM}_x\mathrm{M}_y\mathrm{R}$

Scheme 1.

General Initiation (A,B), Propagation (C,D), and Termination (E) Chemical Reactions for Free Radical Polymerization

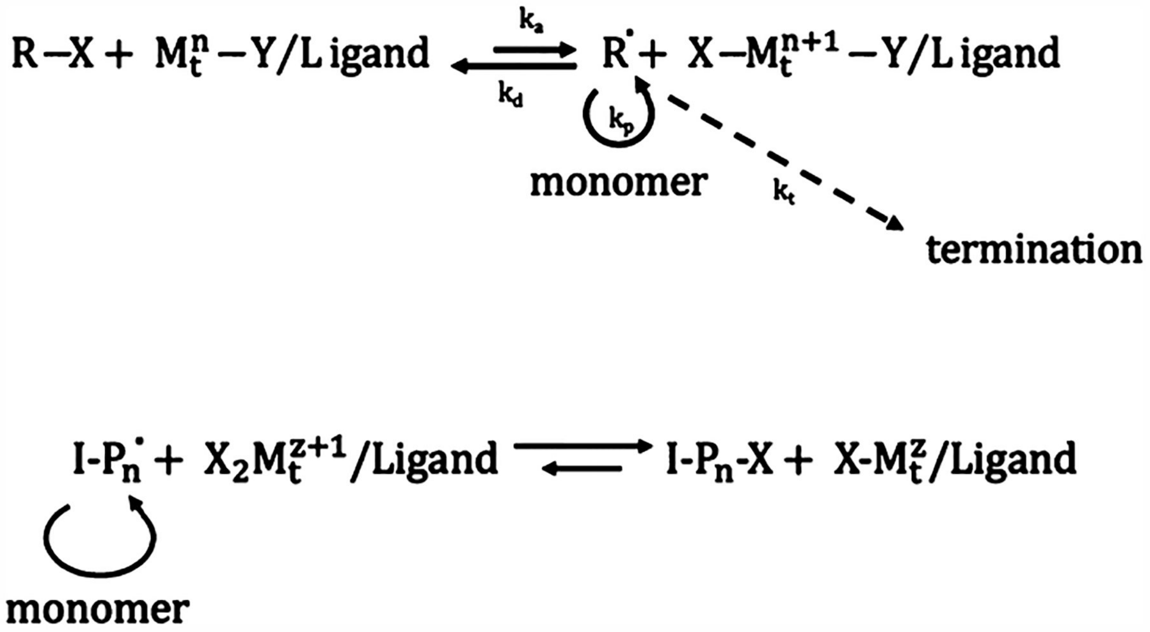

Scheme 2.

(top) Generalized ATRP Reaction Mechanism; (bottom) Generalized Reverse-ATRP Reaction Mechanism

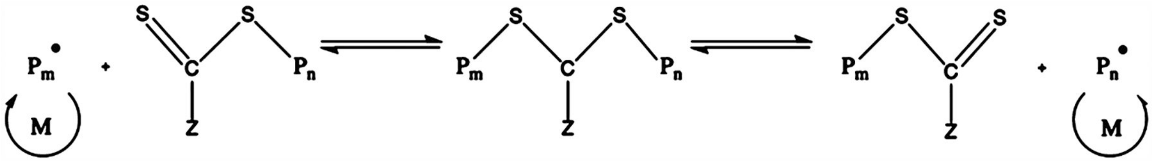

Scheme 3.
Generalized RAFT Reaction Mechanism

Table 1.

Photoinhibitors and Photoabsorbers

type	description	absorption wavelength	cytocompatibility	ref
	Photoinhibitors			
2,2,6,6-tetramethylpiperidin-l-yl)oxyl (TEMPO)	• stable free radical • adds to end of growing polymer chain and quenches reaction • soluble in aqueous media and organic solvents	N/A	cytotoxic	92
butyl nitrite	• alkyl nitrite prepared from n-butanol • UV activation induces photolysis of butyl nitrite to generate nitric oxide that terminates chain propagation	moderate absorbance at near-UV with weak absorbance in the blue region	cytotoxic	87
tetraethylthiuram disulfide (TETD)	• chain transfer reaction with propagating radical species reduces polymerization rates	moderate absorbance at near-UV with weak absorbance in the blue region	cytotoxic	85,86,101,102
bis [2-(*o*-chlorophenyl)-4,5-diphenyl imidazole] (*o*-Cl-HABI)	• activation of lophyl radicals generated upon HABI photolysis terminates chain propagation	moderate absorbance at near-UV with weak absorbance in the blue region	N/A	89
	Photoabsorbers			
tartrazine	• yellow food coloring also known as FD&C yellow 5, E102 • water-soluble	strong absorbance in the near-UV to blue visible light	cytocompatible	93,94
curcumin	• lipophilic • derived from turmeric	strong absorbance in the near-UV to blue visible light	cytotoxic	94–96
anthocyanin	• derived from blueberries • water-soluble	strong absorbance in the blue to yellow visible light range	cytotoxic	94,97,103
inorganic gold nanoparticles	• diameters between 12 and 41 nm	strong absorbance from blue to green visible light region	cytocompatible	100
2-hydroxy-4-methoxy-benzophenone-5-sulfonic acid (HMBS)	• common FDA approved chemical with UV light absorbing properties in sunscreen and cosmetics	UV	cytotoxic	92
reactive orange 16 (ROl6) (disodium(3Z)-6-acetamido-4-oxo-3-[[4-(2-sulfonatooxyethylsulfonyl) phenyl]hydrazinylidene] naphthalene-2-sulfonate)	• anionic azo dye • water-soluble	strong absorbance in the UV and from blue to green visible light region	N/A	98,99

Table 2.

Photopolymerizable Biomaterials Used in Light-Based 3D Printing

biomaterial	strengths	weaknesses	ref
	Natural		
gelatin methacrylate (GelMA)	• biocompatible • biodegradable • cell adhesive properties (i.e., RGD motifs)	• oxygen inhibited • heterogeneous polymer networks due to chain growth photopolymerization	305
Thiol–ene gelatin	• biocompatible • biodegradable • cell adhesive properties (i.e., RGD motifs) • not oxygen inhibited • hmogeneous polymer network • highly efficient step growth photopolymerization	• thiol moieties may spontaneously form disulfide bonds • poor storage stability	306,307
collagen methacrylate	• biocompatible • biodegradable • cell adhesive properties (i.e., RGD motifs)	• oxygen inhibited • heterogeneous polymer networks due to chain growth photopolymerization	308
hyaluronic acid (HA) and derivatives	• biocompatible • biodegradable • high water affinity	• oxygen inhibited • heterogeneous polymer networks due to chain growth photopolymerization • does not support cell adhesion	141,144,159
decellularized extracellular matrix (dECM)	• recapitulates complexity of biochemical constituents within native ECM • biocompatible • biodegradable • cell adhesive properties	• improper decellularization can introduce immunogenicity • inherently mechanically weak and lacks structural integrity thus requires combination with other biomaterials to maintain structural fidelity • batch-to-batch variability	146,148,152
alginate	• biocompatible • biodegradable • low cytotoxicity • minimal foreign body reaction	• does not support cell adhesion • ion leaching can lead to instability	153,161

biomaterial	strengths	weaknesses	ref
	Synthetic		
polyethylene glycol (PEG) derivatives (e.g., PEDGA, PEGMA, multiarmed PEG)	• biocompatible • biodegradable • low cytotoxicity • tunable mechanical strength	• does not support cell adhesion • low degradation rate • lacks biochemical composition of native tissue	170,309
pol(glycerol-co-sebacate) (PGS) derivatives (e.g., PGSA, PGSM)	• biocompatible • biodegradable • elastic nature can withstand dynamic tissue environments	• limited range of mechanical properties • potential cytotoxicity due to acid degradation • rapid degradation kinetics	181,217,310
polyurethane (PU)	• excellent mechanical properties and biocompatibility • low immune response in vivo • can form interpenetrating polymer networks (IPN) with other polymers such as epoxy and acrylates without bulk phase separation • polycarbonate-based and polyolefm-based PUs demonstrate better hydrolytic resistance and oxidative stability	• polyester-based PUs are prone to attacks from hydrolytic enzymes, thus limiting its applications in long-term devices • polyether-based PUs were fragile against stress cracking after implantation	240,241
	Composite		
organic nanomaterials in hydrogels (e.g., carbon nanotubes, graphene oxide)	• enhanced stiffness • electroconductive • cytocompatible in some applications	• brittle • prepolymer opacity increases due to nanofiller addition, which affects printability	265–271
metallic nanomaterials in hydrogels (e.g., gold, silver, iron nanoparticles)	• electroconductivity for sensors • magnetic properties for spatial control • drug delivery • MRI contrast agents	• some MNP variants may affect cell viability and function • little if any improvement on mechanical properties	272,277–282
inorganic nanomaterials in hydrogels (e.g., hydroxyapatite, silicate, glass, silica)	• increase hydrogel toughness • hydroxyapatite is bioactive for promoting osteogenesis • reduces hydrogel swelling	• little to no effect on the compressive modulus • inorganic NPs tend to aggregate as concentration increases • increases opacity with increased nanofiller concentration	283–286
polymeric nanomaterials in hydrogels (e.g., dendrimers, liposomes, polymeric micelles)	• controlled drug release • site-specific drug delivery	• can require organic synthesis (i.e., not off-the-shelf) • generally no improvement on mechanical properties	265,266,287,289

biomaterial	strengths	weaknesses	ref
	• detoxification		
composite natural hydrogels (e.g., GelMA–AlgMA, GelMA–CMCMA, GelMA–HAMA)	• expression of multiple bioactive binding domains • dual cross-linking mechanisms when incorporating with alginate/AlgMA • tunable mechanical and physical properties	• batch-to-batch variability • limited upper range of mechanical properties	297,299
composite synthetic-natural hydrogels (e.g., PEGDA–GelMA)	• improved and wider tunable range of mechanical properties over natural hydrogels alone • tunable degradation time	• synthetic components generally cannot be remodeled by cells • limited MWs and concentrations of synthetic components are cytocompatible	162,297
interpenetrating polymer network (IPN) hydrogels (e.g., thiol—yne and methacrylate systems)	• exceptional increase in toughness as well as other mechanical properties • very compatible with light-based printing techniques	• limited in material choices as it requires two different cross-linking mechanisms and miscible (bio)polymers	301,302,304,311

Table 3.

Light-Based 3D Printing Modalities

type	description	advantages	disadvantages	ref
		Serial		
inkjet	• biomaterials are deposited through a nozzle in a raster-like fashion • construct is cured by light irradiation post printing	• high resolution (nano to micrometer) • can accommodate multimaterial printing	• slow build for larger structures (hours) • limited to low viscosity biomaterials • not scalable • shear stress may decrease cell viability • limited geometric complexity • surface artifacts between layers	308,312
extrusion	• biomaterials are extruded through a nozzle in a raster-like fashion • construct is cured by light irradiation post printing	• moderate build time (minutes) • can accommodate multimaterial printing	• slow build for larger structures (hours) • limited range of compatible biomaterials • shear stress may decrease cell viability • limited geometric complexity • resolution limited to nozzle size and viscosity • surface artifacts between layers	11,150
laser	• laser photopolymerizes biomaterial within a vat in a raster-like contactless fashion	• high resolution can be attained (nanometer to micrometer)	• slow build for larger structures (hours) • not scalable • cannot accommodate multimaterial printing • Not ideal for cell-based printing	313,321
		Planar		
DLP-based layer-by-layer	• planar build via projection of digital patterns into a stationary biomaterial vat	• geometrically complex structures can be fabricated • high resolution (micrometer) • scalable build volume • moderate to rapid build time (seconds to minutes)	• surface artifacts between layers • mechanically weak at interfaces • opaque biomaterials severely limit light penetration and resolution	
DLP-based continuous	• planar build via projection of digital patterns into a biomaterial	• geometrically complex structures can be fabricated	• difficult to build very soft constructs • difficult to incorporate multimaterial print	14,90,323

type	description	advantages	disadvantages	ref
	vat that can be stationary or mobile	• overhanging and hollow structures easily fabricated • smooth surface features • moderate to rapid build time (seconds to minutes) • high resolution (micrometer) • scalable build volume	• opaque biomaterials severely limit light penetration and resolution	
		Volumetric		
DLP-based rotational	• volumetric build via projection of digital patterns into a rotating biomaterial vat	• geometrically complex structures can be fabricated • very soft substrates can be built wholly without support structures • hollow and overhanging structures easily fabricated • no surface artifacts • rapid build of complex large structures (seconds to minutes) • appropriate for bioprinting of cellularized soft hydrogels	• low viscosity biomaterials may compromise resolution • opaque biomaterials severely limit light penetration and resolution • resolution is limited (millimeter) • cannot easily accommodate multimaterial printing • excellent shape fidelity with smooth surface features	17,326
holographic	• volumetric build using holographic patterning of light fields	• geometrically complex structures can be fabricated • a few tens of micrometers resolution • rapid build time of millimeter scale structures (~1–10 s) • very soft substrates can be built wholly without support structures • good shape fidelity with rough surface features • hollow and overhanging structures easily fabricated • utilizes multibeam superposition via single photon absorption process • low power sources (~10–100 W) • less expensive than two-photon polymerization setups	• surface roughness on the scale of 100–200 μm mainly due to laser-speckle induced spatial noise • spatial resolution is dependent on resin viscosity, O_2 diffusivity, and presence of inhibitors with feature sizes limited to 300–400 μm	325

Table 4.

Troubleshooting Strategies to Control Printing Resolution

problem	potential solutions	ref
poor z resolution due to light penetration	i. doping a dye	94,323,348
	ii. using an evanescent field	343
poor resolution due to scattering	i. doping a dye	94,323,348
	ii. flash exposure	345
	iii. mask optimization for printing and material parameters	349
poor resolution due to diffusion	i. using TEMPO	342
	ii. increasing viscosity	350
poor resolution due to aberration	i. decreasing NA	337
	ii. using a narrow-spectrum light source	
poor resolution due to diffraction limit	i. increasing NA	337
	ii. using a shorter wavelength	
poor $x-y$ resolution due to out-offocus plane polymerization (i.e., caused by poor z-resolution)	i. doping a dye	94,323,348
	ii. increasing NA	337
slow (solution) refill causing defect for continuous printing	i. decreasing viscosity	89
	ii. decreasing speed	
	iii. increasing deadzone thickness	
poor resolution due to exposure dose/energy density	i. modifying speed/exposure time	351
poor $x-y$ resolution due to pixel resolution	i. modifying optical magnification	162